Universitat de Girona

SEMIACTIVE CONTROL STRATEGIES FOR VIBRATION MITIGATION IN ADAPTRONIC STRUCTURES EQUIPPED WITH MAGNETORHEOLOGICAL DAMPERS

Mauricio FABIÁN ZAPATEIRO DE LA HOZ

ISBN: 978-84-692-5522-3
Dipòsit legal: GI-976-2009

Universitat de Girona
Departament d'Enginyeria Elèctrica, Electrònica i Automàtica

Semiactive control strategies for vibration mitigation in adaptronic systems equipped with magnetorheological dampers

by

Mauricio Fabián Zapateiro De la Hoz

Advisors

Dr. Ningsu Luo Ren and Dr. Hamid Reza Karimi

DOCTORAL THESIS
Girona, Spain
February, 2009

Universitat de Girona
Departament d'Enginyeria Elèctrica, Electrònica i Automàtica

Semiactive control strategies for vibration mitigation in adaptronic systems equipped with magnetorheological dampers

By

Mauricio Fabián Zapateiro De la Hoz

A dissertation presented to the University of Girona
in partial fulfillment of the requirements of the degree of
DOCTOR OF PHILOSOPHY

Advisors

Dr. Ningsu Luo Ren

Dr. Hamid Reza Karimi

Girona, Spain
February, 2009

To my mother and father.

Universitat de Girona
Departament d'Enginyeria Elèctrica, Electrònica i Automàtica

Abstract

Semiactive control strategies for vibration mitigation in adaptronic systems equipped with magnetorheological dampers

by

Mauricio Fabián Zapateiro De la Hoz

Advisors: Dr. Ningsu Luo and Dr. Hamid Reza Karimi

February, 2009
Girona, Spain

In recent years, the protection of structures against hazardous vibration has gained special interest. Structures such as buildings, bridges and vehicle suspension systems are subject to vibrations that may cause malfunctioning, uncomfort or collapse. It is an extended practice to install damping devices in order to mitigate such vibrations. Furthermore, when the dampers are controllable, the structure act as an adaptronic system. Adaptronic systems are characterized by their ability to respond to external loading conditions and adapt to these changes. These abilities can be exploited to solve the vibration mitigation problems through the installation of controllable dampers and the design of appropriate control laws for an adequate actuation. This dissertation focuses on solving the vibration mitigation problem in buildings and vehicles. Emphasis is made on systems that make use magnetorheological (MR) dampers to accomplish this objective. MR dampers are semiactive devices that can produce high damping forces with less energy requirements than other devices of its class. However, MR dampers are highly nonlinear devices whose dynamics are characterized by a hysteretic force-velocity response. Additionally, the systems where they are installed, are characterized by parametric uncertainties, limited measurement availability and unknown disturbances. The presence of all of these factors makes mandatory the use of complex control techniques in order to get a reliable performance of the control system. This research is intended to contribute with new control algorithms that incorporate these problems in their formulation, especially, the dynamics of the damper. In order to do it, three control methodologies are explored: Backstepping, Quantitative Feedback Theory and Mixed H_2/H_∞. The proposed control laws are applied to different structures equipped with MR dampers. In particular buildings and vehicle suspension systems are studied. Numerical simulations and experimental testing are run to evaluate the performance of the proposed control laws.

Acknowledgements

I would like to seize this opportunity to express my most sincere acknowledgements to my advisors, Dr. Ningsu Luo and Dr. Hamid Reza Karimi. Ningsu's support and clever advices have been definite for the success of my career. I have learnt lots of things from him and I know they will be useful for the success in my professional life. And, despite our short meetings due to the distance, Hamid provided me with several clues that helped me getting successful achievements in my research.

I would like to extend these acknowledgements to all the members of the MICE Laboratory of the University of Girona for their kind support and advice throughout the course of my career. Also, Dr. Shirley J. Dyke and Ellen Taylor, from the WUSCEEL Laboratory (Washington University in St. Louis) and Dr. Billie F. Spencer and Brian Phillips from the SST Laboratory (University of Illinois at Urbana-Champaign). Their support in knowledge and experience were definite in the accomplishment of my research goals.

The time I have spent in Girona during the course of my doctoral studies have certainly been one of the most outstanding periods in my life. This has been possible thanks to many people I have met throughout these years. Some of them, despite their short-time presence, contributed with meaningful things and certainly enriched my life experiences. Yet there are other people who have been there, near me, most of the time and who I have shared amazing moments with. I only have thankfulness words for them, specially for Maira, Yenny and Nicolás, who have offered me an invaluable friendship. My best wishes to them!

I also want to express my most sincere gratitude to my family: my parents Luz María and Gustavo, my sister Laura, my grandmother Esther, my aunt Zully, who have supported me in every sense during my life. And of course, my little nephew Mateo, whose baby's innocence has been enough to make me smile even at the toughest moments. I know that this achievement will fill them up with sincere happiness.

Finally, I want to thank the Department for Innovation, University and Enterprise of the Government of Catalonia (Spain) for supporting me with the FI and BE pre-doctoral and mobility grants. And also, thanks to the Commission of Science and Technology of Spain (CICYT) through the coordinated research projects DPI-2005-08668-C03 and the government of Catalonia through SGR00296 which partially funded this research.

Mauricio F. Zapateiro De la Hoz
Girona, Spain
February 2009

Notation

Unless otherwise noted, the following notation is used in this dissertation.

$\mathbf{A}$, $\mathbf{B}$, $\mathbf{C}$, $\mathbf{D}$	state space matrices.
α	Bouc-Wen model design parameter.
β	Bouc-Wen model design parameter.
c	damping coefficient.
ζ	damping ratio.
$\mathbf{C}$	damping matrix.
d	control system disturbance.
D_d, D_v	seismic motion displacement and velocity bounds.
f_c	Coulomb element frictional force.
f_{mr}	MR damper force.
f_0	MR damper nonzero force.
f_g	ground motion disturbance.
f_{lin}, f_{nonlin}	linear/nonlinear dynamics associated to the MR damper.
F	unknown disturbance bound.
Φ	frictional damper force.
G	controller / compensator transfer function.
G_s	MR damper location vector in a building.
γ	H_∞ performance bound.
h_1, h_2	Backstepping design parameters.
$\mathbf{I}$	identity matrix.
J	performance index.
k	stiffness.
$K_{2\infty}$	mixed H_2/H_∞ controller gain vector.
$\mathbf{K}$	stiffness matrix.
κ	Bouc-Wen model design parameter.
L_s	input disturbance vector in a building.
m	mass.
$\mathbf{M}$	mass matrix.
P	Control system plant.
r_1, r_2, r_3, r_4	Adaptive backstepping design parameters.
s	Laplace variable.
$\mathbf{S_1}$, $\mathbf{S_2}$	LMI design matrices.
S_F, S_L	MR damper force/displacement scaling factors for real time hybrid testing.
u	state space model control input.
v	voltage.
V	Lyapunov function.
φ	Bouc-Wen model design parameter.
w	state space model disturbance.
W	QFT design constraint.
$\mathbf{x}$	state vector.
x, $\dot{x}$, $\ddot{x}$	displacement, velocity, acceleration.
$\mathbf{X_1}$, $\mathbf{X_2}$, $\mathbf{X_3}$, $\tilde{\mathbf{X}}$	LMI variables.
$\mathbf{y}$	state space model measured / controlled signal vector.
y_a, $\dot{y}_a$, $\ddot{y}_a$	building base displacement, velocity and acceleration.
z	Bouc-Wen model hysteresis element.

Contents

List of Figures

List of Tables

Chapter 1

Introduction

1.1 Motivation

In the last three decades, there has been an intense research activity focused on the design of systems able to mitigate the vibrations in civil engineering structures such as buildings, towers and bridges. Vibrations caused by seismic motions, strong winds and heavy traffic may not only be uncomfortable for people but dangerous if these compromise the stability of the structure and the safety of its occupants. Vulnerability of this kind of structures has been patent after the strong earthquakes and hurricanes that have hit different regions around the world and have caused their collapse with the consequent loss of lives.

In order to make structures safer against these phenomena, researchers have taken advantage of the fact that, by the principle of energy conservation, damping devices can be added to the structure as protective systems. This first led to the design and implementation of passive dampers to partially absorb the input energy and thus protect the structure. However, a significative step ahead was made when civil structures were considered as adaptronic systems, i.e. a system characterized by adaptability and multifunctionality (Neumann 1999). Thus, civil structures can be made adaptive or responsive to external loads. Active control was the first step to adaptronics in civil engineering and is an attempt to make them behave like an aircraft or machinery (Hirsch 1999).

One fundamental and powerful concept in adaptronic structures is the control of structural impedance. By modifying the structural impedance, the vibration behavior can be changed and hence, resistance to damage can be increased. Large civil engineering structures can control the transmission of motion and the flow of energy by controlling the impedance of the structure at its base. This can be achieved with electrorheological (ER) and magnetorheological (MR) dampers (Rogers & Giurgiutiu 1999). Particularly, MR dampers feature some interesting characteristics that make them superior than other devices of their class: higher damping force, less power requirements, lower costs, lower size, etc. Hence the efforts that have been devoted to their study (Dyke et al. 2005).

Despite MR damper advantages, they do have a major drawback: MR dampers are highly nonlinear devices and this makes its mathematical treatment a challenging task. Controller design for structures equipped with MR dampers gets more complicated if it is taken into account that the structure-damper system is characterized by model errors, model uncertainties, unknown disturbances, actuator dynamics, nonlinearities, time delays and measurement limitations. The existence of such problems makes imperative the use of complex control methodologies to exploit the best of each device and efficiently solve the vibration problem.

There are several works on control of structures with MR dampers (Dyke 2005). Nevertheless, none of them addresses the problem accounting for all the system characteristics as mentioned previously. It can be found on many of these works, that the controllers are designed as if the MR damper were an active device. Then, a clipping algorithm is applied to approximately command the MR damper force. Thus, these controllers ignore the MR damper nonlinearities in the formulation; others do not guarantee

robustness against the uncertainties of the system; yet there are others that rely on the assumption of the complete system state availability. Furthermore, the control laws are predominantly formulated in the time domain, leaving aside the frequency response of the system.

This research is aimed precisely to surpass some of these issues. By applying adequate control methodologies, it is possible to guarantee robustness by considering the parametric uncertainties and incorporating the actuator nonlinearities in the formulation so as to get a more reliable controller. Yet it is possible to formulate control laws in the frequency domain in order to take into account some frequency response issues that are as important as those in the time domain. Moreover, these control laws can be formulated in such a way that only a few measurements are required to be implemented.

1.2 Open problems

In spite of the progress achieved in the vibration control of civil structures, there are still open problems remaining to be solved. A list of the main problems in structural control is outlined next.

1. ***Unknown disturbances.*** Civil engineering structures are to be protected from hazardous phenomena like seismic motions. It is, however, not possible to predict when an earthquake is going to take place, neither its magnitude nor duration. Unknown disturbances are of major concern because they can excite the structure at its natural frequencies and as a consequence the structure may be severely damaged or even collapse (Pozo et al. 2006, Acho et al. 2008, Zapateiro, Luo & Karimi 2008).

2. ***Uncertain parameters.*** Modeling large-scale structures often lead to model errors. These may result from the neglect of nonlinearities, very fast dynamics, very slow dynamics, coupling between systems and devices, and dynamics of actuators and sensors; mismodeling in material and geometric properties, damping characterization, discretization of continuous models and linear approximation of nonlinearities. Modeling errors can be expected to decrease both the stability and performance robustness of the controlled structure (Rodellar & Luo 2003, Wang et al. 2004, Weber et al. 2006).

3. ***Optimal sensor and actuator location.*** The selection of what variables to measure, which ones to control and therefore, the sensors and actuators is an interdependent problem. There is a need to know which actuators are helping and which are degrading the performance (Skelton 1996). Besides, it must be kept in mind that it is not always possible to measure all the state variables (e.g. displacement, velocity and acceleration) because it would imply the installation of several sensors making this an impractical solution especially when the structure is quite large (a skyscraper, for example). On the other hand, the control performance might be affected by the properties of the channel transmission (latency, delay jitter, signal quantification, loss of data, etc.) and the way that the computational resources are distributed.

4. ***Actuator dynamics and nonlinearities.*** Actuator nonlinearities can generate a high sensitivity to uncertainties in the models and the external excitations. Smart material dampers such as piezoelectric and magnetorheological dampers have limitations associated with nonlinear and hysteretic behavior. They represent a challenge in developing high performance actuation responses over a broad frequency range (Kerschen et al. 2006, Fan & Smith 2008, Kilicarslan et al. 2008). Dampers also exhibit a time delay that must be taken into account because the disturbances occur in short periods of time. Actuator time delay must be added to the delays that exist in the control system and that are a result of the time taken in the online data acquisition from sensors at different locations of the system, the time taken in filtering and processing of the sensory data for the required control force to the actuator and the time taken by the actuator to produce the required control force. Time delay may induce complex behaviors such as oscillation, instability and degraded performances (Karimi et al. 2008*d*).

5. ***Asymmetric structures.*** The asymmetric distribution of stiffness or mass can make a seismic load cause torsional and lateral motions of the structure to be strongly coupled. This behavior

may cause larger responses than in a symmetric structures, resulting in severe localized structural damage. In symmetric buildings the control performance depends primarily on the floor at which the control device is placed; the specific location within the floor is not critical because the centers of mass and rigidity coincide. However, in asymmetric structures, the exact location of the device is critical and larger control forces and controllers based on global responses may be needed (Yoshida et al. 2002, Yoshida & Dyke 2003).

6. ***Coupling.*** The excitation of one structure can be induced in another one if they are coupled. The dynamics of the exciter system may be considered unknown but bounded with no information about its states available. These systems are usually modeled by means of two or more coupled subsystems in which one subsystem includes the measurable dynamics, and the others are unknown with bounded dynamics. The problem is then, to ensure that the control law takes into account the known states and parameters while maintaining the bounds of the structural response.

7. ***Fault tolerance.*** Fault tolerance is the ability of the controlled system to maintain its control objectives in the presence of a fault. Beyond the use of reliable devices and hardware, it is preferable to implement fault detection systems in the structures. Failures in a control system are generally detected by a two-component fault detection system: fault detection and identification, and fault accommodation. To date, very few publications have focussed on fault tolerance in civil engineering structures applications (Dyke 2005).

1.3 Objectives

The general objective of this research is to design semiactive control laws to mitigate the vibrations in adaptronic systems, especially in civil engineering structures equipped with magnetorheological dampers.

An exhaustive theoretical and experimental study of MR dampers is to be performed. Advantages and disadvantages of different MR damper models will be outlined. The goal is to find those models that may be suitable for control design.

New semiactive control strategies will be developed in order to effectively deal with the complexity of hysteretic nonlinearities, parametric uncertainties, measurement limitations and unknown disturbances, and consequently to achieve the robust performance. The formulation of semiactive control laws will be done by introducing, from other application fields, the useful control methodologies into the field of vibration mitigation in adaptronic systems (some of them for the first time) or by making improvements of other control methodologies already applied in this field.

The performance of the semiactive control laws will be validated by means of numerical simulations and/or experimental tests on laboratory specimens.

1.4 Structure of the thesis

This dissertation is organized as follows:

- *Chapter 1* is the introductory chapter. The research motivation, the problem statement and the research objectives are outlined in this chapter.
- *Chapter 2* presents the state of the art of the vibration mitigation problem using MR dampers. It presents the MR damper technology and the control methodologies that have been proposed to reduce vibrations in civil structures equipped with this class of dampers.
- *Chapter 3* is about modeling, identification and experimental testing of an MR damper operating in shear mode. Different models and identification techniques are presented in this chapter as well.
- *Chapter 4* is dedicated to the mathematical models of the structures that will be used throughout the remaining of the document in formulating the control laws and making the numerical and experimental verification.

- *Chapter 5* is devoted to the formulation of controllers in the time domain. The control methodology used is the Backstepping technique and the control laws are formulated so as to take into account the parametric uncertainties, unknown disturbances of the system and the nonlinearities of the MR damper.
- *Chapter 6* is about control formulation in the frequency domain. The technique used is the Quantitative Feedback Theory methodology. This allows to take into account the parametric uncertainties and set constraints for robust performance. The nonlinearities of the MR damper are also taken into account by proposing an uncertain linear representation for it.
- *Chapter 7* addresses the problem of designing mixed H_2/H_∞ controllers. This approach allows for reducing the systems response and control effort while maintaining the response within prescribed intervals in the presence of external disturbances. The output feedback control laws are formulated following an LMI procedure.
- *Chapter 8* outlines the conclusions and contributions of this research as well as the future work.

Chapter 2

State of the art

In this chapter, a survey on damping systems is presented. Emphasis is made on vibration reduction of civil structures using magnetorheological dampers. MR dampers design, applications and mathematical models are discussed. The survey finalizes with a review of the control techniques that have been employed in this class of systems.

2.1 Background on damping vibration systems

This section is a brief survey of the vibration control systems that have been designed and implemented so far to protect the civil structures from hazardous external loadings. Seismic protection systems may be classified in three main categories: passive, active and semiactive. The main characteristics of them will be outlined in what follows.

Passive damping was one of the first solutions proposed to attenuate the vibrations in civil structures. They alleviate the energy dissipation of the main structure by absorbing part of the input energy, thereby reducing the structural damage. Passive dampers can be used as base isolators, as shown in Figs. 2.1(a) and 2.1(b). Base isolators must be rigid enough to support the loadings caused by strong vibrations (Yang et al. 2002). One disadvantage is that the additional damping that base isolation systems provide to the structure may increase the internal motion of the superstructure (Ramallo et al. 2002). Passive dampers can also be installed on the top of a structure, like the tuned mass dampers (TMD). TMD's are viscous damping devices tuned to one of the natural frequencies of the vibrating systems to add damping when in resonance. The classical concept of TMD's is shown in Fig. 2.1(c).

Passive damping has the advantage of not requiring external source powers or other hardware to operate. However, once tuned, they cannot adapt to varying loadings (Johnson et al. 1998). This makes mandatory a deep knowledge of the characteristics of the structure to be protected and the soil where

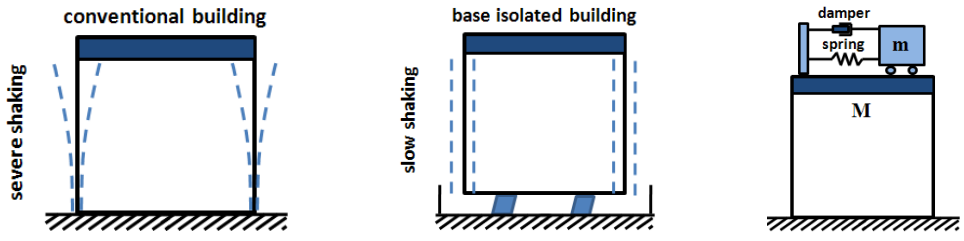

(a) (b) (c)

Figure 2.1: Passive damping. (a) Non isolated structure. (b) Base isolated structure. (c) Tuned mass damper.

it is built on. Furthermore, passive dampers are generally highly nonlinear devices and the vibration reduction is not optimal for a wide range of input ground motion intensities (Yoshioka et al. 2002).

Limitations of passive dampers can be surpassed by active damping systems. In this class of systems, it is possible to determine the forces that stabilize the structure and hence, adapt it to changing loading conditions. Active dampers have already been implemented in a number of civil structures (Housner et al. 1997). A good example is the active mass damper (AMD), which consists of a mass, usually less than 1% of the total mass structure, installed on the top of the structure and is connected to it by an actuator as shown in Fig. 2.2(a). The response of the whole structure is processed by a computer which sends the appropriate signals to the actuator to move the mass and mitigate the vibration. Fig. 2.2(b) is a picture of AMD installed in a Japanese building.

Active control devices, unlike passive dampers, do require external power sources, typically from the electrical network which may fail during an earthquake or hurricane. Moreover, active systems can inject energy to the system and destabilize it in a bounded-input bounded-output sense. Furthermore, additional hardware like sensors and controllers are required (Spencer & Sain 1997).

Despite the successful implementation of passive and active damping systems, there are some concerns that avoid their wide implementation: 1) the reduction of capital cost and maintenance, 2) the elimination of reliance on external power, 3) the increase of system reliability and 4) the acceptance of nontraditional technology (Spencer et al. 1997). These concerns, however, may be addressed by hybrid and semiactive control strategies (Dyke et al. 1998, Jansen & Dyke 2000, Yoshida et al. 2002).

Hybrid control is basically the combination of active and passive devices like, for instance, the hybrid mass damper. It is comprised of a tuned mass damper and an active actuator. The ability of the device to reduce the structural response relies on the natural motion of the TMD. The control actuator is used to improve the performance under changes in the dynamics of the structure. Fig. 2.3(a) shows the schematic of a DUOX systems and Fig. 2.3(b) is a picture of a hybrid mass damper implementation in a Japanese building. Hybrid control systems coupling active and passive dampers into base isolated systems can be designed for enhancing the performance of passive devices (Baratta et al. 2008).

Semiactive control devices, on the other hand, combine the features of active and passive dampers: their properties can be adapted in real time but they cannot inject energy to the system. They are also known as controllable passive dampers (Yi et al. 1999, Yang et al. 2002, Yoshida & Dyke 2003). Semiactive devices have shown to perform significantly better than passive devices and as well as active devices without requiring large power sources, thus allowing for battery operation. Semiactive devices may theoretically be controlled in real-time using a closed loop control scheme. This enables a structure to respond to the earthquake in a theoretical "safe-mode" of vibration via adequate energy dissipating (Spencer & Soong. 1999, Attard et al. 2008). A number of semiactive devices have been studied lately: variable orifice damper, the variable friction damper, the adjustable tuned liquid damper and semi-actively controllable tuned liquid dampers, among others (Symans & Constantinou 1997, Kuruta et al. 1999, Rodellar & Luo 2003, Dyke et al. 2005, Zapateiro & Luo 2007*a*, Ferreira-Oliveira et al. 2008). However, the controllable

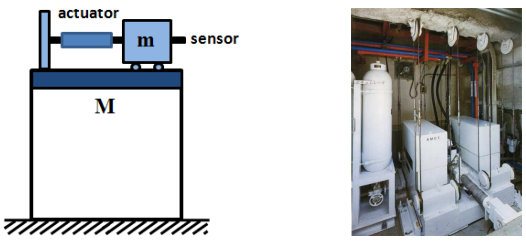

(a) (b)

Figure 2.2: Active mass dampers: (a) AMD system. (b) The AMD at the Kyobashi Seiwa building.

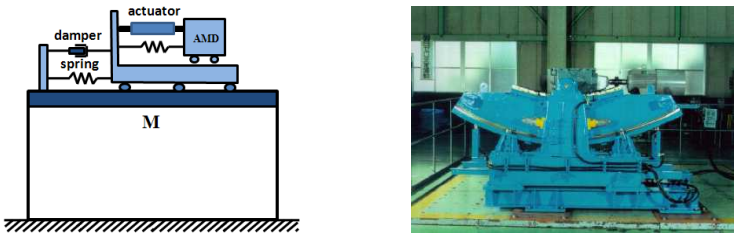

(a) (b)

Figure 2.3: Hybrid mass dampers: (a) HMD schemtaic. (b) HMD at the Rainbow Tower (Japan).

fluid dampers have acquired a particular interest.

Controllable fluid dampers are devices that contain no moving parts other than the piston. They use either an electrorheological (ER) or a magnetorheological (MR) fluid; these fluids have the ability to change their rheological properties in the presence of an electrical (ER case) or magnetic (MR case) field. This change is effective in a few milliseconds and they can generate high forces compared to the other devices, with low power requirements and simple mechanical design which make them an attractive solution for the vibration problem in the large civil structures (Charles 2002, Oh et al. 2004, Christenson & Emmons 2005, Goncalves et al. 2006).

ER and MR fluids have already been applied in several systems to mitigate destructive vibrations. In spite of the early invention of MR fluids (in fact, both of them were first developed in the 1940's), it was approximately two decades ago that researchers devoted their efforts to their study and results were already visible. Practical implementations can be found, for instance, at the Nihon-Kagaku-Miraikan building in Tokyo (the first building to have MR dampers) and at the Dongting Lake Bridge in Yueyang City (China). Nonetheless, MR fluid dampers have some advantages over ER fluid dampers including higher yield strength, lower costs of production, lower energy requirements, faster response and smaller size among others (Yang et al. 2002, Atray & Roschke 2003, Dyke et al. 2005). For this reason, MR dampers have attracted more interest and efforts in research.

2.2 Magnetroheological dampers

2.2.1 Magnetorheological fluids

The invention of magnetorheological fluids is credited to Jacob Rabinow in the 1940's. MR fluids are non colloidal suspensions of micron-sized magnetizable particles in a carrier medium and their main characteristic is their ability to reversibly change their rheological properties in the presence of a magnetic field. In other words, MR fluids can go from a liquid state to a semisolid one when there is a magnetic field present, and this transition can be made effective in a few milliseconds. Thus, it is possible to control the rheological transition by changing the magnitude of the magnetic field. Because of these properties, MR fluids are called smart fluids (Charles 2002, Goncalves et al. 2006).

MR fluids are the magnetic counterpart of electrorheological (ER) fluids. However, there are some drawbacks to the use of ER fluids. MR fluids need lower power requirements for a rheological change than ER fluids. MR fluids are insensitive to contaminants which helps in minimizing the cost of production. ER fluids also exhibit a high dependence on temperature changes. Moreover, MR fluids are 20 to 50 times stronger than ER fluids. The reason that MR fluids exhibit a high dynamic yield strength compared to that of ER fluids is due to the high magnetic energy density that can be established in the fluid. For a typical iron-based MR fluid, the maximum energy density is 0.1 Joule/cm^3 while this density in ER fluids is only 0.001 Joule/cm^3 (Yang 2001).

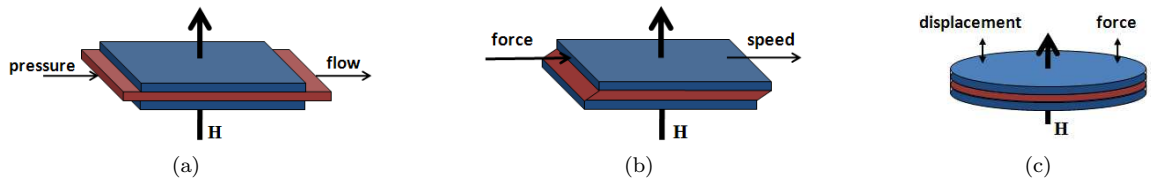

(a) (b) (c)

Figure 2.4: MR damper operation modes: (a) flow or valve mode, (b) shear mode, (c) squeeze mode.

MR fluids have found potential applications in areas such as medicine and engineering. For example, MR fluids have been proposed to treat cancer with a mechanism that blocks the blood vessels to a tumor by injecting an MR fluid and applying a magnetic field (Flores & Liu 2002). MR fluids have been proposed in rehabilitation devices for muscle strengthening and for prosthesis to surpass the disadvantages of active and passive mechanisms used up to date in this kind of devices (Kim & Oh 2001, Dong et al. 2006).

Several applications can be found in engineering. For instance, MR fluid clutches have become an alternative to conventional torque converters and hydraulic starting clutches which suffer from low efficiency, low robustness and uncertainties in the piston stroke (Neelakantan & Washington 2005). MR automotive driveline center bearing have been designed to overcome the noise, vibration and harshness problem present in common bearings (Agrawal et al. 2002). MR fluid suspension seals and MR fluid valves have also been prototyped and tested (Yoo & Wereley 2002, Saito et al. 2006). Perhaps the most important application of MR fluids is found in vibration suppression. Different kinds of MR fluid dampers have been designed, prototyped and tested at different scale and for different systems such as vehicles, industrial machinery, buildings, bridges, etc. (Jolly et al. 1999, Ahn et al. 2005, Milecki & Sedziak 2005, Wang et al. 2006). The next two subsections are devoted to MR fluid dampers.

2.2.2 MR fluid dampers

MR fluid dampers, or simply MR dampers, are a class of controllable fluid dampers where the shear force of the fluid is controlled by an external magnetic field. This kind of damper can be seen as controllable Coulomb dampers where the slope of the Coulomb force trajectories depends on the oil viscosity. MR fluids behave like rigid bodies below yield stress and start to flow above yield stress and then behave like plastic viscous. Because of this, MR dampers exhibit a large yield strength at very small velocities (Weber et al. 2006).

In general, MR dampers work in one of these modes: flow or valve mode, shear mode, squeeze mode or a combination of them (Carlson 1999). Schematics of these operation modes are shown in Fig. 2.4. Shock absorbers, servo-valves, dampers and actuators usually work in the flow mode while clutches, brakes, dampers, chocking and locking devices work in the shear mode. Squeeze mode devices are usually employed in low motion, high force applications such as small-amplitude vibration dampers. Dampers for civil engineering applications are expected to develop large magnitude forces so the flow mode or a combination of flow mode and shear mode is usually employed rather than the other modes individually (Carlson 1999, Jolly et al. 1999, Yang 2001).

Large-scale MR dampers for civil engineering applications have already been built. For instance, a 20-ton MR damper, shown in Fig. 2.5(a), was developed by the Lord Corporation and the University of Notre Dame (United States). It has a stroke of ± 8 cm, a mass of 250 kg, is 1 m long and has 6 liters of MR fluid of which only 90 cm^3 are energized at any given instant (Yang et al. 2002). The Sanwa Teiki Corporation in Tokyo (Japan) designed a 30-ton MR damper for testing at the National Center for Research on Earthquake Engineering in Taipei, Taiwan. The total stroke of the damper piston is 0.24 m and its velocity is limited to 0.50 m/s. The maximum current and voltage that can be applied before saturation is 2.0 A and 1.0 V respectively (Oh et al. 2004). The damper is shown in Fig. 2.5(b).

(a) (b)

Figure 2.5: Large MR dampers: (a) 20-ton MR damper. (b) 30-ton MR damper.

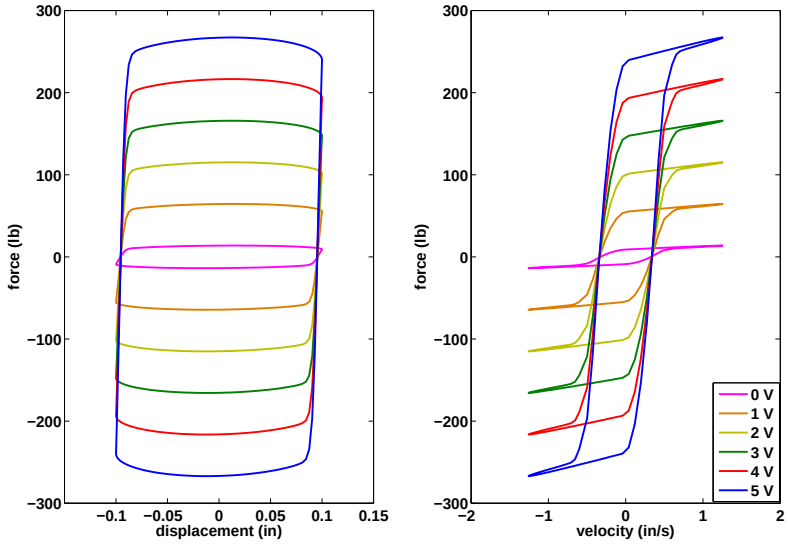

Figure 2.6: Typical force-displacement and force-velocity curves of an MR damper under sinusoidal excitation and different magnetic fields (Yang 2001).

2.2.3 Mathematical models of MR dampers

MR dampers are highly nonlinear devices. Their force-velocity relationship exhibits a hysteretic behavior which is not mathematically easy to model. Fig. 2.6 shows the typical response of an MR damper under sinusoidal excitation at different levels of magnetic field (Yang 2001). Hysteresis can cause serious problems in controlled systems such as instability and loss of robustness. Modeling MR dampers has been an active field during the last years and several solutions have already been proposed. In general, MR damper models can be classified into two groups depending on the way the model is obtained: parametric and non parametric. Parametric models usually make use of physical concepts such as friction and viscosity that help describing the dynamics of the device. On the other hand, non parametric models make use of soft computing techniques such as neural networks and fuzzy logic to build a model based on experimental information.

Parametric models

In this section, some extensively used parametric models are reviewed. As mentioned earlier, these models are built on the base of physical concepts. The Bingham, Bouc-Wen, Hyperbolic tangent, Dahl and other models have been adapted to recreate the MR damper dynamics as described in what follows.

Bingham model. The Bingham model has long been used to characterize ER and MR dampers. It is based on the Bingham plastic model which assumes that a body behaves as a solid until a minimum

yield stress is exceeded and then exhibits a linear relationship between the stress and the rate of shear or deformation (Shames & Cozzarelli 1992). Based on this relationship, a model was proposed for ER dampers. This model, simply known as the Bingham model, consists of a Coulomb friction element placed in parallel with a viscous damper, as shown in Fig. 2.7. The force f_{mr} is given by Eq. 2.1, where c_0 is the damping coefficient, f_c is the frictional force which is related to the fluid yield stress, $\dot{x}$ is the piston velocity and f_0 is the nonzero mean observed in the measured force due to the presence of the accumulator present in some devices. It is well known that the Bingham model does not reproduce the hysteretic behavior of ER and MR dampers. Instead it describes a one-to-one relationship that may not be suitable for control purposes (Butz & von Stryk 2002, Zapateiro, Luo, Taylor & Dyke 2008).

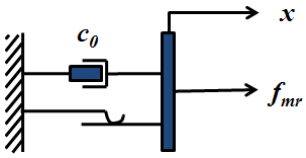

$$f_{mr} = f_c \cdot \operatorname{sgn}(\dot{x}) + c_0 x + f_0 \tag{2.1}$$

Figure 2.7: Bingham mechanical model.

Gamota & Filisko (1991) proposed an extension of the Bingham model to describe the ER behavior in the pre-yield, the post-yield and the yield point. The model consists of the Bingham model in series with a standard model of a linear solid (Zener element), as shown in Fig. 2.8. The force in this system is given by Eq. 2.2, where c_0 is the coefficient associated with the Bingham model and k_1, k_2 and c_1 are associated with the linear solid material.

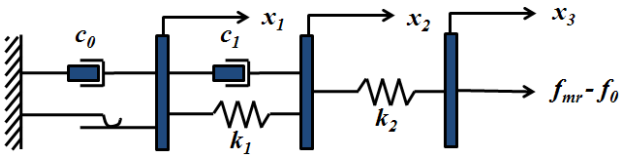

$$f_{mr} = \begin{cases} c_0\dot{x}_1 + f_c \cdot \operatorname{sgn}(\dot{x}_1) + f_0 \\ \quad = k_2(x_3 - x_2) + f_0 & |F| > f_c \\ \\ k_1(x_2 - x_1) + c_1 + f_0\dot{x}_2 + f_0 \\ \quad = k_2(x_3 - x_2) & |F| \leq f_c \end{cases} \tag{2.2}$$

Figure 2.8: Extended Bingham mechanical model.

Bouc-Wen model. The hysteresis model of Bouc as modified by Wen is one of the mathematically simplest yet effective models that can represent a large class of hysteretic behavior (Wen 1976, Sain et al. 1997). A phenomenological model based on the Bouc-Wen model was proposed by Spencer et al. (1997); its schematic is shown in Fig. 2.9. The force of this system is given by Eqs. 2.3-2.4, where $\dot{x}$ is the piston velocity, c_0 is the damping coefficient, k_0 is the stiffness of the device, x_0 accounts for the initial deflection of the spring and z is an unmeasurable evolutionary variable that accounts for the hysteresis behavior. α, β, κ, φ, and n are parameters that can be adjusted to control the shape of the hysteresis loop. The force f_0 is due to an accumulator present in some dampers and is incorporated in the model as the initial deflection x_0 of the spring k_0.

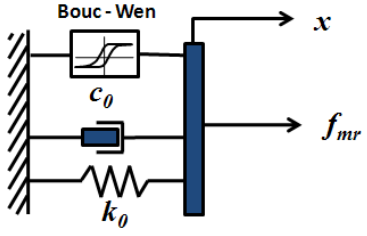

$$f_{mr} = c_0\dot{x} + k_0(x - x_0) + \alpha z \tag{2.3}$$

$$\dot{z} = -\varphi|\dot{x}|z|z|^{n-1} - \beta\dot{x}|z|^n + \kappa\dot{x} \tag{2.4}$$

Figure 2.9: Bouc-Wen mechanical model.

The Bouc-Wen model is able to predict the response of the damper well but it does not roll off in the

region where the acceleration and velocity have opposite signs and the magnitudes of the velocities are small. To overcome this issues, the model was modified by Spencer et al. (1997), as shown in Fig. 2.10. The force of the new system is given by Eqs. 2.5 - 2.7, where c_1 is a dashpot included to account for the effect of the roll off and c_0 is for the viscous damping observed at large velocities; k_1 represents the stiffness of the accumulator present in some MR dampers while k_0 controls the stiffness at large velocities.

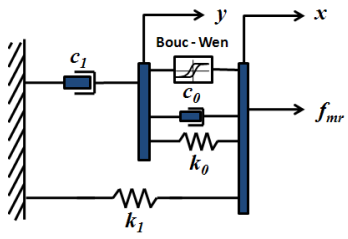

$$f_{mr} = c_1\dot{y} + k_1(x - x_0) \tag{2.5}$$
$$\dot{y} = \frac{1}{c_0+c_1}\{\alpha z + c_0\dot{x} + k_0(x - y)\} \tag{2.6}$$
$$\dot{z} = -\varphi|\dot{x} - \dot{y}|z\ |z|^{n-1} - \beta|z|^n + \kappa(\dot{x} - \dot{y}) \tag{2.7}$$

Figure 2.10: Bouc-Wen mechanical model.

Hyperbolic tangent models. Gavin (2001) and Gavin et al. (2001) proposed a simplified version of the model by Gamota & Filisko (1991) for an ER damper. The model is illustrated in Fig. 2.11. It consists of two Voight elements connected by an inertial element that resists motion through the Coulomb friction element. The equation of the model is given by Eqs. 2.8 - 2.11, where k_1 (spring) and c_1 (dashpot) model the pre-yield viscoelastic behavior while k_0 and c_0 model the post-yield behavior; m_0 is the inertia of the device and the fluid, f_0 is the yield force. $\mathbf{x_0} = [x_0\ \dot{x}_0]^T$, x_0 is the plastic deformation and $\dot{x}_0$ is its rate and they uniquely describe the state of the system. This model takes $\mathbf{x} = [x\ \dot{x}]^T$ as the inputs. There is only one nonlinear term, tanh, and it is separated from the dynamics of the system. The hyperbolic tangent is used as an approximation to the signum function. The whole term $f_0 \tanh(\dot{x}_0/V_{ref})$ approximates the yielding mechanism. V_{ref} is a reference velocity which governs the sharpness of the yield function. The system takes into account the dynamic effects of pre-yield visco-elasticity, bulk compressibility and the device's stiffness and inertia when the velocity changes sign.

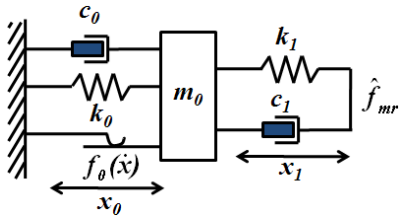

Figure 2.11: Hyperbolic tangent mechanical model by Gavin et al. (2001).

$$\dot{\mathbf{x}}_\mathbf{0} = \Xi_1\mathbf{x_o} + \Xi_2\mathbf{x} + \Xi_3 f_o \tanh(\dot{x}_0/V_r) \tag{2.8}$$
$$\hat{f}_{mr} = \begin{bmatrix} -k_1 \\ -c_1 \end{bmatrix}^T \mathbf{x_o} + \begin{bmatrix} k_1 \\ c_1 \end{bmatrix}^T \mathbf{x} \tag{2.9}$$
$$\Xi_1 = \begin{bmatrix} 0 & 1 \\ -\frac{(k_0+k_1)}{m_0} & -\frac{(c_0+c_1)}{m_0} \end{bmatrix} \tag{2.10}$$
$$\Xi_2 = \begin{bmatrix} 0 & 0 \\ -\frac{k_1}{m_0} & -\frac{c_1}{m_0} \end{bmatrix}, \quad \Xi_3 = \begin{bmatrix} 0 \\ -\frac{1}{m_0} \end{bmatrix} \tag{2.11}$$

Guo et al. (2006) have proposed a similar model which can be considered as a generalization of the Bingham model. In addition, all the parameters have a physical meaning. The proposed model is given by Eq. 2.12, where $\dot{x}$ is the piston velocity, A_1 is the dynamic yield force of the fluid, A_2 and A_3 are parameters related to the post-yield and pre-yield viscous damping coefficients respectively, V_0 and X_0 denote the absolute value of hysteretic critical velocity and hysteretic critical displacement respectively. The mechanical model is shown in Fig. 2.12. Under a sinusoidal excitation ($x = a\sin\theta$, $\dot{x} = a\omega\cos\theta$, $\theta = \omega t + \phi$, $\theta_0 = \arctan(V_0/\omega X_0)$), if $\theta_0 = 0$ and $A_3 = \infty$ Eq. 2.12 reduces to $f_{mr} = A_1 \mathrm{sgn}\dot{x} + A_2 x$, which is the Bingham model. In fact, $\theta_0 = 0$ when the hysteretic behavior is neglected and $A_3 = \infty$ when the pre-yield region of the damper is neglected.

Dahl friction model. Ikhouane & Dyke (2007) and Ikhouane & Rodellar (2007) have studied the overparametrization of the Bouc-Wen model which means that the input-output relationship of the model and the set of Bouc-Wen model parameters is not one-to-one, leading to a non uniqueness of the set of parameters. They have proposed the use of a viscous + Dahl model to describe the device behavior. The

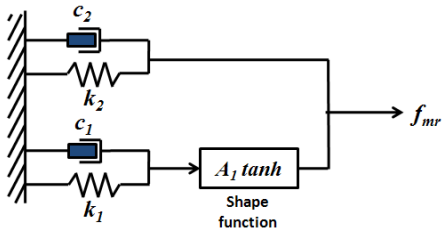

Figure 2.12: Hyperbolic tangent mechanical model by Guo et al. (2006).

$$f_{mr} = A_1 \tanh\left(A_3\left(\dot{x} + \frac{V_0}{X_0}x\right)\right) + A_2\left(\dot{x} + \frac{V_0}{X_0}x\right) \tag{2.12}$$

Dahl model is essentially a Coulomb friction element with a lag in the change of friction force when the direction of motion is changed. The mechanical model proposed for a shear-mode MR damper (viscous + Dahl) is shown in Fig. 2.13. The mathematical model is as in Eqs. 2.13 - 2.14, where k_x and k_w may be voltage-dependent. The model has shown to characterize the MR damper behavior as accurately as the Bouc-Wen model does. The methodology has also been successfully applied to large scale MR dampers as can be seen in Aguirre et al. (2008).

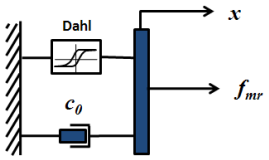

Figure 2.13: Dahl mechanical model.

$$F = k_x(v)\dot{x}(t) + k_w(v)z(t) \tag{2.13}$$

$$\dot{z} = \rho(\dot{x} - |\dot{x}|z) \tag{2.14}$$

Other parametric models. Alvarez & Jiménez (2003) proposed an MR damper model based on the LuGre model that describes friction dynamics (Canudas et al. 1995) and later presented a modification in Jiménez & Álvarez Icaza (2005). The modified model is linear in the parameters, so it is possible to use standard recursive identification algorithms to fit the model parameters to experimental data. Yang & Shen (2006) proposed a three parameter bilinear hysteresis to model MR dampers. Another model is the nonlinear bi-viscous one which utilizes two different linear slopes corresponding to the pre-yield and the post-yield conditions, and a set of piecewise linear functions to describe the hysteresis effect. This model is a good approximation to the actual behavior of the damper but it does not adequately account for variations in the excitation/response conditions. The model parameters need to be updated in time as the excitation conditions vary, which may limit the real-time tracking ability of the control algorithm (Ma et al. 2003).

Non parametric and other models

In this section, techniques such as neural networks, fuzzy logic and polynomial models are presented. These techniques have been widely used to model MR dampers based on experimental data.

Neural network models. Neural networks have extensively been used in many fields of research due to their ability to model nonlinear systems. Neural networks can be trained to learn complicated relationships between sets of inputs and outputs. Their ability to learn complicated nonlinear systems has been exploited to model MR dampers. An important advantage of neural networks is the relative ease to train them to learn the inverse dynamics of a damper, that is, a model that yields the output of a control signal that makes the damper to generate the desired damping force (Zhang & Roschke 1998, Wang & Liao 2001, Du et al. 2006, Zapateiro & Luo 2007*b*).

Fuzzy logic models. Fuzzy logic methodologies such as ANFIS (Adaptive Neuro-Fuzzy Inference System) have been used to model small- and large-scale MR dampers. The structure of an ANFIS model

is similar to that of a neural network that is functionally equivalent to a fuzzy inference system. A network type structure can be used to map inputs through membership functions and associated parameters, and then through output membership functions and associated parameters to outputs (Schurter & Roschke 2000, Peschel & Roschke 2001, Atray & Roschke 2003, Oh et al. 2004).

Other models. $n-$order polynomial equations have been used to model MR dampers. It has been done, for instance, by dividing the force-velocity loop into two regions (positive and negative acceleration) and then, taking into account the varying magnetic field (Choi et al. 2001). In other work, Song et al. (2005) developed an MR damper model using polynomials. They took into account four aspects of the damper behavior and developed a model based on them: a polynomial function describes the maximum damping force as a function of the control current; a shape function, hyperbolic tangent based, describes the bilinear behavior of the force-velocity curve; a first order filter creates the hysteresis loop; and an offset function is included to take into account the effect of the accumulator of some dampers.

2.3 Semiactive control techniques for MR dampers

The development of control algorithms for MR dampers is a challenging task of the structural control design. The nonlinear behavior of the actuators, the limited availability of measurements and the amount of uncertainties which are characteristic of these environments must be taken into account when designing the controller. Control techniques can be divided in two classes: model based control and intelligent technology based control. Some of the most common control techniques used with MR dampers are summarized below.

2.3.1 Model based control

Clipped optimal control. Clipped optimal control was one of the first techniques used for controlling structures with MR dampers. Dyke et al. (1996) proposed a clipped optimal controller based on acceleration feedback, eliminating the need for a full state (velocity and displacement) feedback or velocity feedback, which are measurements difficult to obtain directly. The technique consists of designing a linear optimal controller that calculates the desired control force based on the available measurements. However, the only way to command the force of the MR damper is by varying the magnetic field controlled by voltage or current. The following algorithm is applied to estimate the control signal: the voltage remains the same when the damper is producing the desired force calculated by the controller. If the magnitude of the force produced by the damper is smaller than the magnitude of the desired optimal force and the two forces have the same sign, the voltage applied to the current driver is increased to the maximum level; otherwise, the voltage is set to zero. The MR damper dynamics are ignored in this approach.

The algorithm was successfully applied and extended to multiple MR dampers (Yi et al. 2001) and was also implemented to reduce the coupled lateral and torsional response of asymmetric buildings when subjected to horizontal seismic excitations (Yoshida et al. 2002). Other works where the clipped optimal-like algorithm technique is used are those by (Ramallo et al. 2002, Christenson & Emmons 2005, Johnson et al. 2007).

Control based on Lyapunov's stability theory. According to Lyapunov stability theory, if there exists a function $V(\mathbf{z})$ that is positive definite and the rate of change of such function, $\dot{V}(\mathbf{z})$, is negative semi-definite, the origin is stable in the sense of Lyapunov. The objective of the control design is then to choose the control inputs so as to make $\dot{V}(\mathbf{z})$ as negative as possible. There is not a unique function satisfying these characteristics so this results in a variety of control laws. The works by Jansen & Dyke (2000), Yang (2001), Wang & Gordaninejad (2002), Luo et al. (2003) are about the application of Lyapunov's stability theory to design controllers to reduce vibrations in buildings and bridges with MR dampers. Lyapunov control has also been applied to mitigate vibration in vehicle suspension systems (Park & Jeon 2002).

Bang-bang control. This control technique is useful when the performance index is the pure-minimum time objective of the form $J(t_0) = \int_{t_0}^{t_f} dt = t_f - t_0$. The solution is to apply infinite control energy in an infinitesimal time period. A Lyapunov function is chosen and a possible strategy is to reduce the rate at which the energy is transmitted to the structure. One of the first applications was made by McClamroch et al. (1994) and McClamroch & Gavin (1995). The objective was to minimize the rate at which the mechanical energy in a structure equipped with ER dampers is transmitted to the structure. A Lyapunov function V was chosen to represent the total vibratory energy in the system. The control voltage of the damper is then selected to minimize $\dot{V}$. The resulting control law is of bang-bang type; decentralized, since the electrical field applied to the i-th ER damper depends only on the feedback of the velocity across the i-th ER damper. Jansen & Dyke (2000) also tested this technique in a structure with MR dampers. However, they chose a Lyapunov function relative to the vibratory energy in the system (i.e., excluding the velocity of the ground in the kinetic energy term). The controller was implemented by measuring only the velocity and the damper force.

Sliding mode control. SMC (Utkin 1992) is a robust nonlinear control technique which restricts the state of a system to a sliding surface by switching the control structure on both sides of a stable hyperplane in the state space. The controller design consists of two steps. First, a sliding surface defined by $\sigma = \mathbf{Sx} = 0$ that represents the closed loop control performance is designed. The second step is to design a nonlinear switched feedback control law; i.e., calculate the control gain that makes the state trajectory reach the sliding surface and stay there until it gets to the origin. SMC applications in structural control can be found in (Luo et al. 1999, 2000, 2003, Villamizar et al. 2003, Moon et al. 2003).

Backstepping control. This technique consists of selecting appropriate functions of state variables as pseudo control inputs for lower dimension subsystems of the overall system. Each backstepping stage is a new pseudo control design in terms of the preceding stages. In the final stage, a feedback design for obtaining the true control input results and it achieves the original design objective by virtue of a final Lyapunov function, which is formed by summing up the Lyapunov functions associated with each individual design stage.

Semiactive control nonlinear devices such as hysteretic base isolators and MR dampers by means of backstepping has been approached by Ikhouane et al. (1997), Villamizar et al. (2003), Villamizar (2005), Luo et al. (2006, 2007) and further developed by Zapateiro, Villamizar & Luo (2008) and Zapateiro, Karimi & Luo (2008). The backstepping strategy was applied to generate the control force of an MR damper integrated in a hybrid control system (base isolator + MR damper) in a 10-story building. It was later tested in a 6-story scaled structure available at the Structural Control and Earthquake Engineering Laboratory (Washington University in St. Louis, U.S.A.). Robustness was improved by applying adaptation laws to the structure uncertain parameters.

Quantitative Feedback Theory. QFT is a frequency control technique, initially thought for LTI systems but extendible to nonlinear systems. As one of the frequency structural control strategies, this control technique was firstly introduced by Luo et al. (2004) for the vibration reduction in linear structures and was extended to structures equipped with MR dampers by Villamizar et al. (2004). Numerical simulations and experiments on small scale specimens showed the feasibility of applying QFT control in larger systems. In these works, however, an algorithm similar to the clipped optimal control was followed, i.e. the nonlinear dynamics of the MR damper were ignored. A step further was done by Zapateiro, Luo & Karimi (2008) by proposing the inclusion of the hysteretic dynamics of MR dampers in the QFT control design and its feasibility was proved by numerical simulations.

H_2 and H_∞ control. The suboptimal H_∞ control problem of parameter γ consists of finding a controller that internally stabilizes the closed loop system and the H_∞ norm of the transfer function from the exogenous inputs to the controlled outputs is less than γ. This constraint can be interpreted as a disturbance rejection performance and may be useful to enforce robust stability. On the other hand H_2 control consists of finding a controller that minimizes the H_2 norm of the transfer function from from the inputs to the outputs and it is useful, for example, to avoid actuator saturations. Both techniques, including mixed H_2/H_∞ control have been applied to active and semiactive structural control (Yang

et al. 2003, 2004, Narasimhan & Nagarajaiah 2006, Karimi et al. 2008*b*).

2.3.2 Soft computing based control

Extensive literature about the use of soft computing techniques for structural control can be found. Neural networks, fuzzy logic and genetic algorithms are an example of the methodologies most widely applied to semiactive modeling and control of MR dampers. For instance, Kim et al. (2006) ran full-scale experiments on a single degree of freedom mass equipped with a hybrid base isolation system comprised of a friction pendulum system and a magnetorheological damper. The fuzzy logic controller takes the displacement and acceleration readings of the structure to calculate the appropriate signals to drive the MR damper. Both the friction pendulum system and the MR damper were modeled by ANFIS approaches. This work was later improved by Kim and Roschke Kim & Roschke (2006); they optimized the fuzzy models by using genetic algorithms.

Feasibility of fuzzy logic controllers to reduce the structure response has been studied by Casciati et al. (1999), Choi et al. (2004), Dias (2005), Xu & Guo (2006), Gu & Oyadiji (2007). Applications of neuro fuzzy controllers can be found in Faravelli & Venini (1994), Li et al. (2002), Schurter & Roschke (2001). Neural networks and fuzzy logic have successfully been applied to semiactive control of vehicle suspension as can be seen in Guo et al. (2004), Yu, Dong, Liao & Chen (2006), Yu, Liao, Chen & Huang (2006), Zapateiro, Luo, Karimi & Vehí (2008).

In general, a conclusion that can be found in these works is that the speed of execution of these algorithms is higher than that of model-based controllers. This is an important issue to keep in mind since MR dampers exhibit a time delay response that combined with the time of execution of the control signal can be problematic. Another advantage of soft-computing techniques is that the inverse model of the damper is easier to obtain. Furthermore, these kind of controllers are robust, which is especially desirable in structural control applications characterized by uncertainties. Finally, the implementation of these controllers, particularly neural network controllers, is totally feasible thanks to the existence of high speed, low cost processors such as the digital signal processors.

Chapter 3

Modeling and identification of MR damper dynamics

This chapter presents the results of a series of experiments conducted to model a magnetorheological damper operated in shear mode. The objective is to analyze the performance of different damper models. The control methodologies that will be used in the subsequent chapters require an accurate model of the damper dynamics to be included in the formulation. Moreover, it is desirable that these models are numerically simple for practical implementation and fast execution.

The prototype MR damper consists of two parallel steel plates; a paddle covered with MR fluid coated foam is placed between the plates. The force is generated when the paddle is in motion and the MR fluid is reached by the magnetic field of the coil in one end of the device. Two approaches were considered in this experiment: a parametric approach based on the Bingham, Bouc-Wen and Hyperbolic Tangent models and a non parametric approach based on a Neural Network model. These models have been chosen because, based on other researchers previous experiences, they can be suitable for the class of dampers that are studied in this dissertation. Moreover, these are mathematical simple models that can allow for practical implementation.

This chapter is organized as follows. First, the experimental setup is described. A detailed description of the MR damper to be tested and the experimental environment is given. Then, the proposed models are adjusted. The parameters of the Bingham, Bouc-Wen and Hyperbolic Tangent models are identified using a constrained nonlinear optimization algorithm available in MATLAB. The objective function is the sum of the squared errors between the predicted and the experimental force. Neural networks, on the other hand, are trained with the neural network toolbox that is also available in MATLAB. The simulations are performed in Simulink. Finally, the accuracy to reproduce the MR damper behavior is compared as well as some aspects related to performance are discussed.

3.1 Experimental setup

The experiments to model the MR damper were conducted at the Structural Control and Earthquake Engineering Laboratory (Washington University in St. Louis, Missouri, U.S.A.). The MR damper used works in shear mode and is a prototype from the Lord Corporation (Cary, North Carolina, U.S.A.). A schematic of the MR damper is shown in Figure 3.1(a). It consists of two steel parallel plates separated by 0.635 cm. A paddle covered with a foam saturated with MR fluid is placed between the steel plates. The thickness of the paddle is 0.315 cm. A coil placed in the bottom of the device generates the magnetic field. The dimensions of the device are $4.45 \times 1.9 \times 2.5$ cm. The configuration of the damper allows it to produce forces up to 20 N. The magnetic field is generated by the current supplied by a pulse width modulator (PWM) circuit whose maximum output is 2 A. This device is voltage-controlled and its input-output relationship is linear.

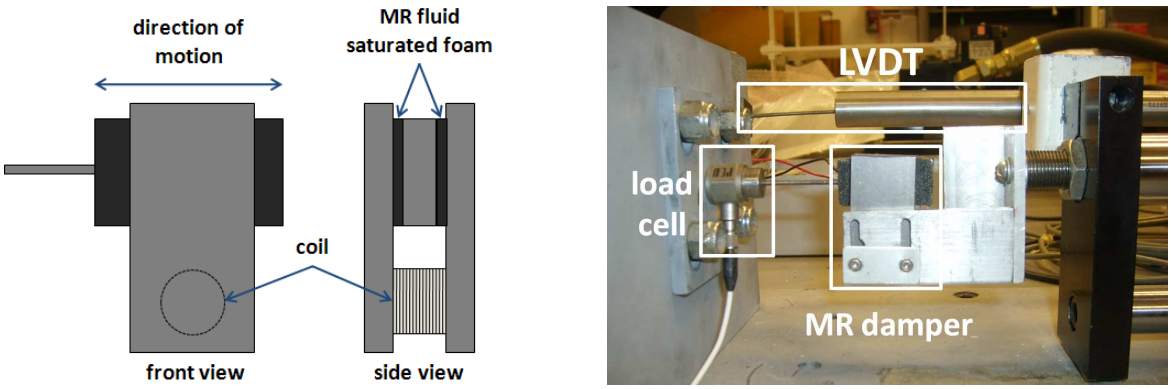

(a) (b)

Figure 3.1: (a) Schematic of the MR damper prototype. (b) Experimental setup.

As shown in Figure 3.1(b), the MR damper is placed on the piston of a hydraulic actuator. This actuator, 2000 lbf rated, is used to apply forces to the MR damper. A force transducer (load cell) is placed in series with the damper and a linear variable differential transformer (LVDT) is used to measure the displacement. The velocity is then calculated using a central differences algorithm.

The experiments are carried out as follows: the MR damper is excited with sinusoidal displacements at frequencies between 0.5 and 5 Hz; currents between 0 and 1.6 A (control voltage between $0.6 - 4$ V); and amplitude displacements between 0.20 and 0.80 cm. Data are sampled at a rate of 256 samples/sec, with null means and the noise is removed with a low pass filter at 80 Hz. The voltage is used as the control signal to vary the magnitude of the magnetic field.

3.2 Numerical results and analysis

The nonlinear dynamics of the MR damper are observed in Figure 3.2. The loops correspond to the experimental response of the damper when it is subject to a sinusoidal displacement at 4 Hz, an amplitude of 0.80 cm and different levels of voltage. The force fluctuations observed in the force-displacement loops as displacement goes from the maximum to the minimum values and viceversa is due to friction in the hydraulic actuator. The force-velocity curve shows that at 0.6 V ($\sim$0 A), the device operation is approximately linear, typical of purely viscous devices. As long as the voltage increases, the force also increases in an almost linear fashion up to a point where the fluid is magnetically saturated and it is not possible for the device to generate higher forces. This case happens at 3 V and above; as can be seen, the force produced at 3 V is almost the same as that at 4 V.

3.2.1 Bingham model

Bingham model parameters (Eq. 2.1) were estimated to compare its ability to predict the force response with other models. Fig. 3.3 shows the results corresponding to the case of 4 Hz sinusoidal displacement at 3 V, in which the parameters obtained were $f_c = 10$ N and $c_0 = 0.2$ N·s/cm. In general, the main concern of using the Bingham model for control analysis is that it reproduces a one-to-one relationship between the force and velocity. However, from the experiments, it is immediately observed that the Bingham model does not reproduce the hysteretic force-velocity loop although it makes a good estimation of the forces at high velocities.

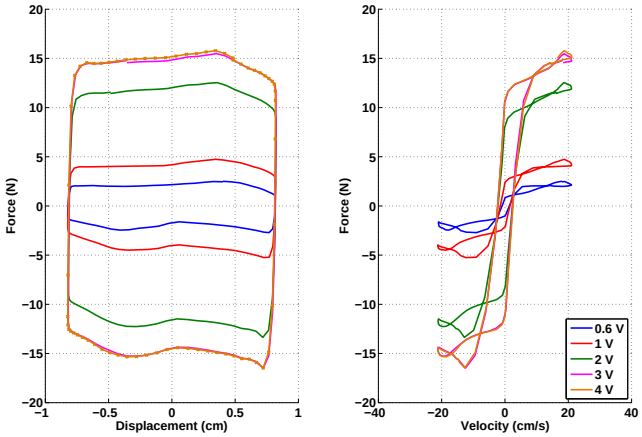

Figure 3.2: Typical displacement-force (left) and force-velocity (right) curves of an MR damper.

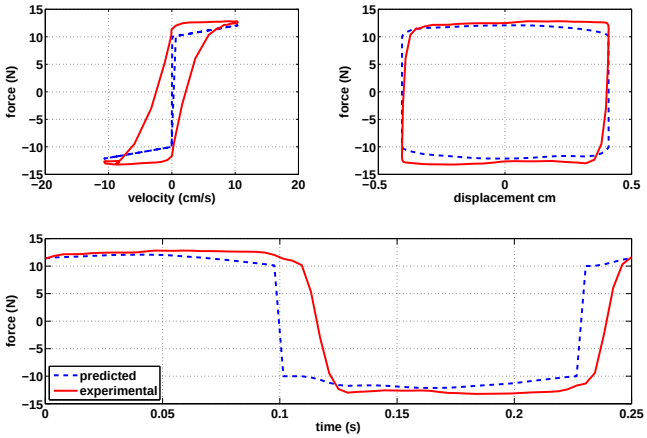

Figure 3.3: Predicted and experimental response using the Bingham model.

3.2.2 Bouc Wen model

The Bouc-Wen model (Eqs. 2.3 and 2.4) is able to reproduce the hysteretic force-velocity response. In order to find a relationship between the predicted force and the magnetic field, several sets of Bouc-Wen parameters were obtained to fit experimental data at different levels of constant voltage. It was found that the damping coefficient (c_0) and α vary linearly with the voltage. These parameters are rewritten as:

$$\alpha(v) = \alpha_a + \alpha_b v, \quad c_0(v) = c_{0a} + c_{ob} v \tag{3.1}$$

where v is the control voltage input to the PWM system. The following parameters, that fit the experimental results, were obtained: $c_{0a} = 0.0055$ N·sec/cm, $c_{0b} = 0.0055$ N·sec/cm·V, $\alpha_a = 1.8079$ N/cm, $\alpha_b = 8.0802$ N/cm·V, $\beta = 46$ cm^{-2}, $\varphi = 84.0253$ cm^{-2}, $\kappa = 80.7337$ and $n = 1$. Furthermore, $k_0 = 0$ because this parameter accounts for the pressure inside the cylinder of dampers working in flow mode. Fig. 3.4 shows a comparison of the predicted and experimental force responses when the damper is subject to a 4 Hz sinusoidal displacement at 3 V, where good agreement is observed.

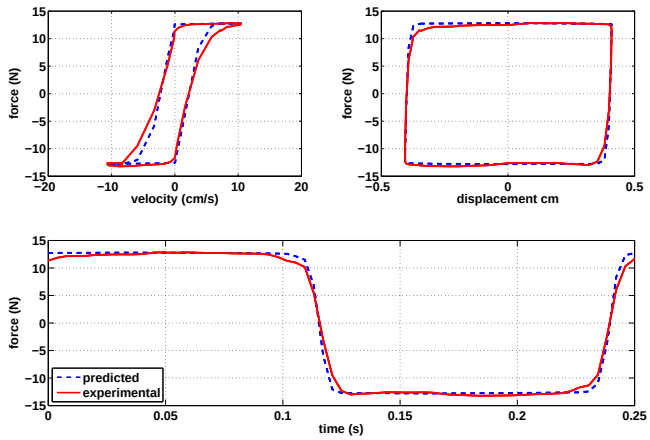

Figure 3.4: Predicted and experimental response using the Bouc-Wen model.

Experimental observations show that the force-velocity loop (Fig. 3.4) appears to be smooth near the zero-velocity region, where the velocity and the acceleration have different signs. However, the predicted response exhibits a discontinuity in slope at this point. This minor difference is not significant.

3.2.3 Hyperbolic tangent model

Using the set of experimental sinusoidal excitations to fit the hyperbolic tangent model (Eqs. 2.8 - 2.11), it was determined that m_0, V_{ref}, and c_0 are independent of the voltage. The following four parameters tend to vary linearly with the voltage:

$$\begin{aligned} k_0(v) &= k_{0a}v + k_{0b} \\ k_1(v) &= k_{1a}v + k_{1b} \\ c_1(v) &= c_{1a}v + c_{1b} \\ f_0(v) &= f_{0a}v + f_{0b} \end{aligned} \tag{3.2}$$

Parameters that fit the experimental results are: $k_{0a} = 0.0193$ N/cm·V, $k_{0b} = 0.5383$ N/cm, $k_{1a} = 148.4435$ N/cm·V, $k_{1b} = -47.4474$ N/cm, $c_0 = 0.7494$ N·s/cm, $c_{1a} = 0.0385$ N·s/cm·V, $c_{1b} = 0.0044$ N·s/cm, $f_{0a} = 4.9328$ N/V, $f_{0b} = -1.3704$ N, $m_0 = 0.00008$ N·s^2/cm and $V_{ref} = 0.330$ cm/s. Fig. 3.5 compares the predicted and experimental force responses when the damper is excited at 4 Hz sinusoidal displacement at 3 V. The sharp change in the slope of the force around 0.12 cm/sec is characteristic of the model, but the perturbation near zero-velocity region in the the force-velocity curve is due to friction in the hydraulic actuator. The hyperbolic tangent model is accurately able to model the hysteretic behavior of the damper.

3.2.4 Neural Networks results

In order to evaluate the feasibility of modeling the MR damper with a neural network, it was trained with data representing different frequencies and voltages. The network takes four inputs: displacement, velocity, voltage and force. The fourth input (force) is fed back from the output. Additionally, the network is dynamic, and the inputs are stored in memory (tapped delay lines, TDL) for a period of time and are updated after each output computation. The structure of the network during the training session is shown in Fig. 3.6(a). This structure allows for fast and more reliable training. Basically, given four inputs, the network must reproduce only the fourth one (damper force). The final model is shown in Fig. 3.6(b). Thus, training the network is a two-step procedure in which the first one is to train the network

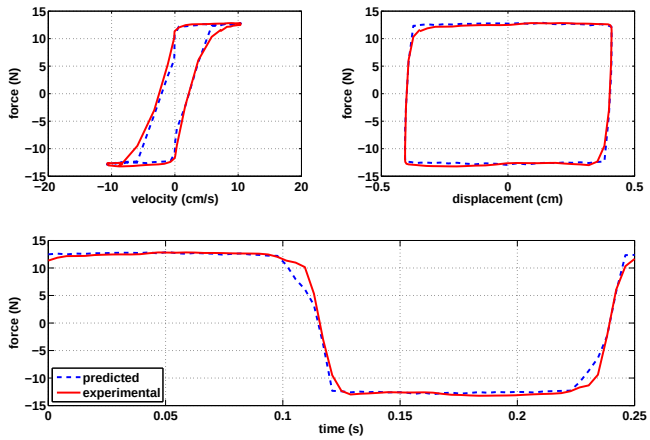

Figure 3.5: Predicted and experimental response using the hyperbolic tangent model.

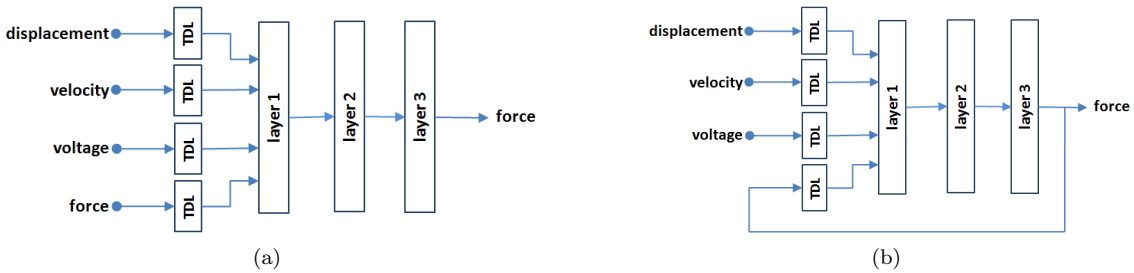

Figure 3.6: (a) Schematic of the NN for training. (b) Schematic of the NN model.

of Fig. 3.6(a) and the second one is to test the network of Fig. 3.6(b) with the same data until a desired performance is achieved. After a trial and error process, it was found that a network with 3 layers (10 neurons in the first layer, 4 neurons in the second one and 1 neuron in the last one) and 4 units-of-time length TDL is good enough to model the MR damper. Sigmoid tangent transfer functions are used in the first two layers while a purely linear transfer function is used in output neuron. Following the training procedure, the estimation of the neural model for a 4 Hz sinusoidal displacement at 3 V is shown in Fig. 3.7 where good performance can be observed.

3.2.5 Analysis of the results

A quantitative comparison is done based upon the errors between the predicted force and the measured force as a function of time, displacement and velocity, as defined in Eq. 3.3:

$$E_t = \frac{\varepsilon_t}{\sigma_F}, \quad E_x = \frac{\varepsilon_x}{\sigma_F}, \quad E_{\dot{x}} = \frac{\varepsilon_{\dot{x}}}{\sigma_F} \tag{3.3}$$

where:

$$\varepsilon_t^2 = \frac{1}{T}\int_0^T (F_{exp} - F_{pre})^2 \, dt \tag{3.4}$$

$$\varepsilon_x^2 = \frac{1}{T}\int_0^T (F_{exp} - F_{pre})^2 \left|\frac{dx}{dt}\right| dt \tag{3.5}$$

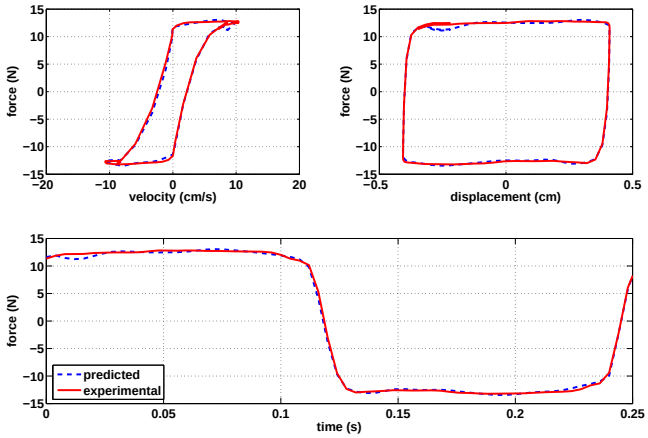

Figure 3.7: Predicted and experimental force using a neural network.

$$\varepsilon_{\dot{x}}^2 = \frac{1}{T}\int_0^T (F_{exp} - F_{pre})^2 \left|\frac{d\dot{x}}{dt}\right| dt \tag{3.6}$$

$$\sigma_F^2 = \frac{1}{T}\int_0^T (F_{exp} - \mu_F)^2 \, dt \tag{3.7}$$

where F_{exp} is the experimental force, F_{pre} is the predicted force and μ_F is the experimental force mean. Table 3.1 shows the error norms between the experimental and predicted responses of each model when compared on a sinusoidal displacement at 4 Hz and 3 V basis. The error calculation is performed using values from one cycle.

Table 3.1: Error norms of the models studied.

Model	E_t	E_x	$E_{\dot{x}}$
Bingham	0.4734	0.3052	5.6954
Bouc-Wen	0.0586	0.1205	1.1656
Hyperbolic Tangent	0.0620	0.1166	1.1785
Neural Network	0.0188	0.0508	0.2232

As expected, the Bingham model shows the greatest error norms in all cases due to its inability to describe the hysteresis loop, while the Bouc-Wen and the hyperbolic tangent models show a similar performance. In terms of computational resources, the Bingham model is by far the most efficient. The simulations performed in Simulink, showed that an integration step size of 10^{-2} is enough to solve the equation. The Bouc-Wen model, on the other hand, requires a step size of at least 10^{-3} to be correctly solved and the hyperbolic tangent model needs a step size of 10^{-6}. In spite of the low computational effort required to solve the Bingham model, it may not be appropriate for accurate simulation of the device or control implementation studies because of its inability to reproduce the hysteresis loop.

Optimization convergence for the Hyperbolic Tangent model is sensitive to the parameters chosen, but with careful selection of them, this model is able to model the hysteretic behavior of the MR damper using fixed time steps. Similar observations about the other two models can be done but convergence is

much faster.

For the range of frequencies studied, i.e., the low pass band up to 5 Hz, the Bouc-Wen model showed a relative independence with respect to the input frequency. No major variations in the behavior of the model were detected in the force-velocity loop when sinusoidal displacements of different frequencies were tested. However, the Hyperbolic Tangent model shows slight frequency dependence. Furthermore, the differences between the force-displacement loops at various frequencies is dependent on the parameters identified from the experimental data.

In both the Bouc-Wen and the Hyperbolic Tangent models, a linear dependence between the voltage and some of the parameters was assumed. However, this assumption is no longer valid near the saturation region, which in this case begins at 3 V, and a force overestimation is perceived beyond this point.

3.3 Summary

In this chapter, four MR damper models have been studied. Three of them are based on the mechanical dynamics of the device, namely, Bingham, Bouc-Wen and Hyperbolic Tangent models while another one was a neural network model. These models were adapted to account for the fluctuating magnetic fields by manipulating some parameters that vary with it.

Good agreement between the experimental and model predicted responses was found in the Bouc-Wen, Hyperbolic Tangent and Neural Network models. The most important characteristics of these models is that they can reproduce the hysteretic force-velocity response, which is something the Bingham model cannot do. Neural network models can learn complicated nonlinear relationships among variables with good prediction results. As expected, the neural network trained could reproduce the force response of the damper to a high degree of accuracy.

Chapter 4

Simulation models and experimental setup

This chapter is devoted to the detailed description of the numerical models and experimental platforms that will be used throughout the remaining of this dissertation. The models correspond to a based isolated building with MR damper; a 3-story building with an MR damper at the first floor; a 6-story building with two MR dampers in the first and second floors; and a semiactive suspension system that makes use of an MR damper as well.

4.1 Base-isolated building with MR damper

Base isolation systems are widely used as a means to mitigate the effects of an earthquake. This is done by isolating the structure and its contents from potentially dangerous ground motion, especially in the frequency range where the building is most affected. The goal is to simultaneously reduce interstory drifts and floor accelerations to limit or avoid damage, not only to the structure but also to its contents, in a cost-effective manner (Ramallo et al. 2002). Experience has shown that base isolation systems can be successful in reducing the inter-story drifts and the absolute accelerations of the structure. However, two main drawbacks are recognized: (i) isolators need to be well tuned to the expected frequency characteristics of the seismic excitations, and (ii) significant absolute base displacements may occur (Luo et al. 2001). To overcome this issue, the use of passive plus active or semiactive dampers have been proposed (Narasimhan et al. 2006).

In this section, a semiactively controlled base isolated structure is studied. It consists of a 10 story building whose base is isolated by means of a passive damper and an MR damper. The objective is to design a controller for the MR damper so that the structure response is reduced when subject to a seismic motion. An important issue in considering the model used for the control formulation is the coordinate system adopted to represent the motion. Systems can be represented in absolute coordinates (with respect to an inertial frame), in which the seismic motion excitation only enters at the base. This gives the chance to consider a single control force at the base level, with the purpose of reducing its absolute motion. Systems can also been represented in relative coordinates (with respect to the ground). In this case, the seismic excitation enters each one of the floors. This means that the ideal distribution of the control actions over the structure is when an actuator applies a control force at each floor of the order of the mass of the floor times the ground peak acceleration. Since this distribution does not sound realistic, many control approaches use a reduced number of actuators, particularly, a single one at the base level. Clearly, the control action transmitted in this case to each floor is not the ideal in the sense discussed above, but a reasonable performance can be achieved in practice (Luo et al. 2001, Pozo et al. 2006).

Consider an uncertain 10-story building whose base is isolated by means of a frictional damper and an MR damper, as shown in Fig. 4.1. Assume that the system is perturbed by an incoming earthquake. The system dynamics can be represented by two coupled subsystems: the main structure (S_r) and the

base (S_c), through the following mathematical models:

$$S_r : \mathbf{M}\ddot{\mathbf{x}}_\mathbf{a} + \mathbf{C}\dot{\mathbf{x}}_\mathbf{a} + \mathbf{K}\mathbf{x}_\mathbf{a} = [c_1, ..., 0]^T \dot{y}_a + [k_1, ..., 0]^T y_a \tag{4.1}$$

$$S_c : m_0\ddot{y}_a + c_0\dot{y}_a + k_0 y_a + f_{bf} = \Phi + f_g + f_{mr} \tag{4.2}$$

$$\Phi = -sgn\left(\dot{y}_a - \dot{x}_g\right)\left[\mu_{max} - \Delta\mu e^{-\nu|\dot{y}_a - \dot{x}_g|}\right] Q \tag{4.3}$$

$$f_g = -c_0\dot{x}_g - k_0 x_g \tag{4.4}$$

$$f_{bf} = c_{bf}(\dot{x}_g - \dot{x}_{a1}) + k_{bf}(y_a - x_{a1}) \tag{4.5}$$

In Eq. (4.1), the a subindex means that the system is represented in absolute coordinates. $\mathbf{M}$, $\mathbf{C}$ and $\mathbf{K} \in \mathbb{R}$ are positive definite matrices representing the mass, damping coefficients and stiffness of the structure, respectively (Eqs. 4.6 - 4.8). The structure remains in the linear region due to the effect of the passive frictional isolator.

$$\mathbf{M} = diag\left(m_i\right),\ i = 1, 2, ..., n \tag{4.6}$$

$$\mathbf{C} = \begin{bmatrix} c_1 + c_2 & -c_2 & 0 & 0 \\ -c_2 & c_2 + c_3 & -c_3 & 0 \\ \vdots & \vdots & \vdots & \vdots \\ 0 & 0 & -c_n & c_n \end{bmatrix} \tag{4.7}$$

$$\mathbf{K} = \begin{bmatrix} k_1 + k_2 & -k_2 & 0 & 0 \\ -k_2 & k_2 + k_3 & -k_3 & 0 \\ \vdots & \vdots & \vdots & \vdots \\ 0 & 0 & -k_n & k_n \end{bmatrix} \tag{4.8}$$

$\mathbf{x_a} = [x_{a1}, x_{a2}, ..., x_{an}]^T \in \mathbb{R}^n$ is the structure horizontal absolute displacement vector, $y_a \in \mathbb{R}$ is the horizontal base absolute displacement and x_g is the displacement of the seismic excitation. Equation (4.2) consists of a linear part, described by the mass m_0, the damping coefficient c_0 and the stiffness k_0 of the base, plus a nonlinear one, characterized by the dynamics of the frictional base isolator (Φ) and the MR damper (f_{mr}). Equation (4.3) describes the dynamics of the frictional base isolator. μ is the friction coefficient, ν is a constant, Q is the force normal to the surface, μ_{max} is the the coefficient for high sliding velocity and $\Delta\mu$ is the difference between μ_{max} and the friction coefficient for low sliding velocity. The term f_{mr} in Eq. (4.2) accounts for the dynamics of the the MR damper which operates in shear mode.

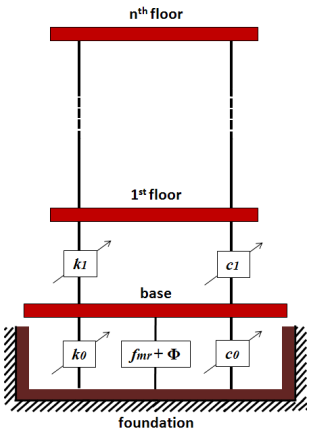

Figure 4.1: Base-isolated 10-story building.

Such dynamics are described by the Bouc-Wen model, as presented in the previous chapters, which takes the following form:

$$f_{mr} = -c_{mr}(v)(\dot{y}_a - \dot{x}_g) - \alpha_{mr}(v)z \tag{4.9}$$

$$\dot{z} = -\varphi|\dot{y}_a - \dot{x}_g|z|z|^{n-1} - \beta(\dot{y}_a - \dot{x}_g)|z|^n + \kappa(\dot{y}_a - \dot{x}_g) \tag{4.10}$$

$$\alpha_{mr}(v) = \alpha_{mra} + \alpha_{mrb}v; \quad c_{mr}(v) = c_{mra} + c_{mrb}v \tag{4.11}$$

where z is an unmeasurable evolutionary variable, the parameters φ, β, κ and n are constant values that can be used to adjust the shape of the hysteresis loop. $\alpha_{mr}(v)$ is related to the hysteretic behavior of the damper and $c_{mr}(v)$ is a damping coefficient; they are both voltage dependent. The voltage is the control signal to be generated: it is the input to a pulse width modulator (PWM) system that generates the current, which in turn creates the magnetic field used to control the MR damper.

Equation 4.4 accounts for the incoming seismic excitation. Equation (4.5) represents the linear force caused by the coupling of the base and the main structure. This force is represented by the damping coefficient $c_{bf} = c_1$, the stiffness $k_{bf} = k_1$ and the relative motion between the base and the first floor of the structure.

The mass of each floor, including that of the base is $m_i = 6 \times 10^5$ kg. The nominal value of the stiffness of the base is $k_0 = 1.184 \times 10^7$ N/m. The stiffness of the structure varies linearly per story from 9×10^8 N/m to 4.5×10^8 N/m. The damping ratio of the base is $\zeta_0 = 0.1$ and that of the structure is $\zeta_i = 0.05$. The parameters of the frictional actuator placed in the base along with the MR damper are: $Q = \sum_{i=1}^{10} m_i$, $\mu = 0.1$, $\nu = 2.0$, $\mu_{max} = 0.185$ and $\Delta\mu = 0.09$. The parameters of the MR damper are: $\varphi = \beta = 3 \times 10^2$ cm^{-1}, $\kappa = 120$, $n = 1$, $\alpha_{mra} = 4.5 \times 10^4$ N/m, $\alpha_{mrb} = 3.6 \times 10^4$ N/m-V, $c_{mra} = 3 \times 10^2$ kNs/m, $c_{mrb} = 1.8 \times 10^2$ kNs/m.

The following propositions about the intrinsic stability of the structure will be used in formulating the control law.

Proposition 1. The unforced main structure subsystem (4.1) (i.e., with the coupling term $[c_1, 0, ..., 0]^T\dot{y}_a$ + $[k_1, 0, ..., 0]^T y_a \equiv 0, t \geq 0$) is globally exponentially stable for any bounded initial conditions.

Proposition 2. If the coordinates $(y_a, \dot{y}_a)$ of the base and the coupling term $[c_1, 0, ..., 0]^T\dot{y}_a$ + $[k_1, 0, ..., 0]^T y_a$ are uniformly bounded, then the main structure subsystem is stable and the coordinates $(\mathbf{x_a}, \dot{\mathbf{x}}_\mathbf{a})$ of the main structure are uniformly bounded for all $t \geq 0$ and any bounded initial conditions.

The proofs of these propositions are detailed in Luo et al. (2000).

4.2 6 story building with 2 MR dampers

The model described in this subsection correspond to that of a 6 story building with 2 MR dampers: one at the first floor and other at the second floor. The structure is a test specimen available at the WUSCEEL Laboratory, at the Washington University in St. Louis (U.S.A.). The schematic of the 6-story building with 2 MR dampers is shown in Figure 4.2. It is assumed that the control forces provided by the control devices are suitable to keep the response of the primary structure within the linear region.

The equation of motion of the structure is given by:

$$\mathbf{M}\ddot{\mathbf{x}}_\mathbf{r} + \mathbf{C}\dot{\mathbf{x}}_\mathbf{r} + \mathbf{K}\mathbf{x}_\mathbf{r} = \mathbf{G_s}\mathbf{f_{mr}} - \mathbf{M}L_s\ddot{x}_g \tag{4.12}$$

where $\mathbf{x_r}$ is the vector of relative displacements, $\ddot{x}_g$ is the incoming earthquake acceleration, $\mathbf{f_{mr}}$ is the vector of measured control forces generated by the MR dampers, G_s is a vector that determines the location of the MR dampers in the structure and L_s is a vector of ones. $\mathbf{M}$, $\mathbf{C}$ and $\mathbf{K}$ are the mass,

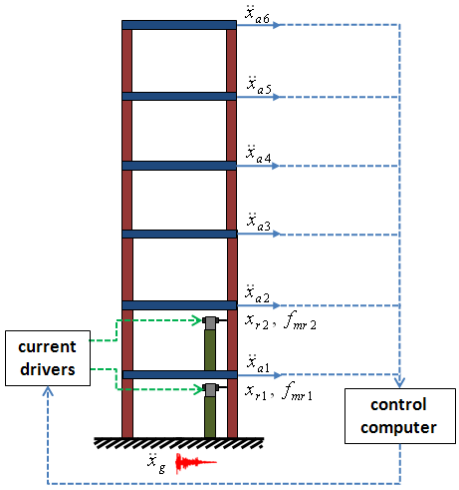

Figure 4.2: 6 story building with 2 MR dampers.

damping coefficient and stiffness matrices of the structure, respectively. These matrices can be written as in Eq. 4.6, while $\mathbf{G_s}$ and L_s are given by:

$$\mathbf{G_s} = \begin{bmatrix} 1 & 0 & 0 & 0 & 0 & 0 \\ 0 & 1 & 0 & 0 & 0 & 0 \end{bmatrix}^T \tag{4.13}$$

$$L_s = \begin{bmatrix} 1 & 1 & 1 & 1 & 1 & 1 \end{bmatrix}^T \tag{4.14}$$

The stiffness and mass of each floor are $k_i = 273$ N/cm and $m_i = 0.227$ N-s^2/cm, respectively. The vector or natural frequencies of the structure is $f_e = [1.29, 3.85, 6.11, 8.22, 9.64, 10.81]$ Hz and the vector of corresponding damping factors is $h_e = [1.38, 0.71, 0.64, 0.56, 0.48, 0.91]$ %. The MR dampers that the structure is equipped with, are similar to the shear-mode dampers used in the experiments described in Chapter 3. The dynamics were fitted to the Bouc-Wen model of Eqs. 4.9 - 4.11. The parameters of these dampers are: $\alpha_{mra} = 8.66$ N/cm, $\alpha_{mrb} = 8.66$ N/cm·V, $c_{mra} = 0.0064$ N-s/cm, $c_{mrb} = 0.0052$ N-s/cm·V, $\varphi = \beta = 300$ cm^{-2}, $n = 2$ and $\kappa = 120$.

4.3 Real time hybrid testing of a 3 story building with MR damper

This section describes the experimental setup of a 3-story building with an MR damper at its first floor. The experiments are performed in a real-time hybrid testing (RTHT) configuration available at the Smart Structures Technology Laboratory, University of Illinois Urbana - Champaign (USA). First, a background on hybrid testing is presented. Then, the configuration is described.

4.3.1 Hybrid testing background

The experimental testing of the control performance in civil engineering structures is an important issue in structural control. It is well known that testing vibration reduction systems at large scale in structures such as buildings or bridges is rather prohibitive because of the dimensions, the power required to do so and the costs that such tests imply. This is why experiments are usually run at small or mid scale laboratory specimens. Experiments can be performed in one of three ways: shaking table tests, quasi-static tests and pseudodynamic or hybrid tests (Shield et al. 2001).

Shaking tables are moved by hydraulic actuators to recreate the motion of the base of the structure in events such as earthquakes, at a correct rate. But these are not suitable for structures that are not well represented at small scale (reinforced concrete, for instance). At smaller scales, it is difficult to investigate structural details like bond, shear and anchorage. Furthermore, shaking tables do not allow the representation of other type of motion such as that of strong winds (Darby et al. 2001, Shield et al. 2001).

Quasi-static testing, on the other hand, is a much simpler testing method that can be used to test structural members at large scales, but these tests require a predefined displacement history, that can later be difficult to relate to the seismic demands on the structure (Mosqueda et al. 2005). The predefined inputs (displacements or forces) are applied to the structural component on an extended time scale (i.e., slow rates); therefore, the interaction with the structure to which it is to be attached and the dynamic and rate-dependent behavior of the structure are not considered. Typically, this type of test is used to investigate the hysteretic or cyclic behavior of structural materials or components under earthquake loading (Carrion & Spencer 2007).

The limitations on the shaking tables and quasi static tests led to development of pseudo dynamic or hybrid tests. This was initially proposed by Hakuno et al. (1969). In these tests, systems are divided into two substructures: a numerical subsystem and a physical subsystem. The numerical subsystem usually corresponds to that of a structure whose dynamics are well known and in general is assumed to exhibit a linear behavior. The physical subsystem is, on the other hand, the critical component of the system and is usually a nonlinear device such as a magnetorheological damper. In this way, large and full-scale experiments can be performed because the main structure is reduced to a numerical model solved in a computer or Digital Signal Processor and the critical components can be physically realized at large or full scale provided reasonable space, energy and costs. Generally, hydraulic actuators are used to drive the physical specimens in the experiment.

One significant advantage of hybrid simulation is that it removes a large source of epistemic uncertainty compared to pure numerical simulations by replacing structural element models that are not well understood with physical specimens on the laboratory test floor (Mosqueda et al. 2005). There are two main drawbacks with the hybrid test method. Firstly, the method relies on the assumption that the mass of the structure is concentrated at discrete points. Secondly, the loading is applied over a greatly expanded time scale so that time-dependent non-linear behavior is not correctly reproduced in the physical component. In hybrid testing, the displacements are imposed on an extended time-scale which typically ranges from 100 to 1000 times the actual earthquake duration to allow for the use of larger actuators without high hydraulic flow requirements, careful observation of the response of the structure during the test, and the ability to pause and resume the experiment. In particular, the method cannot be applied to the testing of highly rate-sensitive components such as visco-elastic dampers and certain active or semi-active structural control devices (Darby et al. 2001, Jung & Shing 2006).

Real-time hybrid testing is a variation of the pseudodynamic test method in which the imposed displacements and response analysis are executed in real time, thus allowing testing of systems with rate-dependent components. Real-time hybrid testing makes possible the testing of a large class of structural components associated with vibration control, including passive, semiactive, and active control devices (e.g., base isolation and dampers), which are typically nonlinear and rate-dependent (Carrion & Spencer 2007, Nakashima & Masaoka 1999). Real-time hybrid testing is challenging because it is necessary to perform all of the calculations, apply the displacements, and measure and feedback the forces within a single time step (typically less than 10 msec). Because the test is conducted in real time, the dynamics of the testing system and specimen become important. For example, when hydraulic actuators are used to apply forces to the test specimen, they inevitably include a response delay, which is equivalent to negative damping in a real-time hybrid experiment (Horiuchi et al. 1999).

It is the response delay one of the main research focus in real time hybrid testing. Researchers have traditionally not differentiated between time delays and actuator lag by treating them as a constant time delay. However, in general, they are frequency dependent; therefore, their approximation as a pure time

delay is valid only in a limited frequency range (e.g., low frequency). The effect of the dynamic response of hydraulic actuators on real-time hybrid experiments was initially considered by Horiuchi et al. (1996), whose method based on polynomial extrapolation is still widely used. Other solutions to this problem have been proposed by Horiuchi et al. (1999), Nakashima & Masaoka (1999), Darby et al. (2001) and Jung & Shing (2006), to name a few. Carrion & Spencer (2007) proposed a method for real-time hybrid testing that incorporates model-based compensation techniques for time delays and actuator dynamics, and combines fast hardware and software (for high-speed computations and communication) with high performance hydraulic equipment, allowing accurate testing of systems with larger natural frequencies (e.g., stiff structures or multi-degree-of-freedom systems) and handling larger delays/lags, typically associated with actuators with high force capacity.

Pseudodynamic tests have also been extended for geographically distributed applications. This allows to run experiments with different substructures located in different places. Because the time required for network communication is relatively large, response prediction-correction methods are required to generate the actuator command signals at continuous or fast-rate tests. See for example the works by Shing et al. (2004), Chang et al. (2005), Spencer et al. (2007) and Mosqueda et al. (2005).

4.3.2 RTHT system

Real-time hybrid testing is particularly suitable for testing structures with rate dependent devices. Recently, special attention has been directed toward the application of this technique to evaluate the response of structures with MR dampers. Real-time hybrid experiments of structures with MR dampers have already been proposed and/or conducted by Emmons & Christenson (2006); Wu et al. (2003), and Carrion & Spencer (2007), among others. The system designed by Carrion & Spencer (2007) is used in this work to implement and evaluate the performance of different semiactive controllers for vibration mitigation in a structure with an MR damper.

The RTHT system schematic used in this work is shown in Figure 1. A fully detailed description of this implementation can be found in (Carrion & Spencer 2007).

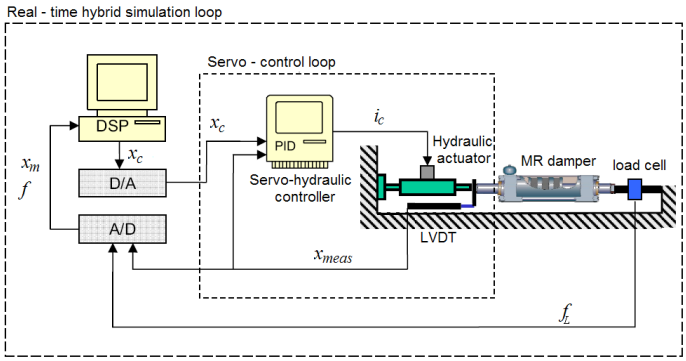

Figure 4.3: RTHT system schematic.

The RTHT system of Figure 4.3 consists of a computer that simulates the structure to be controlled and generates the commanding signals (displacements and control signals); a small-scale MR damper that is driven by a hydraulic actuator which in turn is controlled by a servo-hydraulic controller; and DSP, A/D and D/A hardware for signal processing. Sensors available include a linear variable displacement transformer (LVDT) for displacement measurements and a load cell to measure the MR damper force. In Figure 1, x_c is the commanded displacement, f_L is the MR damper force measured by the load cell, x_{meas} is the displacement measured by the LVDT and i_c is the control current sent to the hydraulic actuator.

4.3.3 Structure model

The schematic of the 3-story building to be controlled is shown in Figure 4.4. The building can be modeled with the second order motion equation:

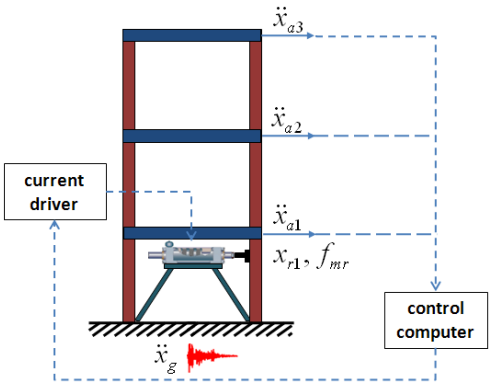

Figure 4.4: Schematic of the 3-story building with MR damper.

$$\mathbf{M}\ddot{\mathbf{x}}_\mathbf{r} + \mathbf{C}\dot{\mathbf{x}}_\mathbf{r} + \mathbf{K}\mathbf{x}_\mathbf{r} = G_s f_{mr} - \mathbf{M}L_s\ddot{x}_g \tag{4.15}$$

where the matrices and vectors $\mathbf{M}$, $\mathbf{C}$, $\mathbf{K}$, G_s and L_s are given by:

$$\mathbf{M_s} = \begin{bmatrix} m_1 & 0 & 0 \\ 0 & m_2 & 0 \\ 0 & 0 & m_3 \end{bmatrix} = \begin{bmatrix} 20253 & 0 & 0 \\ 0 & 20253 & 0 \\ 0 & 0 & 20253 \end{bmatrix} \text{kg} \tag{4.16}$$

$$\mathbf{C_s} = \begin{bmatrix} c_{11} & c_{12} & 0 \\ c_{21} & c_{22} & c_{23} \\ 0 & c_{32} & c_{33} \end{bmatrix} = \begin{bmatrix} 7243.2 & -2070 & 0 \\ -2070 & 4138.2 & -2070 \\ 0 & -2070 & 2070 \end{bmatrix} \text{N} - \text{s/m} \tag{4.17}$$

$$\mathbf{K_s} = \begin{bmatrix} k_{11} & k_{12} & 0 \\ k_{21} & k_{22} & k_{23} \\ 0 & k_{32} & k_{33} \end{bmatrix} = \begin{bmatrix} 9932 & -5661 & 0 \\ -5661 & 11338 & -5661 \\ 0 & -5661 & 5661 \end{bmatrix} \text{N/m} \tag{4.18}$$

$$G_s = [-1, 0, 0]^\text{T} \quad L_s = [1, 1, 1]^\text{T} \tag{4.19}$$

$\mathbf{x_r}$ is the vector of relative displacements, i.e., with respect to the ground (the r subindex means relative coordinates); f_{mr} is the MR damper force and $\ddot{x}_g$ is the incoming earthquake acceleration. $\ddot{x}_{ai}$ is the absolute acceleration of the $i-th$ floor. The relationship between relative and absolute displacements is $x_r = x_a - x_g$. The natural frequencies and the damping ratios of the structure corresponding to the first, second and third mode are 1.09 Hz (0.31%), 3.17 Hz (0.62%) and 4.74 Hz (0.63%), respectively.

4.3.4 MR damper

The MR damper used in the experiments is the RD-1005 manufactured by the Lord Corporation, shown in Figure 4.5. The damper is 216 mm long in its extended position, is 38.1 mm in diameter and has a stroke of 25.4 mm. It contains 50 ml of MR fluid and can generate forces up to 3000 N approximately. The magnetic field is generated by the current from a pulse width modulator (PWM) amplifier (the RD-1002 Wonder Box, from Lord Corp.).

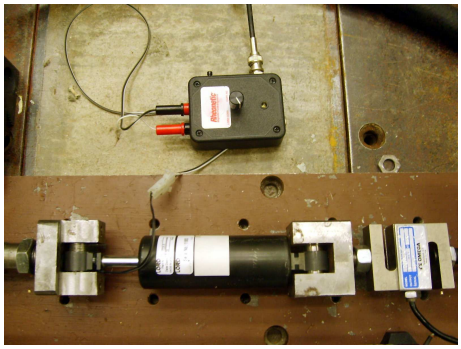

Figure 4.5: MR damper and PWM system.

The dynamics of the damper can be modeled by the Bouc-Wen model, as shown in Eqs. 4.20 - 4.21:

$$f_{mr}^{*} = (c_{mra} + c_{mrb} v_f)\,\dot{x}_p + (k_{mra} + k_{mrb} v_f)\,x_p + (\alpha_{mra} + \alpha_{mrb} v_f)\,z \tag{4.20}$$

$$\dot{z} = -\varphi|\dot{x}_p|z|z|^{n-1} - \beta\dot{x}_p|z|^n + \kappa\dot{x}_p \tag{4.21}$$

where z is an evolutionary variable that describes the hysteretic behavior of the damper, x_p is the piston displacement and v_f is the output of the first order filter introduced to account for the time that the MR fluid takes to reach the rheological equilibrium:

$$\dot{v}_f = -\eta(v_f - v) \tag{4.22}$$

where η is a parameter obtained experimentally. The parameters of the MR damper specimen are: $\alpha_{mra} = 33.27$ N/m, $\alpha_{mrb} = 182.65$ N/m-V, $c_{mra} = 754.41$ N-s/m, $c_{mrb} = 712.73$ N-s/m-V, $k_{mra} = 1137.57$ N/m, $k_{mrb} = 1443.50$ N/m-V, $x_0 = 0$ m, $\varphi = 4209.8$ m^{-2}, $\beta = 4205.2$ m^{-2}, $\kappa = 10246$, $n = 2$, $\eta = 57$ s^{-1}. The following scaling factors are used to integrate the physical small-scale MR damper to the numerical large-scale structure: the first floor relative displacement is reduced by a factor $S_L = 7.25$ to obtain the damper piston displacement (that is, $x_p = x_{1r}/S_L$) and the MR damper force is increased by a factor $S_F = 60$ to obtain the input force to the structure (that is, $f_{mr} = S_F f_{mr}^{*}$).

4.3.5 Hydraulic actuator dynamics

The MR damper is driven by a hydraulic actuator which receives a commanding signal from the computer where the simulation runs to impose a displacement to it. A block diagram that shows the interaction between the numerical model and the dynamic system is illustrated in Figure 4.6.

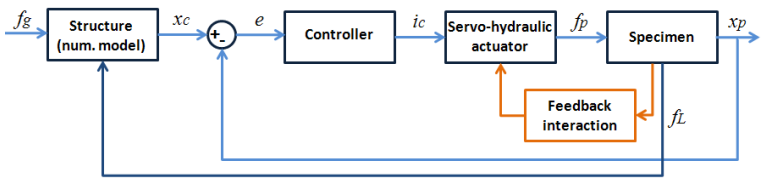

Figure 4.6: Numerical model and physical system interaction.

The entire physical system can be modeled by a transfer function $G_{x_p x_c}(s)$ whose input x_c is the commanded displacement and the output x_p is the piston displacement. Modeling the system dynamics is useful for simulating the RTHT experiments. The transfer function $G_{x_p x_c}(s)$ varies according to the

MR damper input voltage. Two cases are identified corresponding to the damper operating at $V_0 = 0$ V ($G_{x_p x_c, V_0}(s)$) and $V_{max} = 5$ V ($G_{x_p x_c, V_{max}}(s)$) respectively. These transfer functions are given by:

$$G_{x_p x_c, V_0}(s) = \frac{1}{(0.0062s + 1)(2.639 \times 10^{-5}s^2 + 0.059s + 1)} \tag{4.23}$$

$$G_{x_p x_c, V_{max}}(s) = \frac{1}{(0.0094s + 1)(2.618 \times 10^{-5}s^2 + 0.058s + 1)} \tag{4.24}$$

An algorithm was designed by Carrion and Spencer Carrion & Spencer (2007) to provide a smooth transition from $G_{x_p x_c, V_0}(s)$ to $G_{x_p x_c, V_{max}}(s)$ and vice versa when the damper voltage varies during the experiments. A block diagram of this algorithm is shown in Figure 4.7. The Laplace transform of the model is described by:

$$X_d(s) = X_a(s) + X_b(s)V_t(s) \tag{4.25}$$

$$X_a(s) = G_a(s)X_c(s) = G_{x_p x_c, V_0}(s)X_c(s) \tag{4.26}$$

$$X_b(s) = G_b(s)X_c(s) = \left(G_{x_p x_c, V_{max}}(s) - G_{x_p x_c, V_0}(s)\right) X_c(s) \tag{4.27}$$

$$V_t(s) = G_t(s)V(s) \tag{4.28}$$

where $G_t(s)$ is used to model the dynamics of the actuator associated with the change in the voltage of the MR damper, providing a smooth transition between $G_a(s)$ (Eq. 4.26) and $G_b(s)$ (Eq. 4.27), and is given by:

$$G_t(s) = \frac{0.2}{\tau_t s + 1} \tag{4.29}$$

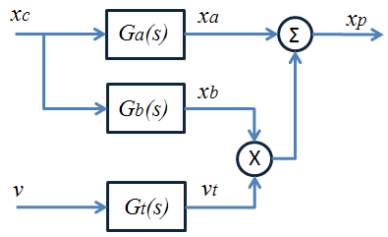

Figure 4.7: Block scheme of the actuator dynamics with bumpless transfer.

where $\tau_t = 0.0048s$ is the transition filter time constant. As the time constant becomes small, the transition becomes faster, approaching a simple switching algorithm, while for large values of the time constant the transition is slower and smoother. Due to the inherent dynamics of the physical system (e.g. time delays), a pre-compensator $G_{ff}(s)$ is added to the system for compensation purposes. In this way, the commanded displacement (x_c, input to the physical system) is calculated based on the desired displacement (x_d, output from the simulations) and the inverse dynamics of the physical system. As a result, $x_p \approx x_d$. A schematic of the compensated system is shown in Figure 4.8.

Once again, two compensators are designed: one for the MR damper operating at $V_0 = 0$ V ($G_{ff,V_0}(s)$) and the other for the damper operating at $V_{max} = 5$ V ($G_{ff,V_{max}}(s)$). The transfer functions are given by

$$G_{ff,V_0}(s) = \frac{(0.062s + 1)(2.639 \times 10^{-5}s^2 + 0.0059s + 1)}{(4.129 \times 10^{-4}s + 1)(1.173 \times 10^{-7}s^2 + 3.909 \times 10^{-4}s + 1)} \tag{4.30}$$

$$G_{ff,V_{max}}(s) = \frac{(0.0094s + 1)(2.618 \times 10^{-5}s^2 + 0.0058s + 1)}{(6.289 \times 10^{-4}s + 1)(1.164 \times 10^{-7}s^2 + 3.857 \times 10^{-4}s + 1)} \tag{4.31}$$

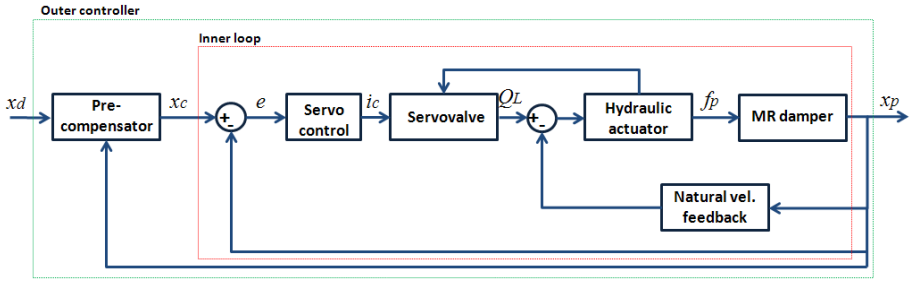

Figure 4.8: Diagram of the complete system with dynamics compensation.

A similar approach to that of Figure 4.7 is followed to provide a smooth transition between both compensators. The block diagram is shown in Figure 4.9 and the model is described by:

$$X_c(s) = X_a(s) + X_b(s)V_t(s) \tag{4.32}$$

$$X_a(s) = G_{ff,a}(s)X_d(s) = G_{ff,V_0}(s)X_d(s) \tag{4.33}$$

$$X_b(s) = G_{ff,b}(s)X_d(s) = \left(G_{ff,V_{max}}(s) - G_{ff,V_0}(s)\right)X_d(s) \tag{4.34}$$

$$V_t(s) = G_t(s)V(s) \tag{4.35}$$

where $G_t(s)$ is the transition filter as given in Eq. 4.29.

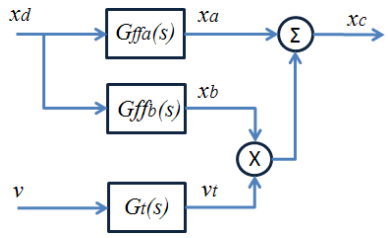

Figure 4.9: Block scheme of the pre-compensator dynamics with bumpless transfer.

4.3.6 RTHT setup performance

The numerical models corresponding to the 3-story building, the compensator, the MR damper, the hydraulic actuator and the controller, are implemented in Matlab/Simulink. The ordinary differential equation solver used is the 4^{th} order Runge-Kutta method with a time step $T_s = 5 \times 10^{-4}$ seconds. Figure 4.10 shows the performance of the compensator. This figure illustrates a comparison between the desired, the commanded and the measured piston displacements during the execution of an experiment. The lower curve is a close-up of the upper one.

On the other hand, Figures 4.11 and 4.12 show a comparison between the experimental dynamics of the MR damper and those predicted by the Bouc-Wen model. In the first case, the damper is subject to a sinusoidal displacement at 5 Hz and 0.254 cm amplitude. The voltage periodically switches from 0 V to 5 V. In the second case, the damper is subject to random displacement and random voltage excitation.

Figure 4.13 compares the MR damper piston displacement as measured during an experiment with that obtained by the model of the overall system. That is, the system of Figure 4.8 was implemented in Simulink and simulated, and the results were compared to the experimental response. To make this comparison, the El Centro seismic motion records and MR damper voltage were taken as inputs to the RTHT system. The results show good accuracy of the system model.

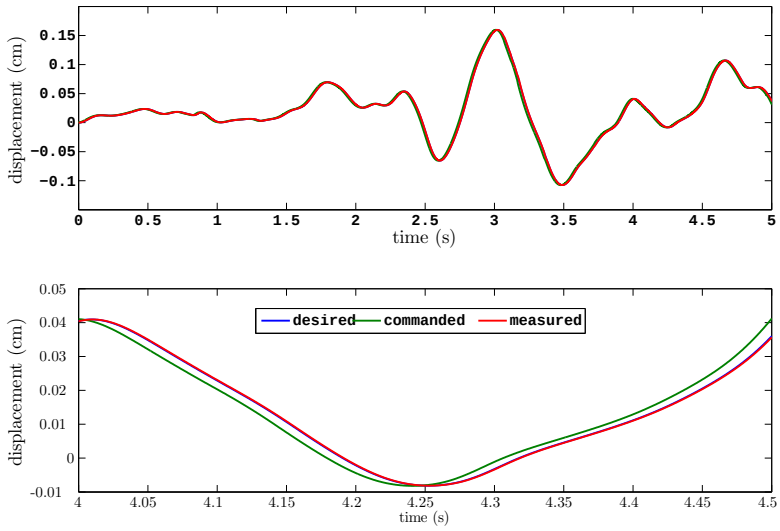

Figure 4.10: Comparison between the desired, commanded and measured piston displacement.

4.4 Semiactive suspension system

A similar problem to that of vibration suppression in civil structures is that of the vehicle suspension systems. The objective of these systems is to protect the vehicle chassis and improve the passengers' comfort by reducing the vibrations caused by the imperfections of the road. MR dampers can be used to achieve this goal. The model to be presented in this section is that of an experimental platform that resembles the suspension system of a vehicle that makes use of an MR damper to suppress the harmful vibrations.

Figure 4.14 shows a picture of the semiactive suspension system (SAS), manufactured by INTECO Ltd. (Cracow, Poland) and available at the Modal Intervals and Control Engineering Laboratory (University of Girona, Spain). It consists of a wheel driven by a DC motor coupled to an eccentric small wheel. The suspended car wheel rolls due to the small wheel rotation and oscillates due to the eccentricity. The geometrical diagram of the semiactive suspension system is depicted in Figure 4.15. The variables and parameters of the model are shown in Table 4.1.

The semiactive suspension system can be modeled by the following set of equations:

$$J_2\dot{\omega}_2 = \sum_{i=1}^{4} M_{2i}; \quad \dot{\alpha}_2 = \omega_2 \tag{4.36}$$

$$J_1\dot{\omega}_1 = \sum_{i=1}^{6} M_{1i}; \quad \dot{\alpha}_1 = \omega_1 \tag{4.37}$$

Equations 4.36 and 4.37 represent the torques of the upper and lower rocking levers, respectively. ω_1 is the angular velocity of the lower rocking lever and ω_2 is that of the upper rocking lever. J_1 and J_2 are the moments of inertia of the lower and upper levers, respectively. The torques actuating on the upper

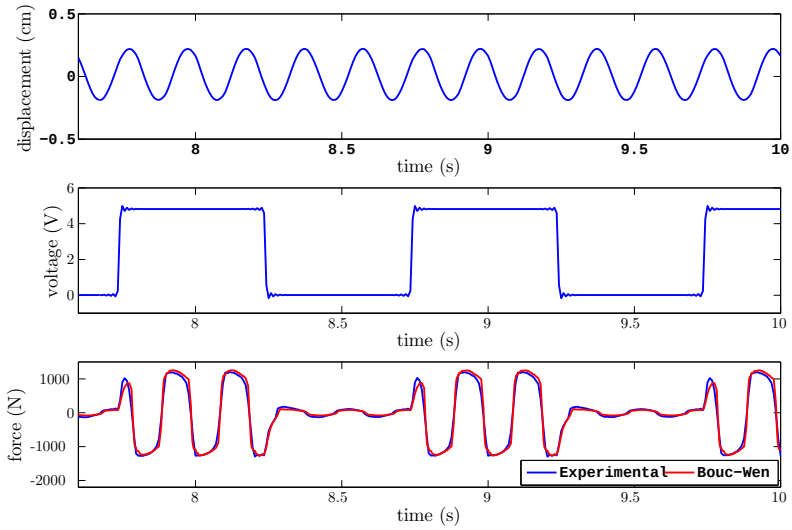

Figure 4.11: Time behavior of the MR damper characteristics: force response to sinusoidal displacement and switching voltage inputs.

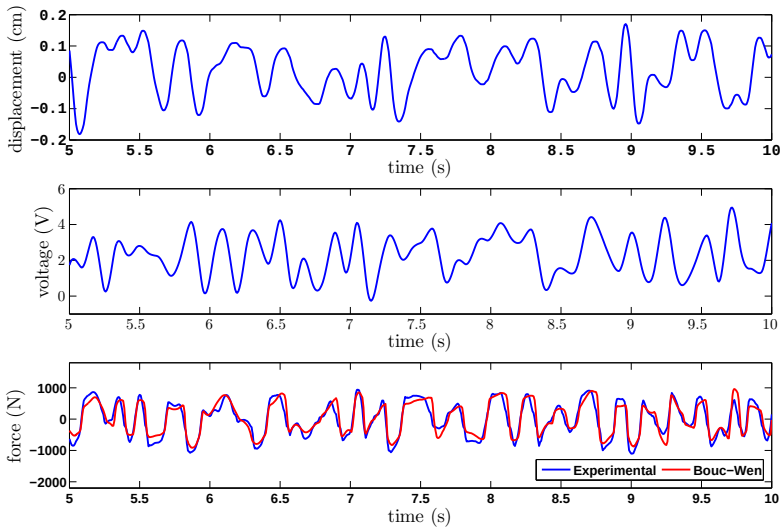

Figure 4.12: Time behavior of the MR damper characteristics: force response to random displacement and voltage inputs.

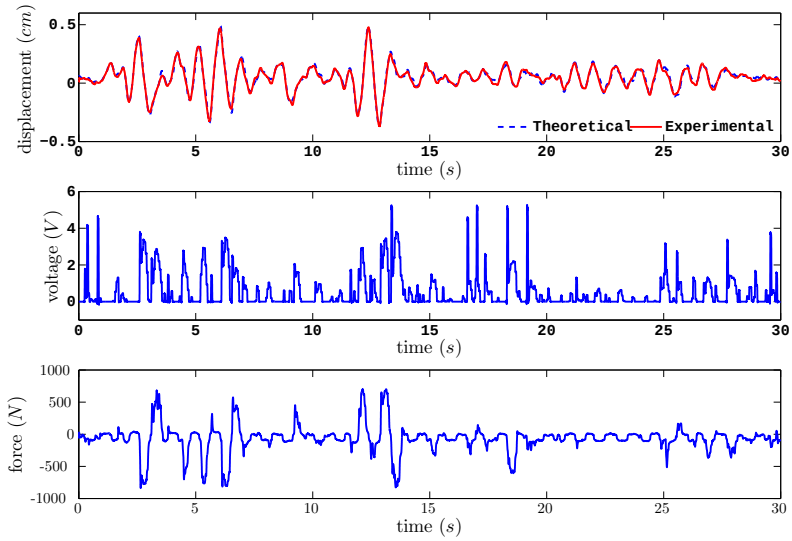

Figure 4.13: Comparison between the experimental and the model displacement response of the RTHT system.

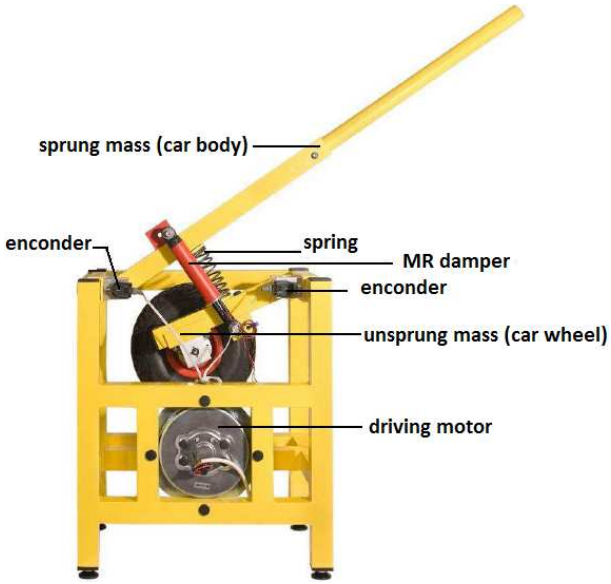

Figure 4.14: Picture of the semiactive suspension system.

Table 4.1: SAS parameters.

Parameter	**Value**	**Comments**
m_1	0.035 m	distance damper joint - upper rocking lever line
m_2	0.035 m	distance damper joint - lower rocking lever line
r_1	0.025 m	distance spring joint - upper rocking lever line
r_2	0.025 m	distance spring joint - lower rocking lever line
r_3	0.05 m	distance wheel axis - lower rocking lever line
l_1	0.125 m	distance damper joint - lower rocking lever pivot
l_2	0.125 m	distance damper joint - upper rocking lever pivot
l_3	0.2 m	distance wheel axis - lower rocking lever pivot
s_1	0.135 m	distance spring joint - lower rocking lever pivot
s_2	0.160 m	distance spring joint - upper rocking lever pivot
r_{1f}	0.1298 rad	lower rotational radius of the damper suspension
r_{2f}	0.1346 rad	upper rotational radius of the damper suspension
r_{1s}	0.1373 rad	lower rotational radius of the spring suspension
r_{2s}	0.0.1619 rad	upper rotational radius of the spring suspension
$R = \sqrt{l_3^2 + r_3^2}$	0.2062 m	rotational radius of the wheel axis
$R = 1$	0.2062 m	length of the lower rocking lever
$R = 2$	0.490 m	length of the upper rocking lever
D_x	0.249 m	minimum eccentricity
l_0	0.07 m	tire thickness
r	0.06 m	radius of the rim
b	0.330 m	distance between the rocking lever rotational axis and the car body
α_{1f}	0.2730 rad	fixation angle of the damper with respect to the lower lever
α_{2f}	0.2630 rad	fixation angle of the damper with respect to the upper lever
α_{1s}	0.1831 rad	fixation angle of the spring with respect to the lower lever
α_{2s}	0.1550 rad	fixation angle of the damper with respect to the upper lever

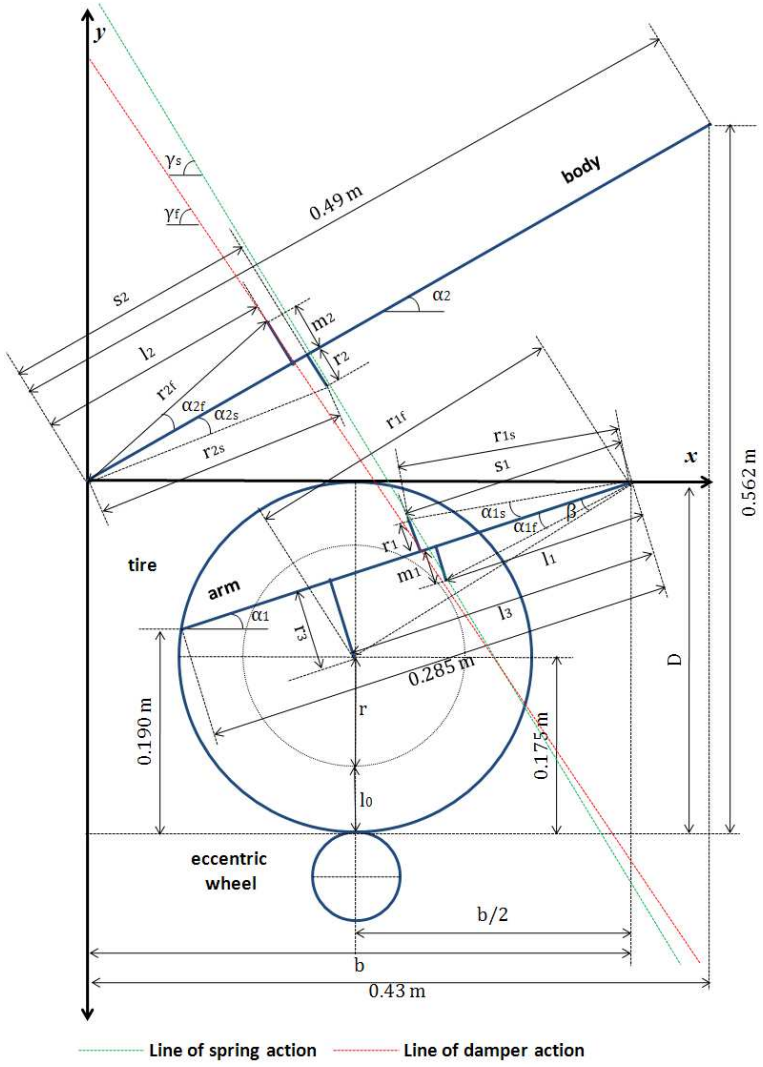

Figure 4.15: Schematic of the Semiactive Suspension System.

rocking lever are given by:

$$M_{21} = -k_2\omega_2 \tag{4.38}$$

$$M_{22} = -m_u g R_2 \cos\alpha_2 \tag{4.39}$$

$$M_{23} = r_{2s}F_s \sin\left(\pi - (\alpha_1 - \alpha_{1s}) - \gamma_s\right) \tag{4.40}$$

$$M_{24} = r_{2f}F_f \sin\left(\pi - (\alpha_{2f} + \alpha_2) - \gamma_f\right) \tag{4.41}$$

where M_{21} is the viscous friction damping torque, M_{22} is the gravitational forces torque, M_{23} is the torque generated by the spring and M_{24} is the torque generated by the MR damper. m_u is the mass of the lever and g is the gravitational acceleration. The angles γ_s and γ_f are the slope angle of the spring operational line and the slope angle of the MR damper operational line, respectively, and are given by:

$$\gamma_s = abs\left(\arctan\left(\frac{-r_{1s}\sin(\alpha_1 - \alpha_{1s}) - r_{2s}\sin(\alpha_2 - \alpha_{2s})}{b - r_{1s}\cos(\alpha_1 - \alpha_{1s}) - r_{2s}\cos(\alpha_2 - \alpha_{2s})}\right)\right) \tag{4.42}$$

$$\gamma_f = abs\left(\arctan\left(\frac{-r_{1s}\sin(\alpha_1 + \alpha_{1s}) - r_{2s}\sin(\alpha_2 + \alpha_{2s})}{b - r_{1s}\cos(\alpha_1 + \alpha_{1s}) - r_{2s}\cos(\alpha_2 + \alpha_{2s})}\right)\right) \tag{4.43}$$

F_f and F_s are the forces generated by the MR damper and the spring, respectively, on the levers. These forces are given by:

$$F_f = f_{mr}\left(\left(\omega_2 r_{2f}\cos\left(-\frac{\pi}{2}+\alpha_2+\alpha_{2f}+\gamma_f\right)\right)-\left(\omega_1 r_{1f}\cos\left(-\frac{\pi}{2}+\alpha_1+\alpha_{1f}+\gamma_f\right)\right)\right) \tag{4.44}$$

$$F_s = K_s\left(l_{0s}-\sqrt{\left(r_{2s}\sin(\alpha_2-\alpha_{2s})+r_{1s}\sin(\alpha_1-\alpha_{1s})\right)^2+\left(b-r_{1s}\cos(\alpha_1-\alpha_{1s})-r_{2s}\cos(\alpha_2-\alpha_{2s})\right)^2}\right) \tag{4.45}$$

where f_{mr} is the dynamics of the MR damper. On the other hand, the actuating torques on the lower rocking lever are given by:

$$M_{11} = -k_1\omega_1 \tag{4.46}$$
$$M_{12} = m_l g R_1\cos(\alpha_1+\beta) \tag{4.47}$$
$$M_{13} = -R_1\cos(\alpha_1+\beta)(K_g(l_0+r+R_1\sin(\alpha_1+\beta)-D_x+e(t))) \tag{4.48}$$
$$M_{14} = f_g\left(\dot{e}-R_1\cos(\alpha_1+\beta)\right) \tag{4.49}$$
$$M_{15} = r_{1s}F_s\sin\left(\pi-(\alpha_2-\alpha_{2s})-\gamma_s\right) \tag{4.50}$$
$$M_{16} = r_{1f}F_f\sin\left(\pi-(\alpha_{1f}+\alpha_1)-\gamma_f\right) \tag{4.51}$$

where M_{11} is the viscous friction damping torque, M_{12} is the gravitational forces torque, M_{13} is the actuating kinematic torque transferred through the tire, M_{14} is the damping torque generated by the gum of tire, M_{15} is the torque generated by the spring and M_{16} is the damping torque generated by the MR damper.

The SAS is equipped with a frictional MR damper, is a frictional damper from the Lord Corporation (RD-1097-01) capable of generating forces of up to 100 N at a current of 1 A. The MR damper dynamics fit the following hyperbolic tangent model:

$$f_{mr} = f_c\tanh\left[\mu(\dot{x}_p+S_d)\right]+c_{mr}(\dot{x}_p+pS_d) \tag{4.52}$$
$$f_c = f_{c1}i+f_{c2} \tag{4.53}$$
$$c_{mr} = c_{mr1}i+c_{mr2} \tag{4.54}$$

where f_c is a parameter associated to the dry friction force, c_{mr} is the viscous damping coefficient, $\dot{x}_p$ is the piston velocity, i is the current that flows through the damper coils; p is a scaling parameter related to hysteresis and μ is a scaling parameter that allows for a smooth transition from negative to positive values. When $\mu\to\infty$, the model is reduced to the Bingham model. The value of the MR damper model parameters are: $f_{c1}=62$ N/A, $f_{c2}=1.5$ N, $c_{mr1}=48$ N-s/A-m, $c_{mr2}=14$ N-s/m, $\mu=130$ s/m and $p=1$ s^{-1}.

Figure 4.16 shows the experimental response of the semiactive suspension system. The velocity of the eccentric wheel is continuously and linearly incremented from 2π rad/s at the beginning during 20 seconds. The current to the MR damper is set to 0 A, so that it is actuating as a passive damper. The figure shows that the resonance frequency of the SAS is at around 1.6 Hz. The goal of the platform is to reduce as much as possible the magnitude of the oscillations in the operational range of applied frequencies.

4.5 Summary

The mathematical models of four systems for simulation and experimentation have been fully described in this chapter. The models correspond to those of buildings equipped with MR dampers and another one that resembles a vehicle suspension system. The main characteristics of each of these models have been annotated. In the remaining of this dissertation, these models will be frequently invoked for control formulation purposes.

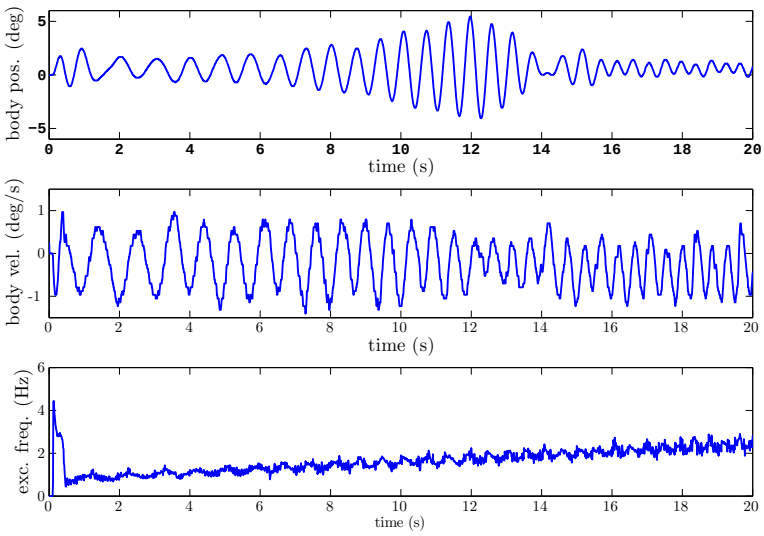

Figure 4.16: SAS experimental response.

Chapter 5

Robust control in time domain: Backstepping control approach

In this chapter, the problem of vibration mitigation in flexible structures with MR dampers is treated from a time-domain perspective. The objective is to reduce the structural response in the presence of actuator nonlinearities, parametric uncertainties, unknown disturbances and limited measurements. This makes mandatory the application on nonlinear control techniques. As discussed previously in Chapter 2, this problem has been solved mainly using methodologies such as Optimal Control (e.g. Linear Quadratic Regulators, Linear Quadratic Gaussian, Clipped Optimal Control), Sliding Mode Control, Lyapunov based control and Neuro-Fuzzy techniques. These solutions have proven to be effective in reducing the response of different structures. Nonetheless, some of controllers formulated do not cover important aspects like actuator nonlinearities or parametric uncertainty while others may require information for the design or implementation that may be impractical to obtain.

As a contribution to the structural control field, it is desired to formulate a controller that surpasses these problems in a systematic and practical way. In order to do it, in this research it is proposed the use of Backstepping control. This methodology allows the introduction of the system nonlinearities in a systematic way because it relies on the successive construction of Lyapunov functions that guarantee the stability of the system. Furthermore, backstepping controllers can be formulated so as to account for the parametric uncertainties by adding adaptation laws. The problem of unknown disturbances is approached by including bounds for the external signals. Finally, the controller is formulated for the subsystem where the actuator is installed. This can be done by taking advantage of the fact that, under certain conditions, stabilization of a part of the structure implies stabilization of the whole structure. This is advantageous because only a few measurements are needed to implement the controller.

This chapter is organized as follows. Section 5.1 introduces the concept of backstepping control. Then, the application of the backstepping methodology to different cases is presented. Thus, in Section 5.2, it is considered the case of a base-isolated 10-story building with an MR damper subject to seismic excitations. The problems of actuator nonlinearities, parametric uncertainty, unknown disturbances and limited measurements are studied. Section 5.3 considers the experimental testing of different backstepping controllers for 3-story building with an MR damper. These experiments are executed in a novel real-time hybrid testing platform which allows the control performance study through a combination of experiments and simulations. Section 5.4 studies the implementation of a backstepping controller to a semiactive suspension system and presents the experiments results as well. The chapter ends with a summary of the obtained results.

5.1 Background on backstepping

The general idea behind the backstepping control design relies in the following assumption (Krstic et al. 1995):

Assumption 5.1.1 *Consider the system:*

$$\dot{x} = f(x) + g(x)u, \;\; f(0) = 0 \tag{5.1}$$

where $x \in \mathbb{R}$ is the state and $u \in \mathbb{R}$ is the control input. There exists a continuously differentiable feedback control law $u = \alpha(x)$ with $\alpha(0) = 0$ and a smooth, positive definite, radially unbounded function $V : \mathbb{R}^n \to \mathbb{R}$ such that:

$$\frac{\partial V}{\partial x}(x)[f(x) + g(x)\alpha(x)] \leq -W(x) \leq 0, \;\; \forall x \in \mathbb{R}^n \tag{5.2}$$

where $W : \mathbb{R}^n \to \mathbb{R}$ is positive semidefinite.

Under this assumption, the control $u = \alpha(x)$ guarantees the global boundedness of $x(t)$ and via the LaSalle-Yoshizawa theorem,

$$\lim_{t \to \infty} W(x(t)) = 0 \tag{5.3}$$

The following lemma states the basis for the backstepping design:

Lemma 5.1.2 *Let the system of Eq. 5.1 be augmented by an integrator:*

$$\begin{aligned} \dot{x} &= f(x) + g(x)\xi \\ \dot{\xi} &= u \end{aligned} \tag{5.4}$$

and suppose that $\dot{x}$ satisfies Assumption 1 with $\xi \in \mathbb{R}$ as its control. If $W(x)$ is positive definite, then:

$$V_a(x, \xi) = V(x) + \frac{1}{2}[\xi - \alpha(x)]^2 \tag{5.5}$$

is a control Lyapunov function for the full system of Eq. 5.4, that is, there exists a feedback control $u = \alpha(x, \xi)$ which renders $x = 0$, $\xi = 0$ the global asymptotic stable equilibrium of Eq. 5.1. If $W(x)$ is only positive semidefinite, then there exists a feedback control which renders $V_a \leq -W_a(x, \xi) \leq 0$, such that $W_a(x, \xi) > 0$ whenever $W(x) > 0$ or $\xi \neq \alpha(x)$. This guarantees global boundedness and convergence of $[x(t), \xi(t)]^T$ to the largest invariance set M_a contained in the set $E_a \left\{[x, \xi]^T \in \mathbb{R}^{n+1} | W(x) = 0, \xi = \alpha(x)\right\}$.

The backstepping technique introduced in this section can easily be extended by recursion to larger order systems and more general cases.

5.2 Base-isolated 10-story building

In this section, an adaptive backstepping controller will be designed for the base-isolated 10 story building described in Section 4.1. The control objective is to reduce the absolute response in the base level and thus to make the base isolator work in its elastic region and also to decouple asymptotically the dynamic motion of the main structure from the base motion. In the control design, it is taken into account the uncertainties in the stiffness and damping coefficients of the base and main structure.

5.2.1 Controller formulation

Recall the equations of motion of the base and main structures (Eqs. 4.1 and 4.2). The controller will be designed for the base substructure. By Propositions 1 and 2 (Section 4.1), the controller can be designed for the base subsystem, while guaranteeing the stability of the whole structure.

Denote $y_1 = y_a$ and $y_2 = \dot{y}_a$. In order to design the backstepping controller, Eq. 4.2 is rewritten in state space form:

$$\dot{y}_1 = y_2 \tag{5.6}$$

$$\dot{y}_2 = -\frac{1}{m_0}\left[c_0 y_2 + k_0 y_1 + f_{bf} - \Phi - f_g - f_{mr}\right] \tag{5.7}$$

Theorem 1. *Consider the system of Eqs. 4.1 - 4.5. The following control law asymptotically attenuates the vibrations and stabilizes the main structure:*

$$\begin{aligned} v = &- \frac{(c_{mra} - m_0 h_1 + \overline{c}_0) y_2 + y_1 \overline{k}_0 + \alpha_{mra} z - \Phi - f_g}{\alpha_{mrb} z + c_{mrb} y_2} \\ &+ \frac{-\overline{c}_{bf}(y_2 - \dot{x}_{a1}) - \overline{k}_{bf}(y_1 - x_{a1}) + m_0 e_1 + m_0 h_2 e_2}{\alpha_{mrb} z + c_{mrb} y_2} \end{aligned} \tag{5.8}$$

for all $\alpha_{mrb} z + c_{mrb} y_2 \neq 0$, otherwise $v = 0$. h_1 and h_2 are positive constants. In order to estimate the uncertain structural stiffness and damping parameters $\overline{c}_0$, $\overline{k}_0$, $\overline{c}_{bf}$ and $\overline{k}_{bf}$, the following adaptation laws are proposed:

$$\dot{\overline{c}}_0 = \frac{r_1}{m_0} e_2 y_2 \tag{5.9}$$

$$\dot{\overline{k}}_0 = \frac{r_2}{m_0} e_2 y_1 \tag{5.10}$$

$$\dot{\overline{c}}_{bf} = \frac{r_3}{m_0} e_2 (y_2 - \dot{x}_{a1}) \tag{5.11}$$

$$\dot{\overline{k}}_{bf} = \frac{r_4}{m_0} e_2 (y_1 - x_{a1}) \tag{5.12}$$

with $r_i, i = 1, ..., 4$ being positive constants. e_1 and e_2 are standard backstepping variables given by:

$$e_1 = y_1 \tag{5.13}$$

$$e_2 = y_2 - \alpha_1 \tag{5.14}$$

$$\alpha_1 = -h_1 e_1 \tag{5.15}$$

Proof Consider the following Lyapunov function candidate:

$$V = \frac{1}{2} e_1^2 + \frac{1}{2} e_2^2 + \frac{1}{2 r_1} \widetilde{c}_0^2 + \frac{1}{2 r_2} \widetilde{k}_0^2 + \frac{1}{2 r_3} \widetilde{c}_{bf}^2 + \frac{1}{2 r_4} \widetilde{k}_{bf}^2 \tag{5.16}$$

where $\widetilde{c}_0 = c_0 - \overline{c}_0$, $\widetilde{k}_0 = k_0 - \overline{k}_0$, $\widetilde{c}_{bf} = c_{bf} - \overline{c}_{bf}$ and $\widetilde{k}_{bf} = k_{bf} - \overline{k}_{bf}$. The derivative of V is given by:

$$\dot{V} = e_1 \dot{e}_1 + e_2 \dot{e}_2 + r_1^{-1}(c_0 - \overline{c}_0)\dot{\overline{c}}_0 + r_2^{-1}(k_0 - \overline{k}_0)\dot{\overline{k}}_0 + r_3^{-1}(c_{bf} - \overline{c}_{bf})\dot{\overline{c}}_{bf} + r_4^{-1}(k_{bf} - \overline{k}_{bf})\dot{\overline{k}}_{bf} \tag{5.17}$$

Deriving (5.13) - (5.15) and substituting (5.6) and (5.7) into the result yields:

$$e_1 \dot{e}_1 = e_1 e_2 - h_1 e_1^2 \tag{5.18}$$

$$\begin{aligned} e_2 \dot{e}_2 = &- \frac{e_2}{m_0}[-\Phi - f_g + \alpha_{mra} z + c_{mra} y_2] + h_1 y_2 e_2 - \frac{c_0}{m_0} e_2 y_2 - \frac{k_0}{m_0} e_2 y_1 \\ &- \frac{e_2(\alpha_{mrb} z + c_{mrb} y_2)}{m_0} v - \frac{c_{bf}}{m_0} e_2 (y_2 - \dot{x}_{a1}) - \frac{k_{bf}}{m_0} e_2 (y_1 - x_{a1}) \end{aligned} \tag{5.19}$$

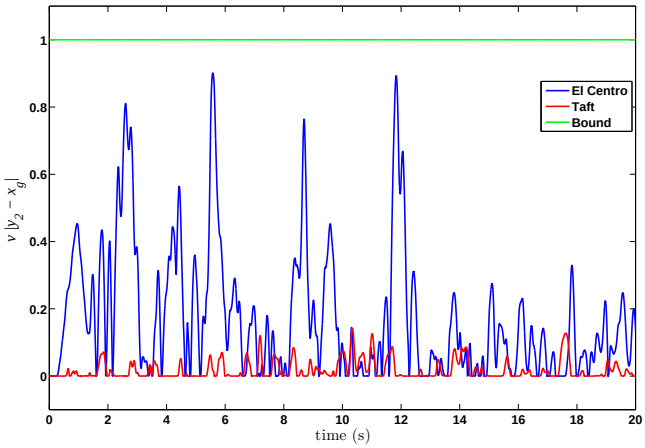

Figure 5.1: Dynamics of the base isolator in the presence of some standard earthquakes.

Substitution of (5.8) into (5.19) yields:

$$\begin{aligned} e_2\dot{e}_2 = &-\frac{1}{m_0}e_2y_2(c_0-\overline{c}_0)-\frac{1}{m_0}e_2y_1(k_0-\overline{k}_0)-h_2e_2^2-e_1e_2-\frac{1}{m_0}e_2(y_2-\dot{x}_{a1})(c_{bf}-\overline{c}_{bf}) \\ &-\frac{1}{m_0}e_2(y_1-x_{a1})(k_{bf}-\overline{k}_{bf}) \end{aligned} \tag{5.20}$$

Substitution of (5.9) - (5.12), (5.18) and (5.20) into (5.17) yields:

$$\dot{V} = -h_1e_1^2 - h_2e_2^2 < 0 \tag{5.21}$$

According to Lyapunov's stability theory, $e_1 \to 0$ and $e_2 \to 0$. Consequently, $y = y_1 = e_1 \to 0$ and $\dot{y} = y_2 = e_2 + h_1e_1 \to 0$. According to Propositions 1 and 2, the vibration of the base is asymptotically attenuated and the asymptotic stability of the main structure is guaranteed.$\diamondsuit$

The controller proposed in (5.8) contains some unmeasurable variables (z, f_g, Φ). In order to address these problems, some assumptions and approximations are made. First, it is assumed that the unknown seismic excitation x_g and $\dot{x}_g$ are bounded by $|x_g| \le D_d$ and $|\dot{x}_g| \le D_v$ and thus, the unknown disturbance force f_g in (4.4) is bounded by:

$$|f_g(t)| \le F \;\; \forall\, t \ge 0 \tag{5.22}$$

with D_d, D_v and F being known positive constants.

On the other hand, the passive control force generated by the frictional actuator can make small the relative movements of the structure during the seismic excitation. Thus, the following relationship holds:

$$\nu|y_2 - \dot{x}_g| < 1 \Rightarrow |y_2 - \dot{x}_g| < 1/\nu \tag{5.23}$$

This fact can be verified with some standard earthquakes, as shown in Figure 5.1. In order to make the simple approximation of the exponential function in the dynamic equation (4.3) of the frictional base isolator, the following Euler approximation is used:

$$e^{-\nu|y_2-\dot{x}_g|} \simeq \frac{1}{1+\nu|y_2-\dot{x}_g|+\frac{\nu^2}{2}|y_2-\dot{x}_g|^2+\frac{\nu^3}{6}|y_2-\dot{x}_g|^3} \tag{5.24}$$

By denoting $|y_2 - \dot{x}_g|_0$ as the maximum value of $|y_2 - \dot{x}_g|$, the passive actuator force can be approximated as:

$$\overline{\Phi} \leq \Delta_0 + \Delta_1 D_v - \Delta_1 y_2 \tag{5.25}$$

$$\Delta_0 = \left(\frac{\mu_{max} - \Delta\mu}{1 + \nu|y_2 - \dot{x}_g|_0 + \frac{\nu^2}{2}|y_2 - \dot{x}_g|_0^2 + \frac{\nu^3}{6}|y_2 - \dot{x}_g|_0^3} \right) Q \tag{5.26}$$

$$\Delta_1 = \left(\frac{\mu_{max}\left[\nu + \frac{\nu^2}{2}|y_2 - \dot{x}_g|_0 + \frac{\nu^3}{6}|y_2 - \dot{x}_g|_0^2\right]}{1 + \nu|y_2 - \dot{x}_g|_0 + \frac{\nu^2}{2}|y_2 - \dot{x}_g|_0^2 + \frac{\nu^3}{6}|y_2 - \dot{x}_g|_0^3} \right) Q \tag{5.27}$$

Finally, the evolutionary variable z is estimated using the following expression:

$$z = \hat{z} + \widetilde{z}, \;\; \dot{\hat{z}} = -\varphi|y_2|\hat{z}|\hat{z}|^{n-1} - \beta y_2|\hat{z}|^n + \kappa y_2 \tag{5.28}$$

Now with these ideas in mind, a modified controller is presented.

Theorem 2. *Consider the system of Equations 4.1 - 4.5. Let* $\widetilde{z} = \lambda e_2$ *and* $h_2 = \lambda\alpha_a/m_0$*, and consider the following characteristics of the shear-mode MR damper used:* $n = 1$ *and* $\varphi \geq \beta > 0$*, the following stabilizing control law is proposed:*

$$\begin{aligned} v = &- \frac{(\overline{c}_0 + \Delta_1 + \delta_a - m_0 h_1)y_2 - (\Delta_0 + \Delta_1 D_v + F)sgn(e_2)}{\alpha_{mrb}\hat{z} + c_{mrb}y_2 + \alpha_{mrb}\lambda e_2} \\ &+ \frac{-f_{bf} - \overline{k}_0 y_1 - \alpha_{mra}\hat{z} + m_0 e_1 + m_0 h_2 e_2}{\alpha_{mrb}\hat{z} + c_{mrb}y_2 + \alpha_{mrb}\lambda e_2} \end{aligned} \tag{5.29}$$

provided that $\alpha_{mrb}\hat{z} + c_{mrb}y_2 + \alpha_{mrb}\lambda e_2 \neq 0$*; otherwise,* $v = 0$*.*

Proof: Consider the following Lyapunov function candidate:

$$V = \frac{1}{2}e_1^2 + \frac{1}{2}e_2^2 + \frac{1}{2}\widetilde{z}^2 + \frac{1}{2r_1}\widetilde{c}_0^2 + \frac{1}{2r_2}\widetilde{k}_0^2 + \frac{1}{2r_3}\widetilde{c}_{bf}^2 + \frac{1}{2r_4}\widetilde{k}_{bf}^2 \tag{5.30}$$

The derivative of V is given by:

$$\begin{aligned} \dot{V} = &e_1\dot{e}_1 + e_2\dot{e}_2 + \widetilde{z}\dot{\widetilde{z}} + r_1^{-1}(c_0 - \overline{c}_0)\dot{\widetilde{c}}_0 + r_2^{-1}(k_0 - \overline{k}_0)\dot{\widetilde{k}}_0 \\ &+ r_3^{-1}(c_{bf} - \overline{c}_{bf})\dot{\widetilde{c}}_{bf} + r_4^{-1}(k_{bf} - \overline{k}_{bf})\dot{\widetilde{k}}_{bf} \end{aligned} \tag{5.31}$$

In order to find the expression for $e_2\dot{e}_2$, the result in (5.19) is used. Substitution of (5.29) into such result yields:

$$\begin{aligned} e_2\dot{e}_2 = &- \frac{e_2}{m_0}[-\Phi - f_g - \Delta_1 y_2 + (c_0 - \overline{c}_0)y_2 + (k_0 - \overline{k}_0)y_1 + (c_{bf} - \overline{c}_{bf})(y_2 - \dot{x}_{a1}) \\ &+ (k_{bf} - \overline{k}_{bf})(y_1 - x_{a1}) + m_0 e_1 + (\Delta_0 + \Delta_1 D_v + F)sgn(e_2)] \end{aligned} \tag{5.32}$$

From (4.10) and (5.28), and taking into account $n = 1$ and $\varphi \geq \beta > 0$, the following expression for $\widetilde{z}\dot{\widetilde{z}}$ is obtained:

$$\begin{aligned} \widetilde{z}\dot{\widetilde{z}} = &- \widetilde{z}[\varphi|y_2|(z|z|^{n-1} - \hat{z}|\hat{z}|^{n-1}) + \beta y_2(|z|^n - |\hat{z}|^n) \\ = &- \varphi|y_2|\widetilde{z}^2 - \beta y_2\widetilde{z}(|z| - |\hat{z}|) \\ \leq &- (\varphi - |\beta|)|y_2|\widetilde{z}^2 \leq 0 \end{aligned} \tag{5.33}$$

Substitution of (5.9) - (5.12), (5.18), (5.32) and (5.33) into (5.31) yields:

$$\dot{V} \leq -\frac{1}{m_0}[(\overline{\Phi} + \Delta_1 y_2)|e_2| - (\Phi + \Delta_1 y_2)e_2 + F|e_2| - f_g e_2] - h_1 e_1^2 - (\varphi - |\beta|)|y_2|\widetilde{z}^2 \leq 0 \tag{5.34}$$

and therefore stability is ensured.$\diamondsuit$

5.2.2 Numerical example

The following example consists in controlling the seismically excited 10-story building. Two different earthquake records are used for the simulations: El Centro and Taft. The mass of each floor, including that of the base is $m_i = 6 \times 10^5$ kg. The nominal value of the stiffness of the base is $k = 1.184 \times 10^7$ N/m. The stiffness of the structure varies linearly per story from 9×10^8 N/m at the first floor to 4.5×10^8 N/m at the top floor. The damping ratio of the base is $\zeta_0 = 0.1$ and that of the structure is $\zeta_i = 0.05$. The parameters of the frictional actuator placed in the base along with the MR damper are: $Q = \sum_{i=1}^{10} m_i$, $\mu = 0.1$, $\nu = 2.0$, $\mu_{max} = 0.185$ and $\Delta\mu = 0.09$. The parameters of the MR damper are: $\varphi = \beta = 3 \times 10^2$ cm^{-1}, $n = 1$, $\alpha_{mra} = 4.5 \times 10^4$, $\alpha_{mrb} = 3.6 \times 10^4$, $c_{mra} = 3 \times 10^2$ kNs/m, $c_{mrb} = 1.8 \times 10^2$ kNs/m. The controller parameters are: $h_1 = 1.5$, $h_2 = 86.3$, $\lambda = 1$, $r_1 = 10$, $r_2 = 1$, $r_3 = 10$ and $r_4 = 1$.

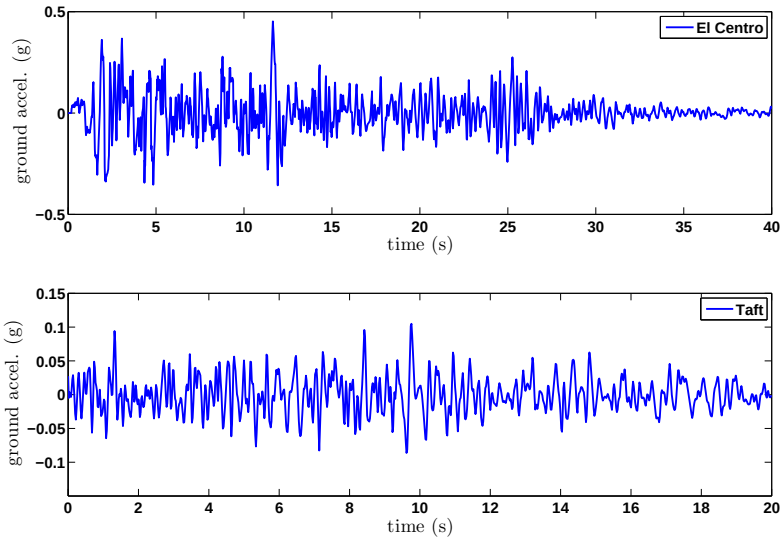

Figure 5.2: El Centro and Taft earthquakes.

Figure 5.2 shows the records of the earthquakes used to excite the structure in the example. Figures 5.3 and 5.4 compare the peak absolute displacement and velocity of each floor in 3 cases: (1) without any type of dampers (*Unc.*); (2) with only the passive damper (*Pas.*); and (3) with the hybrid scheme, i.e., the passive damper plus the MR damper (*Ad. BS*). These figures also show the reduction in displacement and velocity response when the hybrid scheme is implemented compared to the case of no dampers actuating on the structure. The control effort of the MR damper when subject to the El Centro and Taft earthquakes is shown in Figure 5.5.

5.3 Real-time hybrid testing of backstepping controllers

In this section, backstepping controllers are designed for a 3-story building with an MR damper and tested in the real-time hybrid testing setup described in Section 4.3.

5.3.1 Controller formulation

To begin with the design of the backstepping controller, the structure model of Eq. 4.15 is divided into two subsystems accounting for the first floor dynamics, where the MR damper is attached, and the rest of the structure i.e., the two upper floors. Thus, the building can be modeled by the following set of

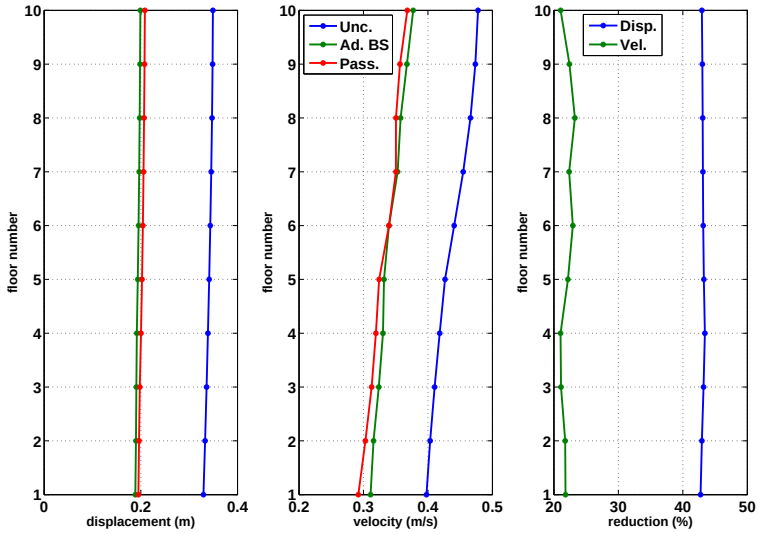

Figure 5.3: El Centro: Peak relative response and reduction percentage with respect to the uncontrolled case.

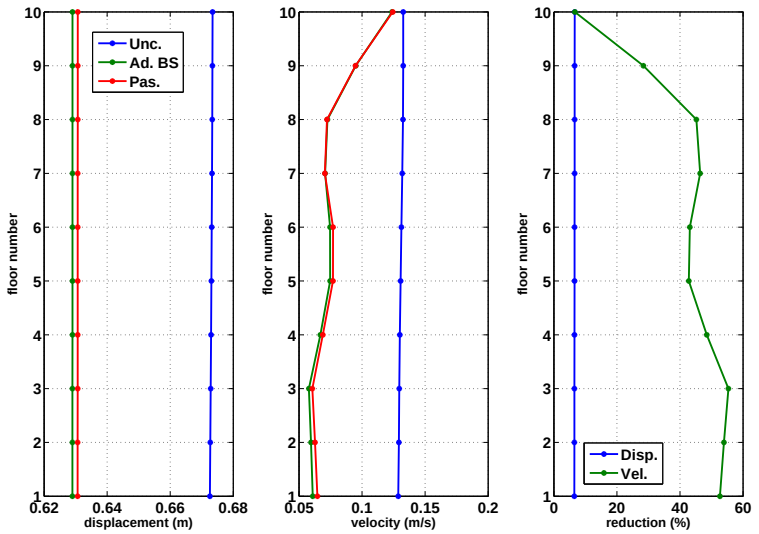

Figure 5.4: Taft: Peak relative response and reduction percentage with respect to the uncontrolled case.

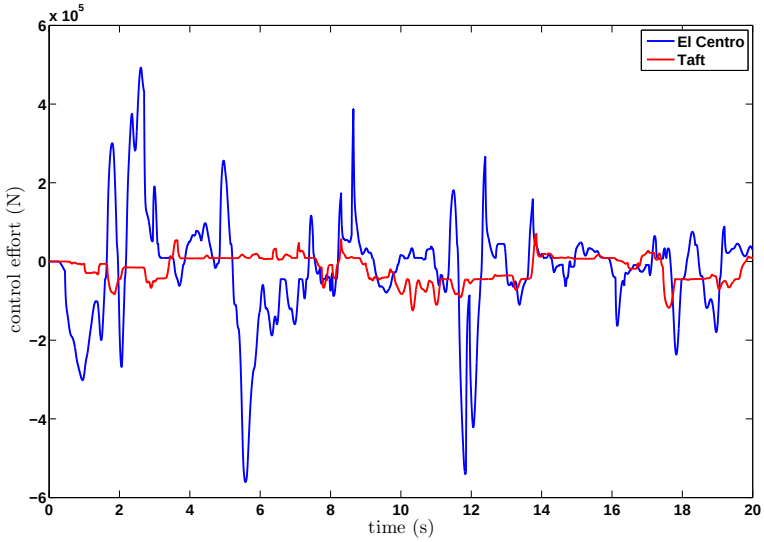

Figure 5.5: MR damper control effort.

equations:

$$S_m : \mathbf{M_{23}}\ddot{\mathbf{x}}_{\mathbf{a23}} + \mathbf{C_{23}}\dot{\mathbf{x}}_{\mathbf{a23}} + \mathbf{K_{23}}\mathbf{x_{a23}} = \mathbf{B_{23}}\mathbf{x_{a1}} + \mathbf{F_g} \tag{5.35}$$

$$S_b : m_1\ddot{x}_{a1} + c_{11}\dot{x}_{a1} + k_{11}x_{a1} = -f_{mr} - f_c + f_g \tag{5.36}$$

where S_m stands for the super substructure subsystem (the two upper floors, subsystem without control) and S_b is the first floor subsystem (controlled system). The a sub-index means absolute coordinates; $\mathbf{x_{a23}} = [x_{a2}, x_{a3}]^{\mathrm{T}}$ is the absolute displacement vector of the two upper floors and $\mathbf{x_{a1}} = [x_{a1}, \dot{x}_{a1}]^{\mathrm{T}}$ is a vector composed of the absolute displacement and velocity of the first floor. $\mathbf{F_g} = [(c_{21} + c_{22} + c_{23)})\dot{x}_g + (k_{21} + k_{22} + k_{23)})x_g, 0]^{\mathrm{T}} \approx [0, 0]^{\mathrm{T}}$. The matrices $\mathbf{M_{23}}$, $\mathbf{C_{23}}$, $\mathbf{K_{23}}$ and $\mathbf{B_{23}}$ are given by:

$$\begin{aligned} \mathbf{M_{23}} &= \begin{bmatrix} m_2 & 0 \\ 0 & m_3 \end{bmatrix} & \mathbf{C_{23}} &= \begin{bmatrix} c_{22} & c_{23} \\ c_{32} & c_{33} \end{bmatrix} \\ \mathbf{K_{23}} &= \begin{bmatrix} k_{22} & k_{23} \\ k_{32} & k_{33} \end{bmatrix} & \mathbf{B_{23}} &= \begin{bmatrix} -k_{21} & -c_{21} \\ 0 & 0 \end{bmatrix} \end{aligned} \tag{5.37}$$

f_c is the coupling force between the first floor subsystem and the superior substructure and f_g is the force due to the seismic motion:

$$f_c = c_{12}\dot{x}_{a2} + k_{12}x_{a2} \tag{5.38}$$

$$f_g = (c_{11} + c_{12})\,\dot{x}_g + (k_{11} + k_{12})\,x_g \tag{5.39}$$

The propositions about the intrinsic stability of the structure that were stated in Section 4.1 will be used in formulating the control laws. These propositions are reformulated as follows:

Proposition 1. *The unforced superior substructure subsystem S_m is globally exponentially stable for any bounded initial conditions.*

Proposition 2. *If the coordinates $(x_{a1}, \dot{x}_{a1})$ of the first floor and the coupling term $\mathbf{B_{23}x_{a1}}$ are uniformly bounded, then the superior substructure subsystem is stable and the coordinates $(x_{a2,a3}, \dot{x}_{a2,a3})$ of the superior substructure are uniformly bounded for all $t \geq 0$ and any bounded initial conditions.*

In this way, the controller is designed for the first floor subsystem assuming that it will stabilize the overall system. Finally, to proceed with the controller formulation, Eq. 5.36 is written in state space form so that the backstepping technique can be applied:

$$\dot{y}_1 = y_2 \tag{5.40}$$

$$\dot{y}_2 = -\frac{k_{11}}{m_1} y_1 - \frac{c_{11}}{m_1} y_2 - \frac{1}{m_1}(f_{mr} + f_c - f_g) \tag{5.41}$$

where $y_1 = x_{a1}$ is the first floor absolute displacement and $y_2 = \dot{x}_{a1}$ is the first floor absolute velocity.

Consider the system of Eqs. 5.40 - 5.41. The following control law attenuates the vibrations and stabilizes the main structure:

$$f_{mr} = (m_1 - k_{11} + h_1 h_2 m_1)\, y_1 + (h_1 m_1 - c_{11} + h_2 m_1)\, y_2 - f_c + f_g \tag{5.42}$$

where h_1 and h_2 are positive constants. To demonstrate it, consider the following standard backstepping variables:

$$e_1 = y_1 \quad e_2 = y_2 - \alpha_1 \quad \alpha_1 = -h_1 e_1 \tag{5.43}$$

Now consider the following Lyapunov function candidate and its derivative:

$$V = \tfrac{1}{2} e_1^2 + \tfrac{1}{2} e_2^2 \tag{5.44}$$

$$\dot{V} = e_1 \dot{e}_1 + e_2 \dot{e}_2 \tag{5.45}$$

Substitution of Eqs. 5.40, 5.41 and 5.43 into Eq. 5.45 yields:

$$\begin{aligned} \dot{V} &= e_1 \dot{e}_1 + e_2 \dot{e}_2 \\ &= e_1 y_1 + e_2 (\dot{y}_2 - \dot{\alpha}_1) = e_1 y_1 + e_2 \dot{y}_2 + h_1 \dot{e}_1 \\ &= e_1 y_1 + e_2 \left[-\frac{k_{11}}{m_1} y_1 - \frac{c_{11}}{m_1} y_2 - \frac{1}{m_1}(f_{mr} + f_c - f_g) \right] + h_1 y_2 \end{aligned} \tag{5.46}$$

Substitution of Eq. 5.42 into Eq. 5.46 yields:

$$\dot{V} = -h_1 e_1^2 - h_2 e_2^2 < 0 \tag{5.47}$$

According to Lyapunov's stability theory, $e_1 \to 0$ and $e_2 \to 0$. Consequently, $x_{a1} = y_1 = e_1 \to 0$ and $\dot{x}_{a1} = y_2 = e_2 + h_1 e_1 \to 0$. According to Propositions 1 and 2, the vibration of the base is asymptotically attenuated and the asymptotic stability of the main structure is guaranteed.

The control law of Eq. 5.42 cannot be implemented directly because the force to the MR damper cannot be commanded. Instead, a voltage signal must be sent to the damper to approximately generate the desired force. Two approaches are now considered to determine the voltage to the MR damper that can produce the damping force required to mitigate the vibrations.

The first approach is based on the Clipped Optimal Control algorithm by Dyke et al. (1996). The algorithm is graphically depicted in Figure 5.6. The dynamics of the MR damper are ignored and the control signal (i.e., the voltage) takes only two values, 0 V and 5 V, according to the following algorithm:

$$v = V_{max} H \left\{ (f_{mr} - f_{meas})\, f_{meas} \right\} \tag{5.48}$$

where $H\{\cdot\}$ is the Heaviside function, f_{mr} is the force generated by the backstepping controller and f_{meas} is the actual damping force actuating on the system.

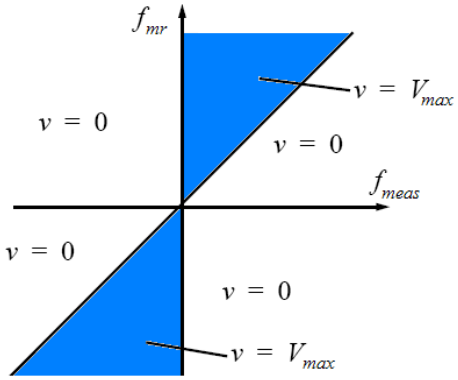

Figure 5.6: Graphical representation of the Clipped Optimal Algorithm.

The second approach consists in using the Bouc-Wen model of the MR damper so that its nonlinear dynamics are included in the controller design. Substituting $f_{mr} = S_F f^*_{mr}$, with f^*_{mr} as given in Eq. 4.20, and S_F being the force scaling factor of the RTHT setup, the following control law is obtained by solving for v:

$$\begin{aligned} v = & \frac{(m_1 - k_{11} + h_1 h_2 m_1)\, y_1 + (h_1 m_1 - c_{11} + h_2 m_1)\, y_2}{S_F \left[c_{0b} \frac{\dot{x}_{r1}}{S_L} + k_{mrb} \frac{x_{r1}}{S_L} + \alpha_{mrb} z \right]} \\ & - \frac{+f_c - f_g + S_F \left[c_{mra} \frac{\dot{x}_{r1}}{S_L} + k_{mra} \frac{x_{r1}}{S_L} + \alpha_{mra} z \right]}{S_F \left[c_{mrb} \frac{\dot{x}_{r1}}{S_L} + k_{mrb} \frac{x_{r1}}{S_L} + \alpha_{mrb} z \right]} \end{aligned} \tag{5.49}$$

provided that $S_F \left[c_{mrb} \frac{\dot{x}_{r1}}{S_L} + k_{mrb} \frac{x_{r1}}{S_L} + \alpha_{mrb} z \right] \neq 0$, otherwise $v = 0$.

The stability of the controller of Eq. 5.49 can be proved in a similar way as that of Eq. 5.42. Consider again the backstepping variables of Eq. 5.43 and the Lyapunov function candidate and its derivative of Eqs. 5.44 and 5.45. Substitution of Eqs. 4.20, 5.40 - 5.43 and 5.49 into Eq. 5.45 also yields $\dot{V} = -h_1 e_1^2 - h_2 e_2^2 < 0$, which guarantees the stability of the system.

5.3.2 Experimental results

The backstepping controllers were tested in the RTHT setup described previously. The numerical model, i.e. the 3-story building and the controller, are implemented in Matlab/Simulink. The ordinary differential equation solver used is the 4^{th} order Runge-Kutta method with a time step $T_s = 5 \times 10^{-4}$ seconds. The structure is subject to three different earthquake records, namely, El Centro, Loma Prieta and Northridge as shown in Figure 5.7; the scale amplitude used is 0.4. The controllers are implemented with $h_1 = 1 \times 10^{-3}$ and $h_2 = 1 \times 10^{-6}$. Table 5.1 shows the performance indices used to evaluate the controller performance.

The performance index for the different seismic excitations are shown in Table 5.2. Figures 5.8 - 5.11 show the structure response and the MR damper performance when subject to the El Centro seismic excitation. Figures 5.8 and 5.10 show the performance of the MR damper (the actual damper, i.e. not scaled), and particularly, a comparison of the dynamics predicted by the Bouc-Wen model and that obtained experimentally.

Performance indices J_1 - J_4 show that both controllers have a similar performance. However, performance indices J_5 and J_6 show that the control effort in the case of the controller based on the modified

Index	Description
$J_1 = max_{i,t}\left(\frac{\lvert\ddot{x}_{ai}(t)\rvert}{\ddot{x}_a^{max}(t)}\right)$	Normalized peak floor acceleration.
$J_2 = max_{i,t}\left(\frac{\lVert\ddot{x}_{ai}(t)\rVert}{\lVert\ddot{x}_a^{max}\rVert}\right)$	Normed peak acceleration
$J_3 = max(\lvert x_{r1}(t)\rvert)$	1^{st} floor peak relative displacement under control.
$J_4 = max(\lvert\ddot{x}_{a1}(t)\rvert)$	1^{st} floor peak absolute acceleration under control.
$J_5 = max_{t,i}\left(\frac{\lvert f_{mrd}(t)\rvert}{W}\right)$	Maximum control force.
$J_6 = \left(\frac{1}{\tau}\int_0^\tau [\dot{x}_m(t)]^2 dt\right)^{1/2}$	RMS control power.

Table 5.1: Performance indices.

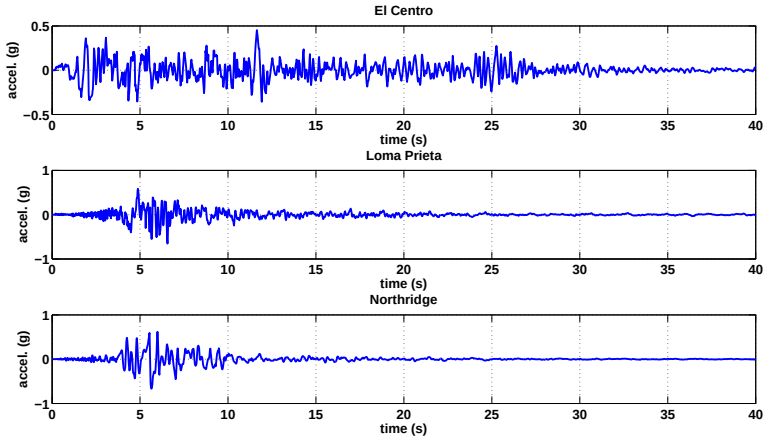

Figure 5.7: Records of El Centro, Loma Prieta and Northridge earthquakes.

clipped optimal algorithm is greater than that of the controller based on the dynamics of the MR damper. This can be explained by the fact that in the first case, the voltage is switching between two extreme cases (no current flowing through the damper coil and maximum current flowing through the damper coil). In the second case, the control signal changes in a smoother fashion and consequently, the control effort is reduced. According to the performance indices and the structure response, the control objectives were satisfactorily accomplished, i.e. a reduction in displacement and acceleration response was achieved with both backstepping controllers.

Earthquake	Controller	J_1	J_2	J_3 (cm)	J_4 (m/s^2)	J_5	J_6 (N)
El Centro	Clipped BS.	0.55	0.28	3.11	3.40	0.12	338.71
	Mod. based BS.	0.48	0.31	3.20	3.06	0.08	253.42
Loma Prieta	Clipped BS.	0.58	0.34	3.19	3.27	0.12	288.58
	Mod. based BS.	0.48	0.34	3.21	2.34	0.09	227.54
Northridge	Clipped BS.	0.72	0.38	4.61	4.51	0.12	286.87
	Mod. based BS.	0.75	0.41	5.82	3.29	0.11	231.07

Table 5.2: Controller performance indices under El Centro, Loma Prieta and Northridge earthquakes.

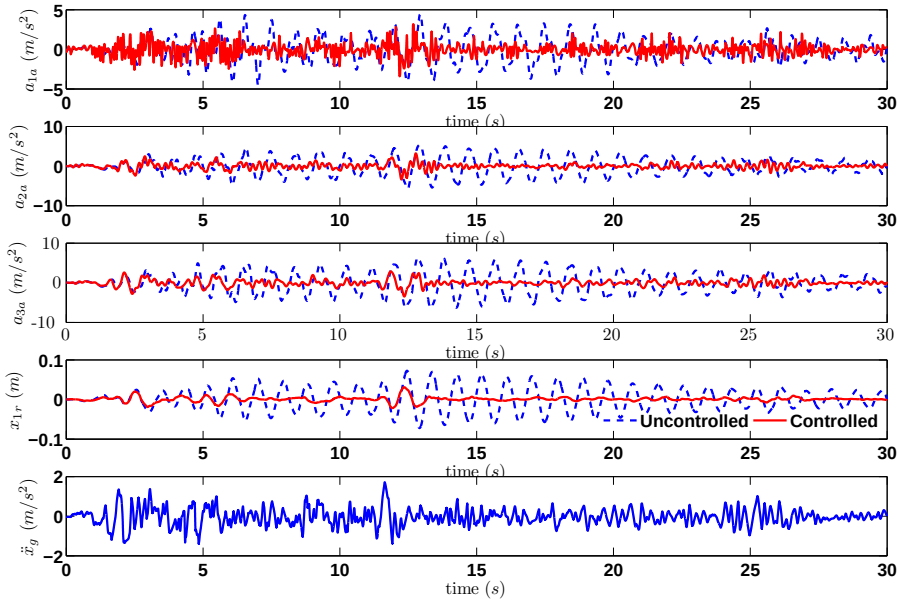

Figure 5.8: Clipped Backstepping: Structure response under El Centro earthquake.

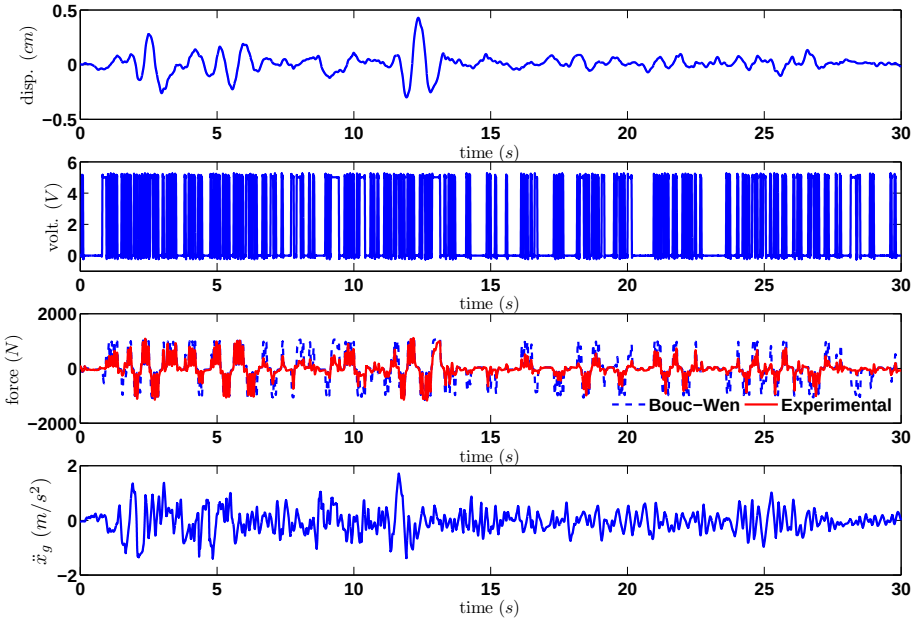

Figure 5.9: Clipped Backstepping: MR damper response under El Centro earthquake.

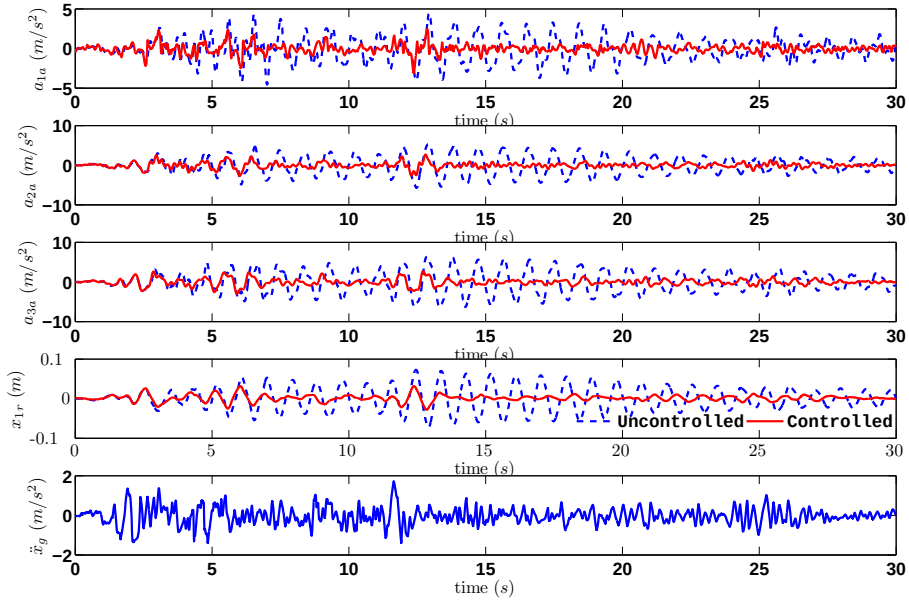

Figure 5.10: Model based Backstepping: Structure response under El Centro earthquake.

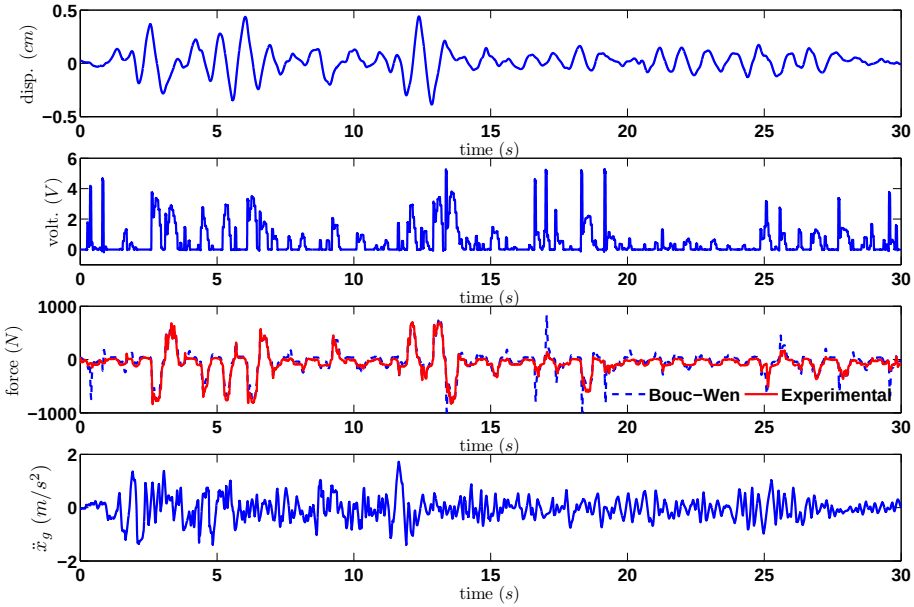

Figure 5.11: Model based Backstepping: MR damper response under El Centro earthquake.

5.4 Semiactive suspension system

In this section, a backstepping controller is designed for the semiactive suspension system described in Section 4.4.

5.4.1 Controller formulation

Consider the system of equations of the upper rocking lever, repeated here for convenience:

$$\dot{\alpha}_2 = \omega_2 \tag{5.50}$$
$$\dot{\omega}_2 = J_2^{-1}(M_{21} + M_{22} + M_{s2}) + J_2^{-1} r_{2f} f_{mr} \sin(\pi - \alpha_{2f} - \alpha_2 - \gamma_f) \tag{5.51}$$

where α_2 and ω_2 are the angular position and angular speed of the upper lever respectively. M_{21}, M_{22} and M_{s2} are the viscous friction damping torque, the gravitational forces torque and the spring torque action on the lower lever, respectively.

The objective of the semiactive control is to reduce the vibrations of the car body (the upper rocking lever) at the natural frequency (1.6 Hz). This can be achieved by reducing the angular velocity of the lever (ω_2). Thus, the system of Eqs. 5.50 and 5.51 will be controlled assuming that the lower rocking lever dynamics constitute the disturbances. The equilibrium point of the system is $(\alpha_{2equ}, \omega_{2equ}) = (0.55\,\text{rad}, 0)$, $f_{mr} = 0$. A change of coordinate is made so that the equilibrium point is set to $(0, 0)$. Thus, define z_1 and z_2 as the new coordinates according to:

$$(z_1, z_2) = (\alpha_2 - \alpha_{2equ}, \omega_2) \tag{5.52}$$

In the new coordinates, the system of Eqs. 5.50 and 5.51 becomes:

$$\dot{z}_1 = z_2 \tag{5.53}$$
$$\dot{z}_2 = J_2^{-1}(M_{21} + M_{22} + M_{s2}) + J_2^{-1} r_{2f} F_{eq} \sin(\pi - \alpha_{2f} - z_1\alpha_{2equ} - \gamma_f) f_{mr} \tag{5.54}$$

Define f and g as:

$$f = J_2^{-1}(M_{21} + M_{22} + M_{s2}) \tag{5.55}$$
$$g = J_2^{-1} r_{2f} F_{eq} \sin(\pi - \alpha_{2f} - z_1\alpha_{2equ} - \gamma_f) \tag{5.56}$$

The backstepping technique can now be applied to the system of Eqs. 5.53 and 5.54. First, define the following standard backstepping variables and their derivatives:

$$\begin{array}{ll} e_1 = z_1 & \dot{e}_1 = z_2 \\ e_2 = z_2 - \delta_1 & \dot{e}_2 = \dot{z}_2 + h_1 z_2 \\ \delta_1 = -h_1 e_1,\ h_1 > 0 & \dot{\delta}_1 = -h_1 z_2 \end{array} \tag{5.57}$$

Now define the following Lyapunov function candidate:

$$V = \frac{1}{2}V_1^2 + \frac{1}{2}V_2^2 = \frac{1}{2}e_1^2 + \frac{1}{2}e_2^2 \tag{5.58}$$

Deriving Eq. 5.58 and subsitution of Eqs. 5.53, 5.54 and 5.57 in the result yields:

$$\begin{aligned} \dot{V} =& e_1\dot{e}_1 + e_2\dot{e}_2 \\ =& e_1 e_2 - h_1 e_1^2 + e_2 f + e_2 g f_{mr} + h_1 z_2 e_2 \\ =& -h_1 e_1^2 - h_2 e_2^2 + e_2\left[(\alpha_2 - \alpha_{2equ})(1 + h_1 h_2) + (h_1 + h_2)\omega_2 + f + g f_{mr}\right] \end{aligned} \tag{5.59}$$

In order to make $\dot{V}$ negative, the following control law is proposed to generate the force f_{mr}:

$$f_{mr} = -\frac{(\alpha_2 - \alpha_{2equ})(1 + h_1 h_2) + (h_1 + h_2)\omega_2 + f}{g} \tag{5.60}$$

Substitution of Eq. 5.60 into Eq. 5.59 yields:

$$\dot{V} = -h_1 e_1^2 - h_2 e_2^2 < 0 \ \ \forall h_1, h_2 > 0 \tag{5.61}$$

Thus, according to the Lyapunov stability theory, the system is asymptotically stable. Therefore $e_1 \to 0$ and $e_2 \to 0$, and consequently $\alpha_2 \to \alpha_{2equ}$ and $\omega_2 \to 0$.

However, since the control force f_{mr} cannot be commanded directly, voltage or current signals are used as the control input to approximately generate the desired damping force. Assuming the f_{mr} is given by Eqs. 4.52 - 4.54, the current commanding signal is derived from Eq. 5.60 as follows:

$$i = \frac{-(\alpha_2 - \alpha_{2equ})(1 + h_1 h_2) - (h_1 + h_2)\omega_2 f - g\left[f_{c2}\tanh(\mu(\dot{x}_p + S_d)) + c_{mr2}(\dot{x}_p + pS_d)\right]}{g\left[f_{c1}\tanh(\mu(\dot{x}_p + S_d)) + c_{mr1}\right]} \tag{5.62}$$

5.4.2 Experimental results

The backstepping controller was implemented in Matlab/Simulink and different scenarios were tested. Figures 5.12 - 5.14 show the response of the semiactive suspension system in two cases: uncontrolled, i.e., no current is flowing through the MR damper coils and controlled, i.e., the backstepping controller is on. Each figure shows the angular position of the upper rocking lever with respect to the equilibrium point, the angular velocity, the PWM control signals and the estimated MR damper force.

Figure 5.12 shows the response when the SAS is excited in a range of frequencies from 0.75 Hz to 2 Hz. At 1.6 Hz approximately, the system is in resonance. Figure 5.13 shows the response when the SAS is being excited at 1.6 Hz, i.e., the resonance frequency. Finally, Figure 5.14 shows the response to a step input from 1.6 Hz to 0.1 Hz. In all cases, it can be seen that the backstepping controller is able to reduce the response of the system at the frequency of resonance. The control effort is always within the limits of the damper ($\pm 500N$).

5.5 Summary

In this chapter, new semiactive controllers based on the backstepping technique have been proposed to reduce the vibrations in different structures equipped with MR dampers. Three backstepping controllers were proposed. The first one is an adaptive backstepping controller that accounts for the uncertainties of the system and the unmeasurable variables. The uncertainties that characterize the stiffness and damping coefficients have been approached by deriving adaptive laws that estimate their values. The proposed control law also takes into account the nonlinearities of the frictional and hysteretic dampers as well as the unknown disturbances that the structure is subject to. The second controller is a modification of the the clipped optimal algorithm which is characterized by switching between two control signals and ignoring the damper dynamics. The third one is a simpler approach than the first, which does not include adaptation laws. The controllers were tested in numerical simulations and experimental platforms. All controllers successfully achieved the goal of reducing the system response when subject to external vibrations.

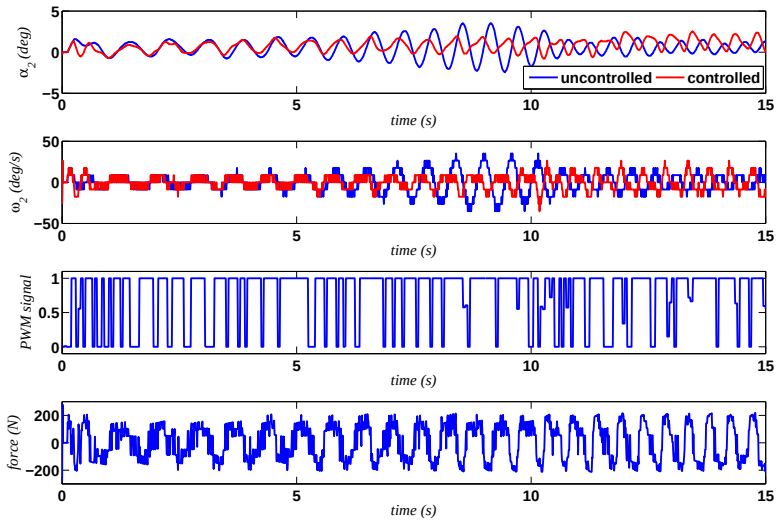

Figure 5.12: Backstepping controller for the SAS: chirp excitation.

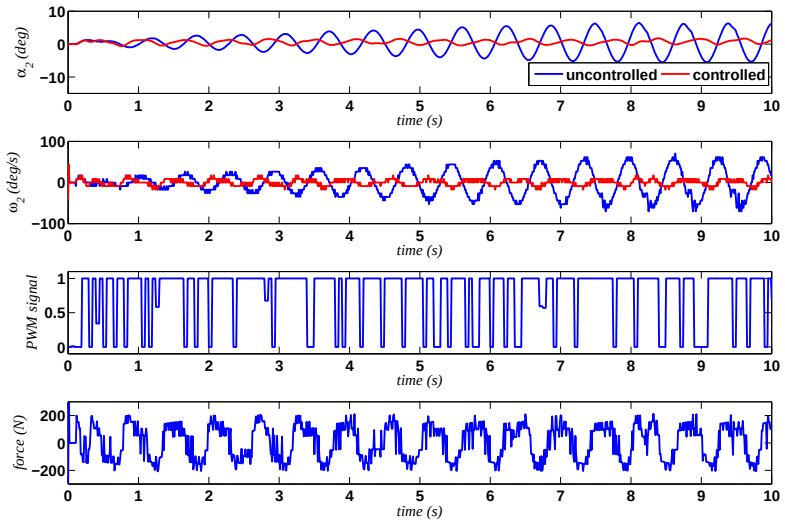

Figure 5.13: Backstepping controller for the SAS: excitation at resonance frequency.

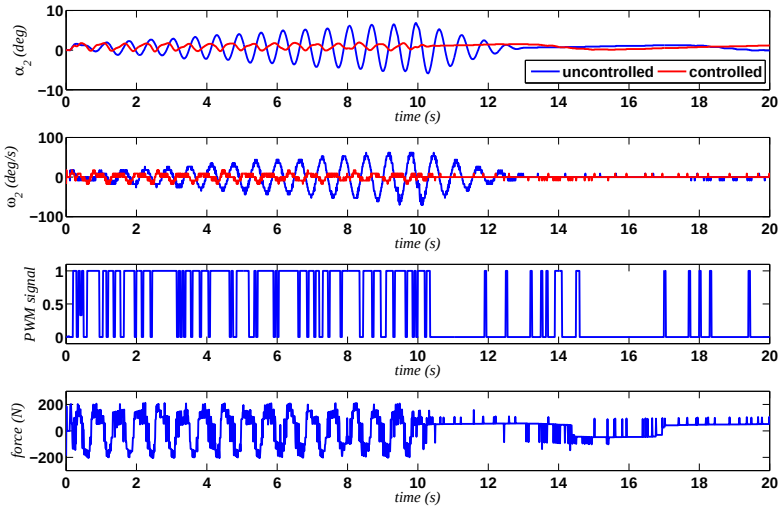

Figure 5.14: Backstepping controller for the SAS: step excitation.

Chapter 6

Robust control in frequency domain: Quantitative Feedback Theory based control

The vibration mitigation problem in flexible structures with MR dampers is covered in this chapter from a frequency-domain perspective. It had been discussed previously in this dissertation (Chapters 2 and 5) how to approach this problem with time-domain techniques. In fact, most of semiactive structural control strategies are based on the idea of attenuating vibrations or maintaining structural time response within certain acceptable ranges, when external forces such as earthquakes or strong winds act on the structures. The controller design is usually done in time-domain by considering that the system model and its associated parameters are known or uncertain but with known upper and lower bounds. Since the behavior of controlled structures depends not only on the magnitude of the external excitation but also on its frequency modes, the modal frequency control is of a great interest for achieving the structural safety and human comfort.

One of the goals of this research is to contribute with a new frequency-based methodology to mitigate vibrations in flexible structures. It has been chosen the Quantitative Feedback Theory (QFT) control because it is a methodology that systematically accounts for several factors such as parametric uncertainties, disturbance rejection and nonlinearities. Thus, the controller can be designed so as to guarantee stability and robustness at each frequency of interest. This is advantageous in structural control because the controller can be formulated accounting for the natural frequencies of the system. Additionally, the actuator nonlinearities can be incorporated in the control formulation by choosing an appropriate representation of its dynamics. This representation is an uncertain linear system whose uncertain parameters take the appropriate values so as to approximately describe the true dynamics of the system.

This chapter is organized as follows. Section 6.1 introduces the concept of Quantitative Feedback Theory. Then, the application of the QFT methodology to different cases is presented. Thus, in Section 6.2, it is considered the case of a 6-story building with two MR dampers subject to seismic excitations. The goal is to explore the QFT control application to this class of structures. Furthermore, an uncertain linear system representation is proposed to approximate the dynamics of the MR dampers so that the actuator nonlinearities can be incorporated in the controller formulation. Section 6.3 considers the experimental testing of different QFT controllers for 3-story building with an MR damper. These experiments are executed in the real-time hybrid testing platform used previously to test the backstepping controllers. The chapter concludes with a summary of the obtained results.

6.1 Quantitative Feedback Theory

QFT is a frequency control methodology based on the notion that feedback is only necessary when there is uncertainty and unmeasurable disturbances actuating on the plant. The basic developments with QFT are focused on the control design problem for uncertain Linear Time Invariant (LTI) Systems, as shown in Figure 6.1. In this figure, **R** represents the command input set, **P** the plant set and **T** the transfer function set. For each $R(s) \in \mathbf{R}$, $P(s) \in \mathbf{P}$, the closed loop output will be $Y(s) = T(S)R(s)$ for some $T(s) \in \mathbf{T}$. For a large class of such problems, QFT is executable, i.e., a pair of controller $F(s)$ and $G(s)$ can be found to guarantee that $Y(s) = T(S)R(s)$. Suppose that the plant $P(s)$ is an uncertain but known member of the set **P**. The designer is free to choose the prefilter $F(s)$ and the compensator $G(s)$ in order to ensure that the system transfer function $T(s) = F(s)P(s)G(s)/(1 + P(s)G(s))$ satisfies the assigned specifications.

The uncertain plant model $P(s)$ and its frequency and time domain specifications are represented in the Nichols chart through the use of the Borowitz-Sidi bounds. These bounds determine the regions where the nominal open loop transfer function $L_0(s) = G(s)P_0(s)$ may lie so that all the design specifications can be achieved.

The QFT methodology design can be summarized as follows (Houpis et al. 2006):

- **Plant model, template generation and nominal plant election.** The plant is represented in the Laplace domain; each uncertain parameter is assigned a range of variation and the frequencies of interest are chosen within the expected operation range. At each frequency of interest and for each possible value of the uncertain parameters, the plant model $P(j\omega)$ becomes a complex number that can be represented in the Nichols chart (dB, Φ). This set of complex numbers is called the templates.

- **Design specifications.** The inputs to the system of system of Figure 6.1 are $R(s)$ (the reference), $W(s)$, $D_1(s)$ and $D_2(s)$ (the disturbances) and $N(s)$ (the noise). $Y(s)$ is the variable to be controlled, $E(s)$ is the error and $U(s)$ is the control signal. The following transfer functions can be obtained:

$$Y = \frac{1}{1+PGH}D_2 + \frac{P}{1+PGH}D_1 + \frac{PG}{1+PGH}(W+FR) - \frac{PGH}{1+PGH}N \tag{6.1}$$

$$U = \frac{G}{1+PGH}(W+FR) - \frac{GH}{1+PGH}(N+D_2+D_1) \tag{6.2}$$

$$E = -\frac{H}{1+PGH}D_2 + \frac{PH}{1+PGH}D_1 + \frac{PGH}{1+PGH}W + \frac{1}{1+PGH}FR - \frac{H}{1+PGH}N \tag{6.3}$$

By limiting the transfer function magnitudes of Eqns. 6.1 - 6.3, it is possible to set the stability and robustness specifications such as disturbance rejection, tracking and noise rejection.

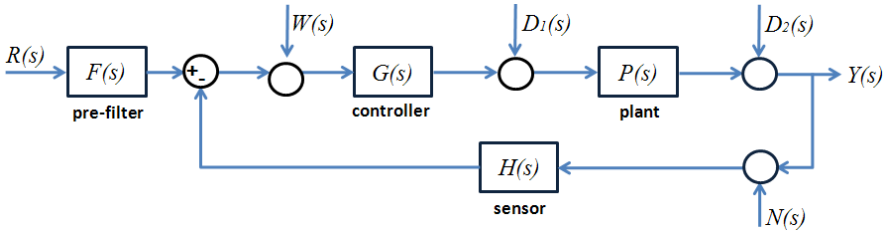

Figure 6.1: Schematic of the QFT control system.

- **Bound generation.** Once chosen the nominal plant, the next step is to transform the closed loop specifications of uncertainty plants in a set of restriction curves or bounds as known as Horowitz-Sidi bounds for each frequency of interest on the Nichols chart. This information synthesis allows the design of the controller using only the nominal plant. For each frequency and for each design specification there is one bound. When all these bounds are calculated, then the most restrictive one per frequency is kept.
- **Loop shaping.** When the most restrictive bounds are found, the controller is synthesized by adding a gain, poles and zeros such that the loop function $L_0(j\omega)$ lies in the Nichols chart in the regions where the design specifications can be achieved. The optimal controller is the one that, having the minimum gain, lies on the bounds at each frequency of interest. In this case, it is possible to affirm that the controller accomplishes all the design specifications.
- **Prefilter.** When tracking specifications are required, the prefilter $F(s)$ must be designed. The prefilter synthesis is similar to that of the controller.
- **Design validation.** This step involves the performance evaluation of the controller and its adjustment until all the design specifications are satisfied within acceptable limits.

Most of the design process can be done with the help of software packages such as the QFT toolbox for MATLAB. The loop shaping process is left to the ability and experience of the designer.

6.2 QFT controllers for the 6-story building with 2 MR dampers

This section is devoted to explore the feasibility of the application of QFT techniques to the design of controllers for systems with 2 MR dampers (Section 4.2).

6.2.1 Controller formulation

In order to do it, firstly recall Eq. 4.12 that represents the dynamics of the 6-story building with two MR dampers. The equations of motions of the first and second floors are:

$$S_{f1} : m_1\ddot{x}_{r1} + (c_1 + c_2)\dot{x}_{r1} - c_2\dot{x}_{r2} + (k_1 + k_2)x_{r1} - k_2x_{r2} = -f_{mr1} - m_1\ddot{x}_g \tag{6.4}$$

$$S_{f2} : m_2\ddot{x}_{r2} - c_2\dot{x}_{r1} + (c_2 + c_3)\dot{x}_{r2} - c_3\dot{x}_{r3} - k_2x_{r1} + (k_2 + k_3)x_{r2} - k_3x_{r3} = -f_{mr2} - m_2\ddot{x}_g \tag{6.5}$$

where m_i, c_i and k_i are the mass, damping coefficient and stiffness of each floor, respectively; x_{ri} are the relative displacements of each floor, f_{mri} are the MR damper forces and $\ddot{x}_g$ is the seismic acceleration input. Taking the Laplace transform to Eqs. 6.4 and 6.5 yields:

$$\begin{aligned} m_1s^2X_{r1}(s) &= -(c_1 + c_2)sX_{r1}(s) + c_2sX_{r2}(s) - (k_1 + k_2)X_{r1}(s) + k_2X_{r2}(s) - F_{mr1}(s) - m_1\ddot{X}_g(s) \\ X_{r1}(s) &= \frac{1}{m_1s^2 + (c_1 + c_2)s + k_1 + k_2}\left[-F_{mr1}(s) + c_2sX_{r2}(s) + k_2X_{r2}(s) - m_1\ddot{X}_g(s)\right] \end{aligned} \tag{6.6}$$

Similarly, by taking the Laplace transform of the second floor subsystem, it is obtained:

$$\begin{aligned} m_2s^2X_{r2}(s) &= c_2sX_{r1}(s) - (c_2 + c_3)sX_{r2}(s) + c_3sX_{r3}(s) + k_2X_{r1}(s) - (k_2 + k_3)X_{r2}(s) + k_3X_{r3}(s) \\ &\quad - F_{mr2}(s) - m_2\ddot{X}_g(s) \\ X_{r2}(s) &= \frac{1}{m_2s^2 + (c_2 + c_3)s + k_2 + k_3}\left[-F_{mr2}(s) + c_2sX_{r1}(s) + c_3sX_{r3}(s) + k_2X_{r1}(s) + k_3X_{r3}(s)\right] \\ &\quad - \frac{1}{m_2s^2 + (c_2 + c_3)s + k_2 + k_3}m_2\ddot{X}_g(s) \end{aligned} \tag{6.7}$$

Evidently, the terms $F_{mr1}(s)$ and $F_{mr2}(s)$ from Eqs. 6.6 and 6.7 cannot be computed because these are the nonlinear dynamics of the MR damper. To overcome this problem, it is proposed a simple

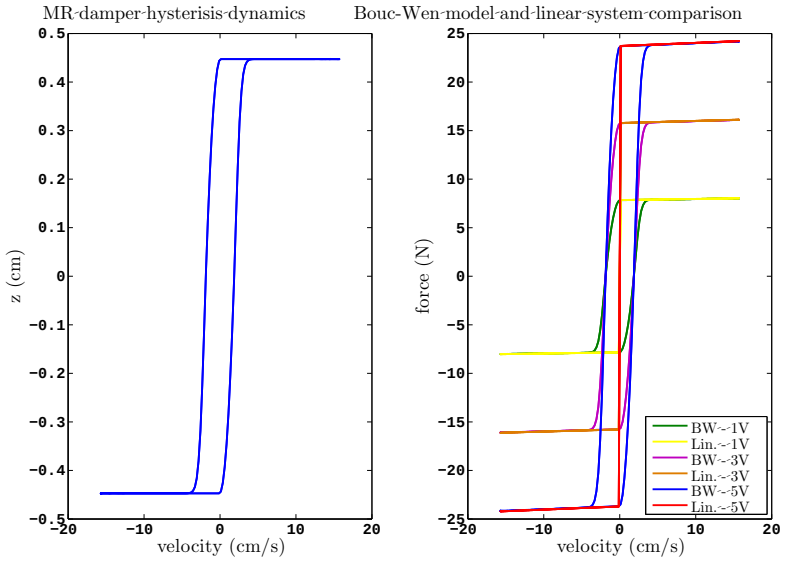

Figure 6.2: Left: MR damper hysteretic dynamics. Right: Bouc-Wen model and linear approximation comparison.

representation of the MR damper dynamics as an uncertain linear system. In order to do it, consider the Bouc-Wen model of the MR dampers installed in the structure (Eqs. 4.9 - 4.11). It can be decomposed into two parts: one linear and another nonlinear. Thus, the force f_{mri} of each MR damper can be represented as:

$$f_{lin} = (c_{mra} + c_{mrb}v)\,\dot{x}_{ri} = a_1\dot{x}_{ri} \tag{6.8}$$

$$f_{nonlin} = (\alpha_{mra} + \alpha_{mrb}v)\,z_0 = u_d z_0 \tag{6.9}$$

$$f_{mri} = f_{lin} + f_{nonlin} \tag{6.10}$$

From Eq. 6.8, it is observed that the parameter a_1 varies only with the input voltage (v). The second parameter, z_0 in Eq. 6.9 (left hand), is a bounded parameter. At high velocities, z is approximately constant and thus, z_0 could take either the maximum or the minimum value depending on the signs of velocity, as can be seen in Figure 6.2. In this way, Eqs. 6.8 and 6.9 can be seen as a plant with 2 uncertain parameters namely, a_1 and z_0 that describe the dynamics of the damper. In this way, the damper dynamics appear to follow the Bingham model. Figure 6.2 (right hand) illustrates this approach with a sinusoidal displacement excitation at 3 levels of voltage.

The uncertain linear plant representation of the MR damper can now be incorporated into Eqs. 6.6 and 6.7. The Laplace transform of Eq. 6.10 is given by:

$$F_{mri}(s) = a_1 s X_{ri}(s) + z_o U_d(s) \tag{6.11}$$

Replacing Eq. 6.11 into Eqs. 6.6 and 6.7 yields:

$$X_{r1}(s) = \frac{z_0}{m_1 s^2 + (c_1 + c_2 + a_1)s + k_1 + k_2}\left[-U_{d1}(s) + \frac{1}{z_0}\left(c_2 s X_{r2}(s) + k_2 X_{r2}(s) - m_1\ddot{X}_g(s)\right)\right] \tag{6.12}$$

$$\begin{aligned} X_{r2}(s) = {} & \frac{z_0}{m_2 s^2 + (c_2 + c_3 + a_1)s + k_2 + k_3}\left[-U_{d2}(s) + \frac{1}{z_0}\left(c_2 s X_{r1}(s) + c_3 s X_{r3}(s)\right)\right] \\ & + \frac{z_0}{m_2 s^2 + (c_2 + c_3 + a_1)s + k_2 + k_3}\left[\frac{1}{z_0}\left(k_2 X_{r1}(s) + k_3 X_{r3}(s) - m_2\ddot{X}_g(s)\right)\right] \end{aligned} \tag{6.13}$$

From Eqs. 6.12 and 6.13, and following the notation of Figure 6.1, the plants $P_1(s)$ and $P_2(s)$, the control inputs $U_1(s)$ and $U_2(s)$, and the disturbances to plant $D_{1,1}(s)$ and $D_{1,2}(s)$ are obtained as follows, respectively:

$$P_1(s) = \frac{z_0}{m_1 s^2 + (c_1 + c_2 + a_1)s + k_1 + k_2} \tag{6.14}$$

$$U_1(s) = -U_{d1}(s) + c_2 s X_{r2}(s) + k_2 X_{r2}(s) \tag{6.15}$$

$$D_{1,1}(s) = -m_1 \ddot{X}_g(s) \tag{6.16}$$

$$P_2(s) = \frac{z_0}{m_2 s^2 + (c_2 + c_3)s + k_2 + k_3} \tag{6.17}$$

$$U_2(s) = -U_{d2}(s) + c_2 s X_{r1}(s) + c_3 s X_{r3}(s) + k_2 X_{r1}(s) + k_3 X_{r3}(s) \tag{6.18}$$

$$D_{1,2}(s) = -m_2 \ddot{X}_g(s) \tag{6.19}$$

The uncertain parameters and QFT controller specifications are: $a_1 = [0.0064, 0.0324]$ N-s/cm, and $z_0 = \{-0.448, 0.448\}$ cm. The stiffness and damping coefficients of the structure vary in ± 10 %. The frequencies of interest are the natural frequencies of the system, i.e., 1.29 Hz, 3.85 Hz, 6.11 Hz, 8.22 Hz, 9.64 Hz and 10.81 Hz. The controller performance should accomplish the following bounds: robust performance $W_{s1} = 1.2$ and disturbance rejection $W_{s3} = 3.4 \times 10^{-4}$.

Figures 6.3 - 6.5 depict different stages of the controllers design: templates and initial approach ($G_1(s) = 0$) and final loop. Figure 6.6 shows the analysis of the closed loop response for the robust performance and disturbance rejection problems for the range of frequencies studied. The final controller of the first floor, $G_1(s)$, with a displacement input measured in centimeters and output $U_{d1}(s)$ (measured in Newton-centimeter), is given by:

$$G_1(s) = 7735.14 \frac{1.44 \times 10^{-6} s^3 + 0.0011 s^2 + 0.192 s + 1}{3.887 \times 10^{-7} s^3 + 2.3762 \times 10^{-4} s^2 + 0.405 s + 1} \tag{6.20}$$

The controller of the second floor is designed in a similar way, with the same parameters and design constraints. The resulting controller is:

$$G_2(s) = 6574 \frac{7.05 \times 10^{-6} s^3 + 7.16 \times 10^{-4} s^2 + 0.0320 s + 1}{2.045 \times 10^{-6} s^3 + 5.225 \times 10^{-4} s^2 + 0.044 s + 1} \tag{6.21}$$

6.2.2 Numerical results

In order to verify the performance of the controllers, simulations were performed using scaled versions of the El Centro, Loma Prieta and Northridge earthquakes. Figures 6.7 and 6.8 show the response of the MR damper in the case of El Centro seismic excitation. These figures show the displacement response of the first and the second floor in the case there is not any damper on the structure and the case when the controllers are active. Additionally, Table 6.1 lists the performance index discussed outlined in Table 5.1. Indices J_3 - J_6 were calculated for the first and second floors where the MR dampers are installed. The performance indices show a clear reduction in absolute acceleration and relative displacements with a reasonable control effort, within the damper capabilities.

6.3 Real-time hybrid testing of QFT controllers

In this section, QFT controllers will be formulated for the real-time hybrid testing of 3-story building structure with an MR damper (Section 4.3).

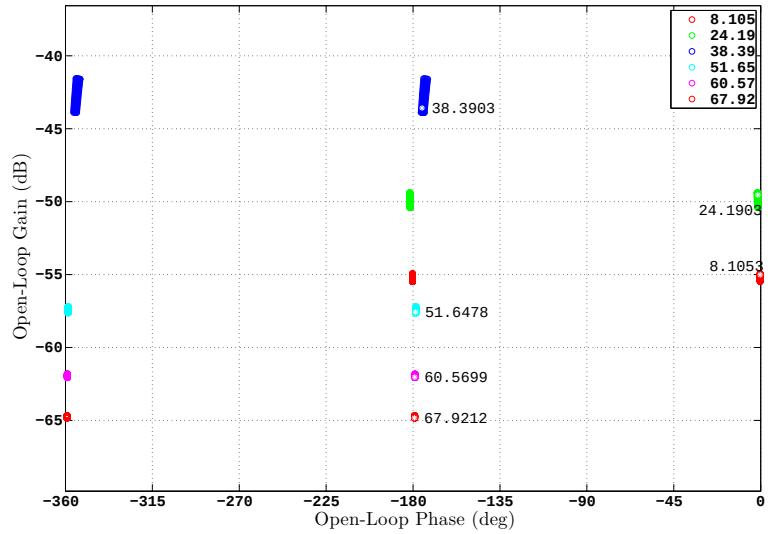

Figure 6.3: Templates for the first floor controller.

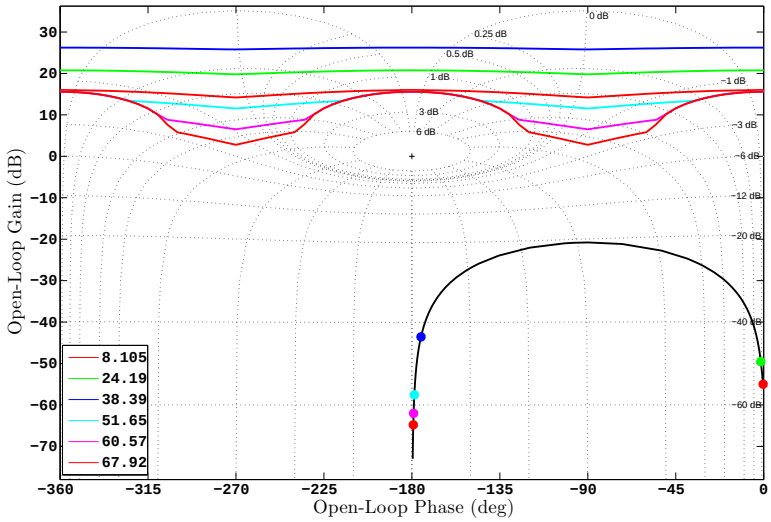

Figure 6.4: First floor QFT controller initial loop.

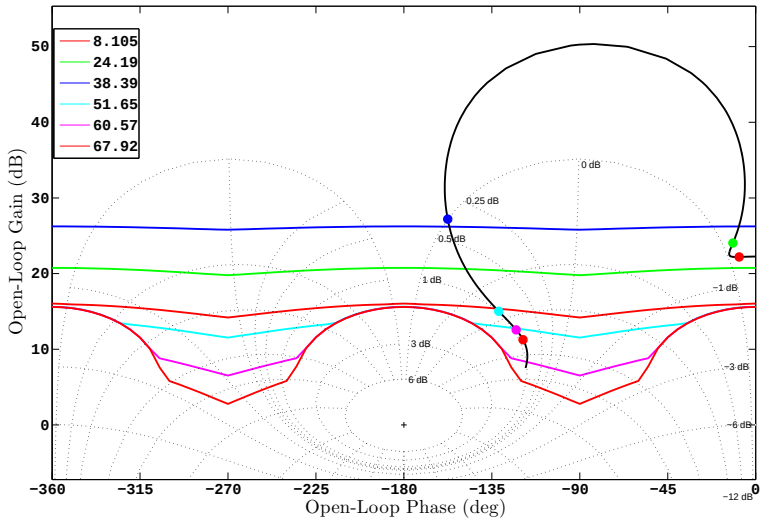

Figure 6.5: First floor QFT controller final loop.

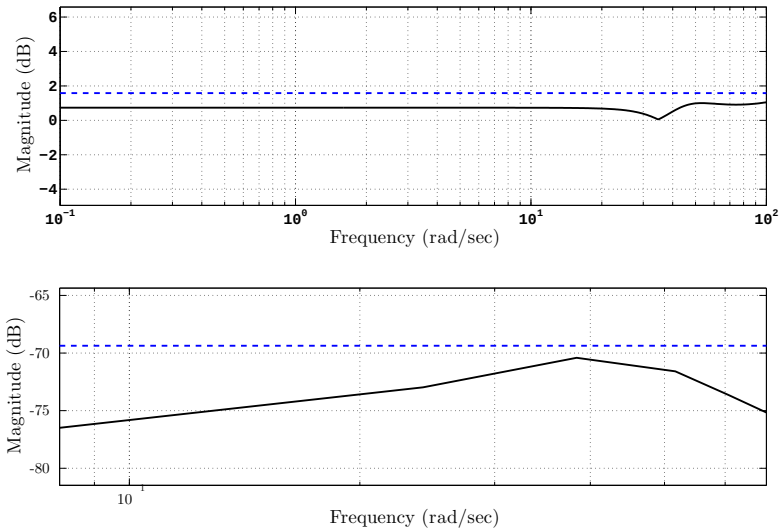

Figure 6.6: First floor controller closed loop analysis. Upper: robust performance. Lower: disturbance rejection.

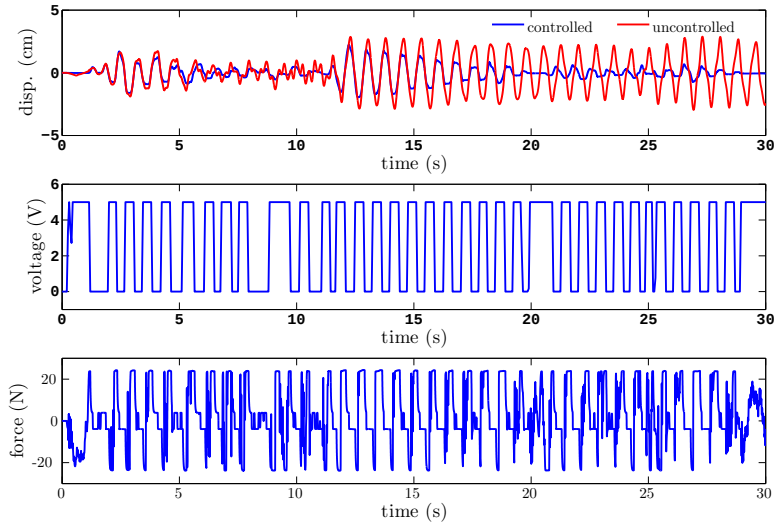

Figure 6.7: First floor MR damper response.

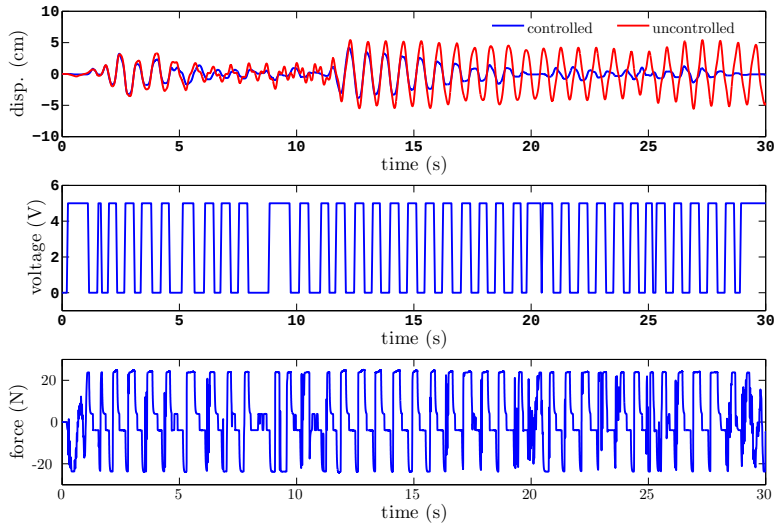

Figure 6.8: Second floor MR damper response.

Index	El Centro	Loma Prieta	Northridge
J_1	0.8185	0.6268	0.8244
J_2	0.4657	0.4131	0.4371
$J_{3,1}$ (cm)	2.1810	2.8493	2.8053
$J_{3,2}$ (cm)	4.1162	5.4729	5.3824
$J_{4,1}$ (cm/s^2)	352.6457	427.5446	643.4298
$J_{4,2}$ (cm/s^2)	518.1071	658.9434	863.4917
$J_{5,1}$	0.0183	0.0185	0.0187
$J_{5,2}$	0.0187	0.0191	0.0194
$J_{6,1}$ (N)	14.8913	14.7541	13.1978
$J_{6,2}$ (N)	16.0763	15.6517	15.3756

Table 6.1: Controller performance indices under El Centro, Loma Prieta and Northridge earthquakes.

6.3.1 Controller formulation

To begin with the design of the controllers, recall the system of Eqs. 5.35 and 5.36 in Section 5.3.1 where it was also discussed that the controller can be designed for the first floor while guaranteeing the stability of the whole structure. Now consider Eq. 5.36, repeated here for convenience:

$$S_b : m_1\ddot{x}_{a1} + c_{11}\dot{x}_{a1} + k_{11}x_{a1} = -f_{mr} - f_c + f_g \tag{6.22}$$

This equation written in relative coordinates becomes:

$$m_1\ddot{x}_{r1} + c_{11}\dot{x}_{r1} - c_{12}\dot{x}_{r2} + k_{11}x_{r1} - k_{12}x_{r2} = -f_{mr} - m_1\ddot{x}_g \tag{6.23}$$

Taking the Laplace transform of Eq. 6.23 yields:

$$m_1s^2X_{r1}(s) + c_{11}sX_{r1}(s) - c_{12}sX_{r2}(s) + k_{11}X_{r1}(s) - k_{12}X_{r2}(s) = -F_{mr}(s) - m_1\ddot{X}_g(s) \tag{6.24}$$

Rearranging terms from Eq. 6.24 yields:

$$X_{r1}(s) = \frac{1}{m_1s^2 + c_{11}s + k_{11}}\left[-F_{mr}(s) + c_{12}sX_{r2}(s) + k_{12}X_{r2}(s) - m_1\ddot{X}_g(s)\right] \tag{6.25}$$

From Eq. 6.25, and following the notation of Figure 6.1, it can be deduced that the plant $P_1(s)$, the input to the plant $U_1(s)$ and the input disturbance $D_1(s)$ are, respectively:

$$P_1(s) = \frac{1}{m_1s^2 + c_{11}s + k_{11}} \tag{6.26}$$

$$U_1(s) = -F_{mr}(s) + c_{12}sX_{r2}(s) + k_{12}X_{r2}(s) \tag{6.27}$$

$$D_1(s) = m_1\ddot{X}_g(s) \tag{6.28}$$

The force to the MR damper cannot be directly commanded. Instead, a voltage signal must be sent to the damper to approximately generate the desired force. Two approaches are now considered to determine the voltage to the MR damper that can produce the damping force required to mitigate the vibrations.

The first approach is based on the Clipped Optimal Control algorithm by Dyke et al. (1996) as discussed in Section 5.3.1. Following this approach, the controller is designed with these specifications: $c_{11} = 7243.2 \pm 5\%$ N-s/m, $k_{11} = 9932 \pm 5\%$ N/m; the frequencies of interest are the natural frequencies of the system, i.e., 1.09 Hz, 3.17 Hz and 4.74 Hz. The controller performance should achieve the following

bounds: robust performance $W_{s1} = 2$ and disturbance rejection $W_{s3} = 3 \times 10^{-2}$.

Figure 6.9 - 6.11 show different stages of the QFT controller design: the templates, the initial and final loops. Figure 6.12 shows the analysis of the closed loop response for the robust performance and disturbance rejection problems for the range of frequencies studied. The final controller, with input $X_{r1}(s)$ (the displacement, measured in meters) and output $U_1(s)$, (force, measured in Newtons) is given by:

$$G_1(s) = \frac{27541034(0.002s+1)(0.068s+1)(1.960s+1)}{(0.151s+1)(0.188s+1)^2} \tag{6.29}$$

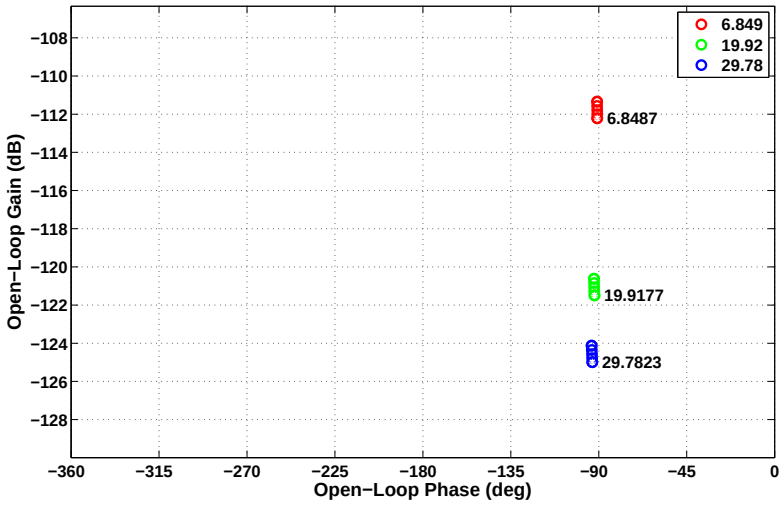

Figure 6.9: Templates of the system of Eq. 6.26.

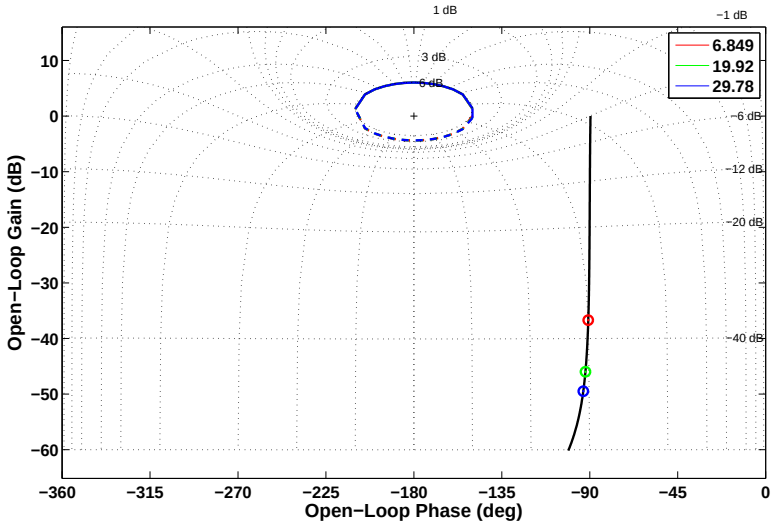

Figure 6.10: QFT controller initial loop: $G_1(s) = 1$.

The second approach consists of replacing the term $F_{mr}(s)$ with a Laplace representation of the damper dynamics, as it was done in Section 6.2. Consider again the Bouc-Wen model of the MR damper

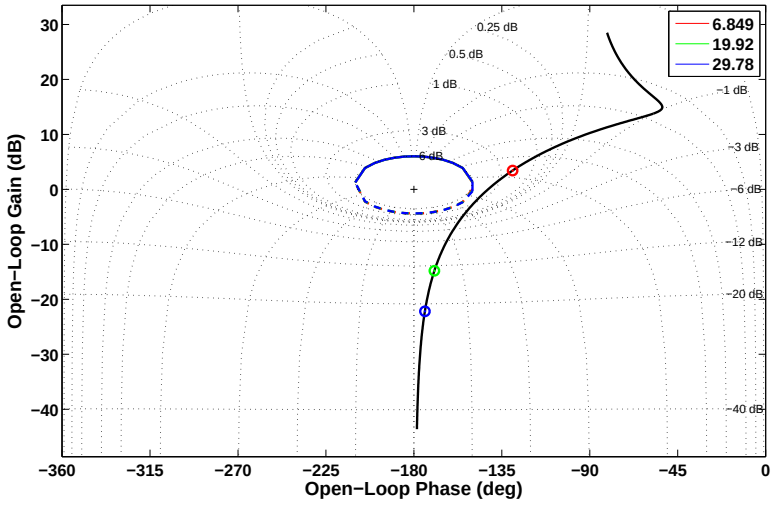

Figure 6.11: QFT controller final loop.

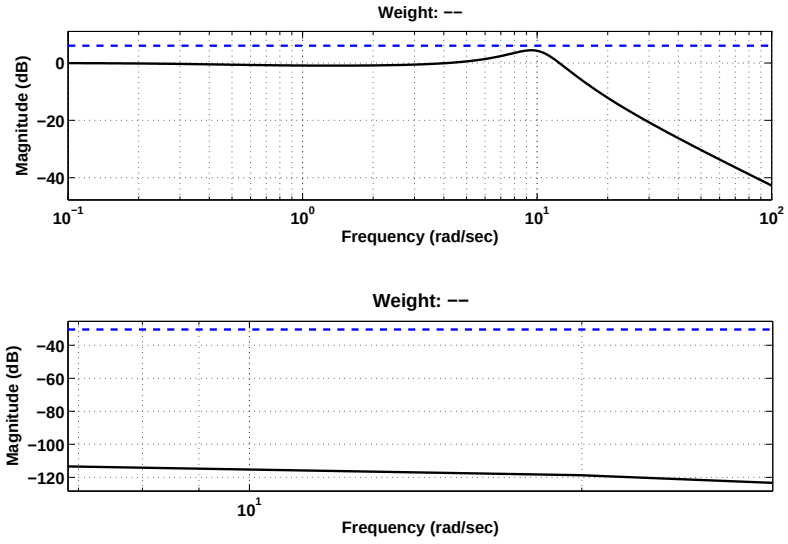

Figure 6.12: QFT controller closed loop analysis. Upper: robust performance. Lower: Disturbance rejection.

of Eq. 4.20. It can be decomposed into two parts: one linear and another nonlinear. Thus:

$$f_{lin} = (c_{mra} + c_{mrb}v)\,\dot{x}_{r1} + (k_{mra} + k_{mrb}v)\,x_{r1} = a_1\dot{x}_{r1} + a_2 x_{r1} \tag{6.30}$$

$$f_{nonlin} = (\alpha_{mra} + \alpha_{mrb}v)\,z_0 = z_0 u_d \tag{6.31}$$

$$f_{mr} = f_{lin} + f_{nonlin} \tag{6.32}$$

Eqns. 6.30 and 6.31 can be seen as a plant with 3 uncertain parameters namely, a_1, a_2 and z_0 that describe the dynamics of the damper. Figure 6.13 illustrates this approach with a sinusoidal displacement excitation at 3 levels of voltage.

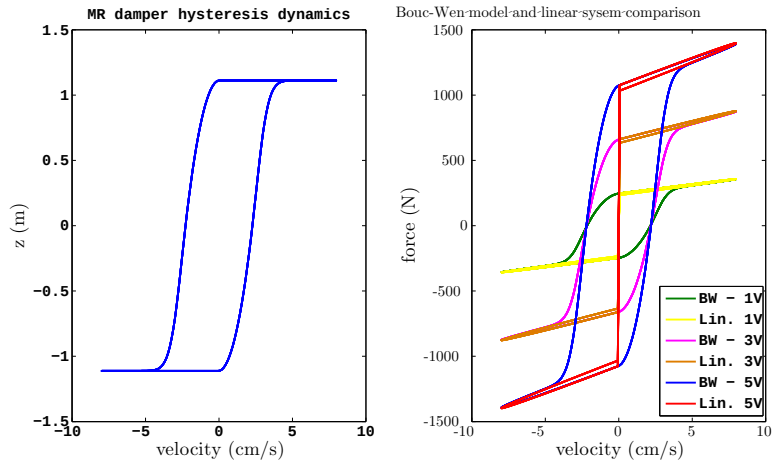

Figure 6.13: Left: MR damper hysteretic dynamics. Right: Bouc-Wen model and linear approximation comparison.

The representation of the MR damper as an uncertain linear plant can now be incorporated into Eq. 6.24. The Laplace transform of Eqns. 6.30 - 6.32 yields:

$$F_{mr}(s) = \frac{a_1 S_F}{S_L} s X_{r1}(s) + \frac{a_2 S_F}{S_L} X_{r1}(s) + S_F z_0 U_d(s) \tag{6.33}$$

Substitution of Eq. 6.33 into Eq. 6.24 yields:

$$X_{r1}(s) = \frac{-S_F z_0 U_d(s) + c_{12} s X_{r2}(s) + k_{12} X_{r2}(s) - m_1 \ddot{X}_g(s)}{m_1 s^2 + (c_{11} + \frac{a_1 S_F}{S_L})s + (k_{11} + \frac{a_2 S_F}{S_L})} \tag{6.34}$$

The plant $P_2(s)$ is now given by:

$$P_2(s) = \frac{S_F z_0}{m_1 s^2 + (c_{11} + a_1 S_F/S_L)s + (k_{11} + a_2 S_F/S_L)} \tag{6.35}$$

and the voltage can be estimated by manipulating the following equation:

$$U_2(s) = -U_d(s) + \frac{1}{S_F z_0}\left(c_{12} s X_{r2}(s) + k_{12} X_{r2}(s)\right) \tag{6.36}$$

The uncertain parameters and QFT controller specifications are: $a_1 = [754.41, 4318.06]$ N-s/m, $a_2 = [1137.57, 6855.07]$ N/m and $z_0 = \{-1.11, 1.11\}$ m. The frequencies of interest are the natural

frequencies of the system, i.e., 1.09 Hz, 3.17 Hz and 4.74 Hz. The controller performance should accomplish the following bounds: robust performance $W_{s1} = 2$ and disturbance rejection $W_{s3} = 3 \times 10^{-2}$.

Figures 6.14 - 6.16 depict different stages of the controllers design: templates and initial approach ($G_2(s) = 1$) and final loop. Figure 6.17 shows the analysis of the closed loop response for the robust performance and disturbance rejection problems for the range of frequencies studied. The final controller $G_2(s)$ with a displacement input measured in meters and output $U_i(s)$ (measured in Newton-meter), is given by:

$$G_2(s) = \frac{298(0.016s^2 + 0.073s + 1)(7.3 \times 10^{-4}s^2 + 0.051s + 1)(4.7 \times 10^{-3}s^2 + 2.15 \times 10^{-3}s + 1)}{(0.017s + 1)(0.033s + 1)(0.015s^2 + 0.095s + 1)(4.65 \times 10^{-3}s^2 + 0.060s + 1)} \quad (6.37)$$

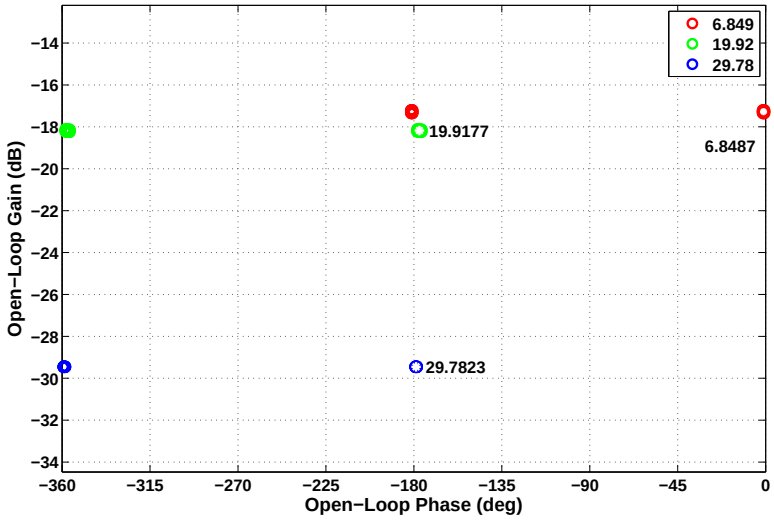

Figure 6.14: Templates of the system of Eq. 6.35.

6.3.2 Experimental results

The QFT controllers are now tested in the RTHT setup described previously. The numerical model, i.e. the 3-story building and the controller, are implemented in Matlab/Simulink. The ordinary differential equation solver used is the 4^{th} order Runge-Kutta method with a time step $T_s = 5 \times 10^{-4}$ seconds. The structure is subject to three different earthquake records, namely, El Centro, Loma Prieta and Northridge with a scale amplitude of 0.4.

The performance indices used to evaluate the controller performance are those of Table 5.1. The resulting indices for the different seismic excitations are shown in Table 6.2. Figures 6.18 - 6.21 show the structure response and the MR damper performance when subject to the Loma Prieta seismic excitation. Figures 6.19 and 6.21 show the performance of the MR damper (the actual damper, i.e. not scaled), and particularly, a comparison of the dynamics predicted by the Bouc-Wen model and that obtained experimentally.

Performance indices J_1 - J_4 show that both controllers have a similar performance and in most of cases, the QFT controllers based on the MR damper dynamics is better than the other. However, performance indices J_5 and J_6 show that for this controller to perform better in reducing the structure response, it makes use of a greater control effort. According to the performance indices and the structure response, the control objectives were satisfactorily accomplished, i.e. a reduction in displacement and acceleration

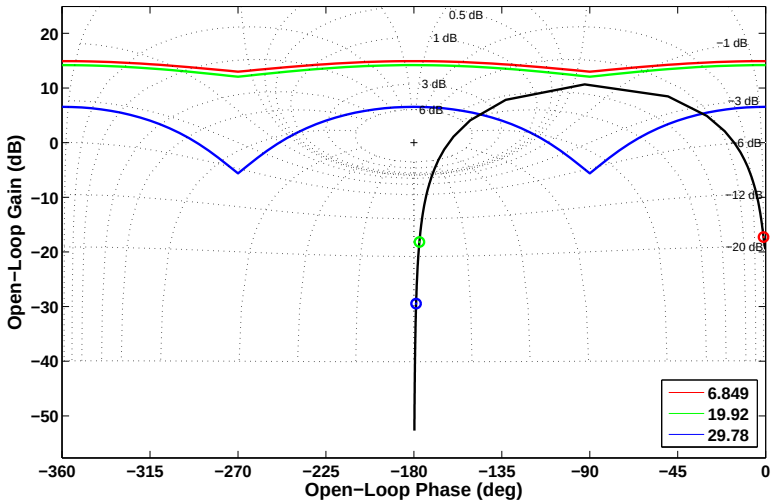

Figure 6.15: QFT controller initial loop: $G_2(s) = 1$.

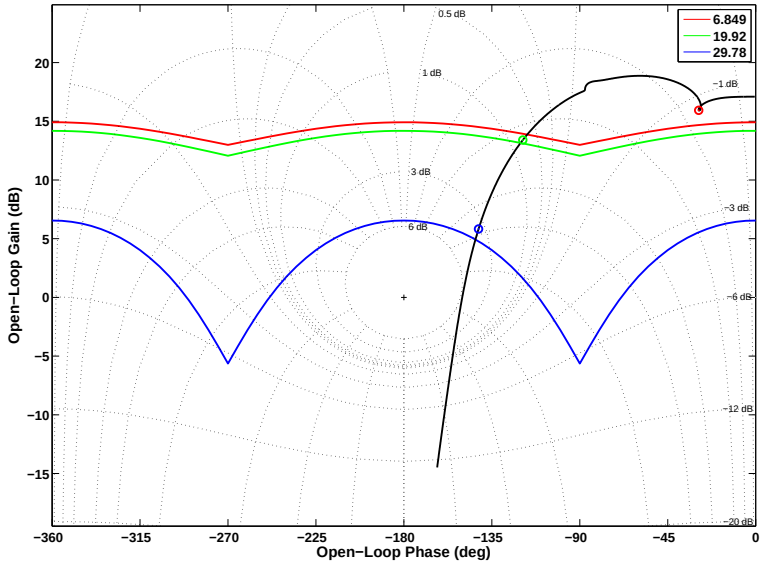

Figure 6.16: QFT controller final loop.

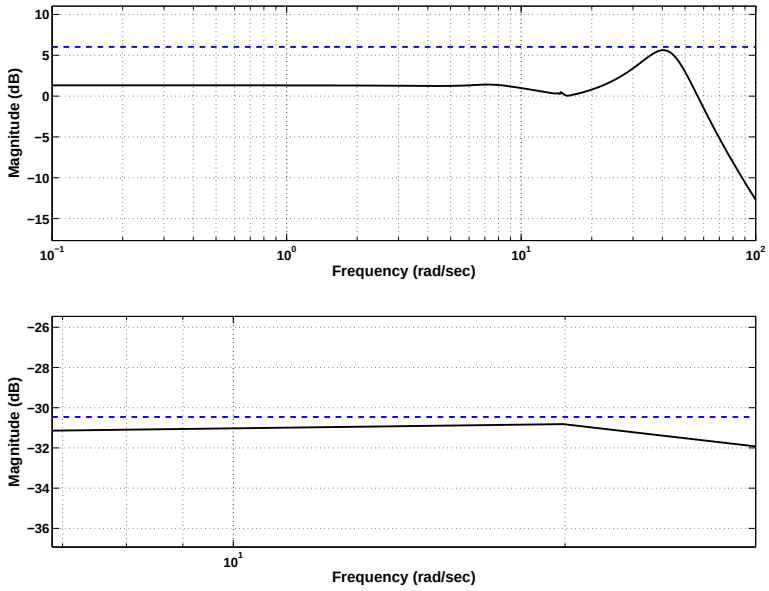

Figure 6.17: QFT controller closed loop analysis. Upper: robust performance. Lower: Disturbance rejection.

Earthquake	Controller	J_1	J_2	J_3 (cm)	J_4 (m/s^2)	J_5	J_6 (N)
El Centro	Clipped QFT	0.67	0.40	3.36	3.77	0.12	259.64
	Model based QFT	0.62	0.30	2.31	3.92	0.11	346.05
Loma Prieta	Clipped QFT	0.92	0.47	3.38	5.25	0.11	178.04
	Model based QFT	0.92	0.41	3.64	5.47	0.11	283.86
Northridge	Clipped QFT	0.73	0.52	6.27	5.94	0.11	202.37
	Model based QFT	0.64	0.42	4.76	5.06	0.11	302.42

Table 6.2: Controller performance indices under El Centro, Loma Prieta and Northridge earthquakes.

response was achieved with both QFT controllers.

6.4 Summary

This chapter has presented a novel QFT controller for vibration reduction in buildings equipped with MR dampers. A simple characterization of the nonlinear hysteretic cycle was proposed to represent the whole plant in the Nichols chart that contains the uncertainty template, by using the bounded LTI systems based on the LTI nominal one. The advantage of using QFT in structural control is that the design is made in the frequency domain, which is a very important issue, taking into account that disturbances are unknown and vibrations can excite the structure at its natural frequencies. The QFT based control design has taken into account these considerations. The applicability and effectiveness of the technique was demonstrated by means of both numerical simulations and experimental tests.

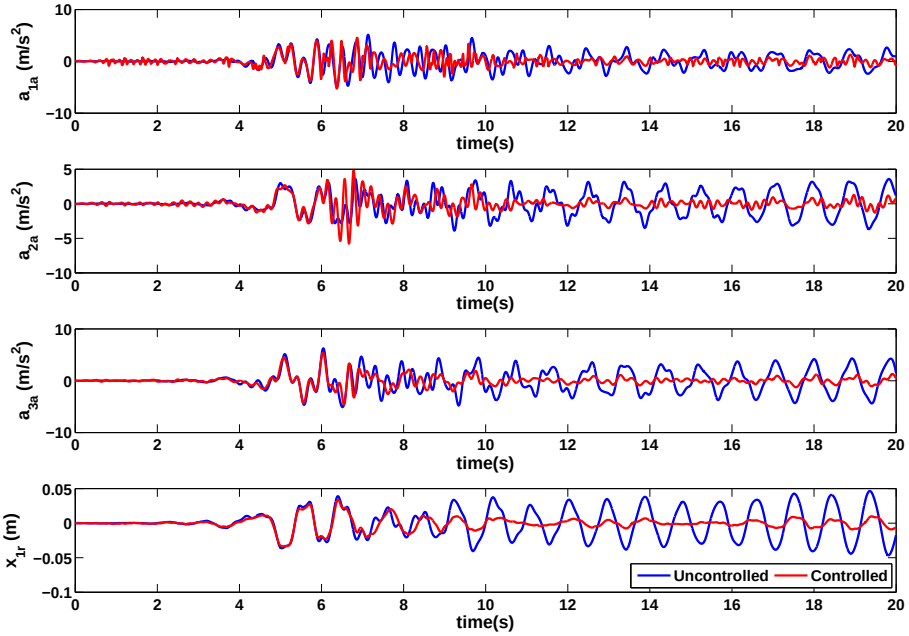

Figure 6.18: Clipped QFT: Structure response under Loma Prieta earthquake.

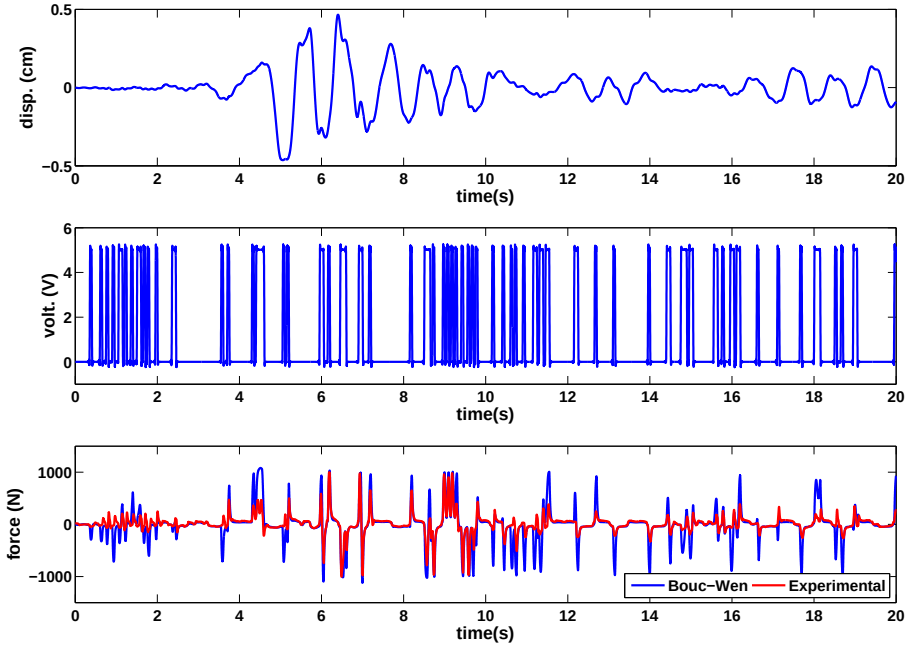

Figure 6.19: Clipped QFT: MR damper response under Loma Prieta earthquake.

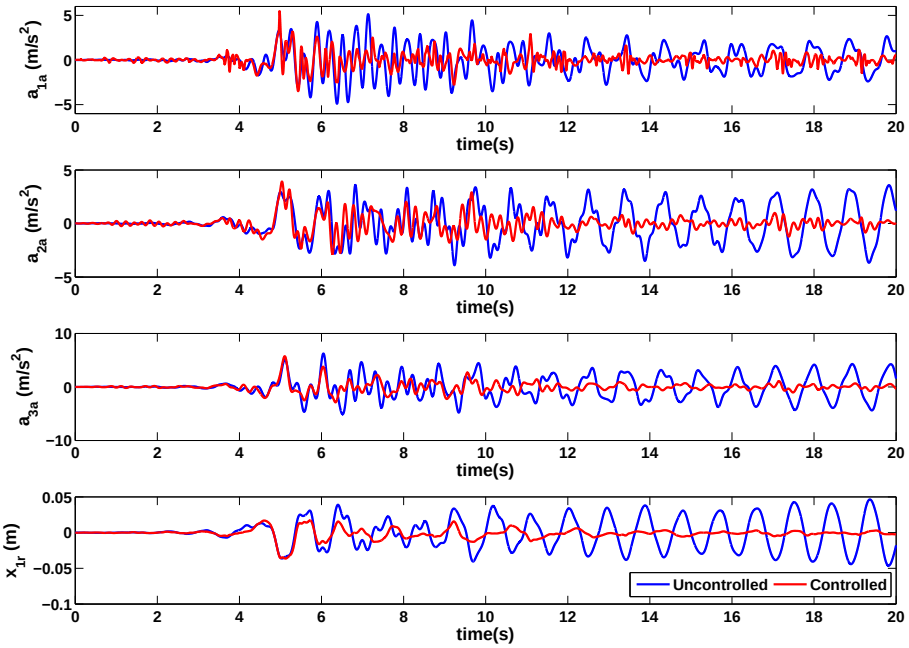

Figure 6.20: Model based QFT: Structure response under Loma Prieta earthquake.

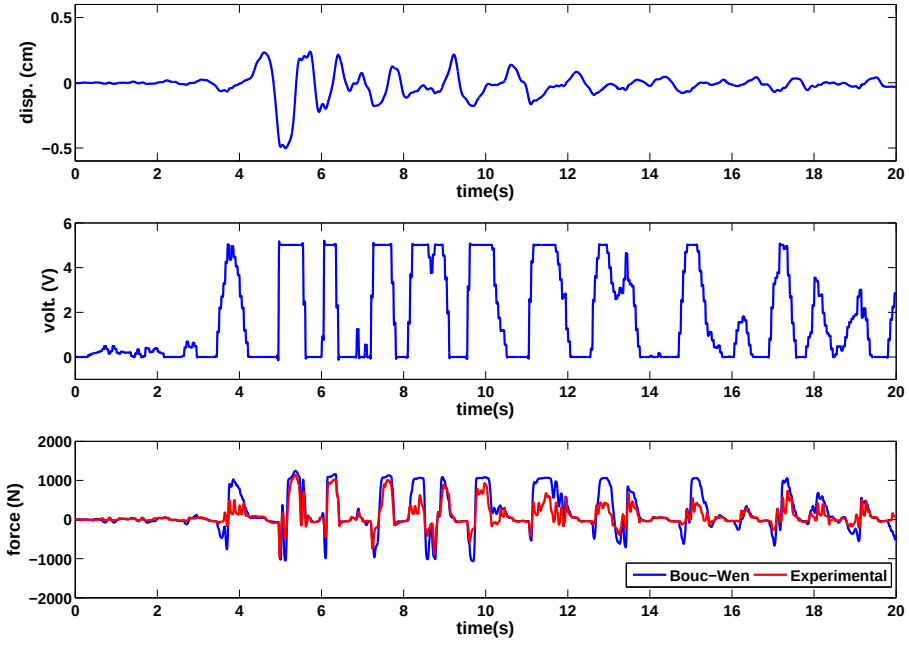

Figure 6.21: Model based QFT: MR damper response under Loma Prieta earthquake.

Chapter 7

Mixed H_2/H_∞ control

In this chapter, the vibration problem is considered from a mixed time-frequency domain perspective. It is desirable that the vibration mitigation problem can be solved not only by reducing the time response but the frequency response as well. This can be approached by the mixed H_2/H_∞ control methodology. The objective is to find an H_∞ controller that achieves the robust performance of the system by minimizing its controlled output response against the external disturbances within the frequency range, while combing it with the H_2 control approach in order to reduce the structural time response and control effort.

H_2 and H_∞ controllers (and hence the mixed controllers) can be formulated feeding back either the state or the output. Despite the simplicity of the state feedback design, it may not be a good option when dealing with large systems with several (and possibly inaccessible) states. Thus, the output feedback seems to be a better option for this class of systems. In this dissertation, the output feedback option was chosen. In this way, the controller accounts for the limited measurements and the external disturbances. Based on the Lyapunov theory, some required sufficient conditions are established in terms of linear matrix inequalities (LMIs) for the stability and stabilization of the considered system using some free matrices. The desired robust mixed H_2/H_∞ output feedback control is derived based on a convex optimization method such that the resulting closed-loop system is asymptotically stable and satisfies H_2 performance with a guaranteed cost and a prescribed level of H_∞ performance, simultaneously. An algorithm is also proposed to include the dynamics of the actuator in order to estimate the control signal.

This chapter is organized as follows. The problem of mixed H_2/H_∞ control is described in Section 7.1. Section 7.2 is devoted to the details of the formulation of the output feedback mixed H_2/H_∞ controller. LMIs for the H_2 and H_∞ performances are developed. These LMIs form the set that solves the problem of the mixed constraints. Then, in Section 7.3 the results of the experimental validation of the controllers are presented. The controllers are designed for the 3-story building with an MR damper of the real-time hybrid testing setup. Finally, the conclusions are outlined at the of the chapter.

7.1 Problem definition

Consider the state space model representation of a system:

$$\dot{\mathbf{x}} = \mathbf{A}\mathbf{x} + \mathbf{B_1}\mathbf{u} + \mathbf{B_2}\mathbf{w} \tag{7.1}$$

$$\mathbf{y_c} = \mathbf{C_1}\mathbf{x} + \mathbf{D_{11}}\mathbf{u} + \mathbf{D_{12}}\mathbf{w} \tag{7.2}$$

$$\mathbf{y_o} = \mathbf{C_2}\mathbf{x} + \mathbf{D_{21}}\mathbf{u} \tag{7.3}$$

where $\mathbf{x}$ is the state vector, $\mathbf{u}$ is the input vector, $\mathbf{w}$ is the exogenous input vector, $\mathbf{y_c}$ is the vector of controlled outputs and $\mathbf{y_o}$ is the vector of measured outputs. The H_2 performance measure of the systems 7.1 - 7.3 is defined as:

$$J_{H_2} = \int_0^\infty \left(\mathbf{x}^{\mathrm{T}}\mathbf{S_1}\mathbf{x} + \mathbf{u}^{\mathrm{T}}\mathbf{S_2}\mathbf{u}\right) dt \tag{7.4}$$

where $\mathbf{w} = \mathbf{0}$ and the constant matrices $\mathbf{S_1}$ and $\mathbf{S_2}$ are given. On the other hand, the H_∞ performance measure is defined as:

$$J_\infty = \int_0^\infty \left(\mathbf{y_c}^{\mathrm{T}}\mathbf{y_c} - \gamma^2 \mathbf{w}^{\mathrm{T}}\mathbf{w}\right) dt \tag{7.5}$$

where γ is a given positive scalar. Then, the mixed H_2/H_∞ performance measure is defined as:

$$Min\ \{J_0 | J_\infty < 0\ and\ J_{H_2} \leq J_0\} \tag{7.6}$$

which is equivalent to minimize the upper bound J_{H_2} $(J_0 > 0)$ subject to $J_\infty < 0$. The minimization of J_{H_2} will result in the reduction of the system response and control effort while the achieving $J_\infty < 0$ will keep the system response within prescribed intervals in the presence of external disturbances.

7.2 LMI formulation of the output feedback controller

Recall the state space model of Eqs. 7.1 - 7.3. Suppose that the aim is to design the following static output controller:

$$\mathbf{u} = \mathbf{K_{2\infty}}\mathbf{y_o} \tag{7.7}$$

where $\mathbf{K_{2\infty}}$ is the controller gain. Then, the system of Eqs. 7.1 - 7.3 can be rewritten as follows:

$$\dot{\mathbf{x}} = \bar{\mathbf{A}}\mathbf{x} + \mathbf{B_2}\mathbf{w} \tag{7.8}$$

$$\mathbf{y_c} = \bar{\mathbf{C}}\mathbf{x} + \mathbf{D_{12}}\mathbf{w} \tag{7.9}$$

$$\mathbf{y_o} = (\mathbf{I} - \mathbf{D_{21}}\mathbf{K_{2\infty}})^{-1}\mathbf{C_2}\mathbf{x} \tag{7.10}$$

where $\bar{\mathbf{A}} = \mathbf{A} + \mathbf{B_1}\mathbf{K_{2\infty}}(\mathbf{I} - \mathbf{D_{21}}\mathbf{K_{2\infty}})^{-1}\mathbf{C_2}$ and $\bar{\mathbf{C}} = \mathbf{C_1} + \mathbf{D_{11}}\mathbf{K_{2\infty}}(\mathbf{I} - \mathbf{D_{21}}\mathbf{K_{2\infty}})^{-1}\mathbf{C_2}$. Now, represent the system of Eqs. 7.8 - 7.10 in a model descriptor form as follows:

$$\dot{\mathbf{x}} = \eta_{\mathbf{d}} \tag{7.11}$$

$$\mathbf{0} = -\eta_{\mathbf{d}} + \bar{\mathbf{A}}\mathbf{x} + \mathbf{B_2}\mathbf{w} \tag{7.12}$$

Define the following Lyapunov functional:

$$\mathbf{V} = \mathbf{x}^{\mathrm{T}}\mathbf{P_1}\mathbf{x} := \begin{bmatrix} \mathbf{x}^{\mathrm{T}} & \eta_{\mathbf{d}}{}^{\mathrm{T}} \end{bmatrix} \mathbf{T}\mathbf{P} \begin{bmatrix} \mathbf{x} \\ \eta_{\mathbf{d}} \end{bmatrix} \tag{7.13}$$

where $\mathbf{T} = diag\{\mathbf{I}, \mathbf{0}\}$, $\mathbf{P_1} = \mathbf{P_1}^{\mathrm{T}} > 0$ and $\mathbf{P} = \begin{bmatrix} \mathbf{P_1} & \mathbf{0} \\ \mathbf{P_3} & \mathbf{P_2} \end{bmatrix}$, such that P_2 and P_3 are some free matrices. Differentiating $\mathbf{V}$ along the system trajectories (Eq. 7.8) yields:

$$\dot{\mathbf{V}} = 2\begin{bmatrix} \mathbf{x}^{\mathrm{T}} & \eta_{\mathbf{d}}{}^{\mathrm{T}} \end{bmatrix}\mathbf{P}^{\mathrm{T}} \left\{ \begin{bmatrix} \mathbf{0} & \mathbf{I} \\ \bar{\mathbf{A}} & \mathbf{I} \end{bmatrix} \begin{bmatrix} \mathbf{x} \\ \eta_{\mathbf{d}} \end{bmatrix} + \begin{bmatrix} \mathbf{0} \\ \mathbf{B_2} \end{bmatrix} \mathbf{w} \right\} \tag{7.14}$$

Before proceeding with the controller formulation, a lemma that will be further used is stated next.

Lemma 1 (Ho & Lu 2003). *For a given $\mathbf{M} \in \mathbb{R}^{p\times n}$ with $rank(\mathbf{M}) = p < n$, assume that $\mathbf{Z} \in \mathbb{R}^{n\times n}$ is a symmetric matrix, then there exists a matrix $\hat{\mathbf{Z}} \in \mathbb{R}^{p\times p}$ such that $\mathbf{MZ} = \hat{\mathbf{Z}}\mathbf{M}$ if and only if*

$$\mathbf{Z} = \mathbf{V} \begin{bmatrix} \mathbf{Z_1} & \mathbf{0} \\ \mathbf{0} & \mathbf{Z_2} \end{bmatrix} \mathbf{V^T} \tag{7.15}$$

$$\hat{\mathbf{Z}} = \mathbf{U}\hat{\mathbf{M}}\mathbf{Z_1}\hat{\mathbf{M}}^{-1}\mathbf{U^T} \tag{7.16}$$

where $\mathbf{Z_1} \in \mathbb{R}^{p\times p}$, $\mathbf{Z_2} \in \mathbb{R}^{(n-p)\times(n-p)}$ and the singular value decomposition of the matrix $\mathbf{M}$ is represented as $\mathbf{M} = \mathbf{U}\begin{bmatrix} \hat{\mathbf{M}} & \mathbf{0} \end{bmatrix}\mathbf{V}^{\mathrm{T}}$ with the unitary matrices $\mathbf{U} \in \mathbb{R}^{p\times p}$, $\mathbf{V} \in \mathbb{R}^{n\times n}$ and a diagonal matrix $\hat{\mathbf{M}} \in \mathbb{R}^{p\times p}$ with positive diagonal elements in decreasing order.

H_∞ performance

Under zero initial conditions, the H_∞ performance measure can be written as:

$$\begin{aligned} J_\infty &\leq \int_0^\infty \left[\mathbf{y_c}^{\mathrm{T}} \mathbf{y_c} - \gamma^2 \mathbf{w}^{\mathrm{T}} \mathbf{w} \right] dt - \mathbf{V}|_{t=0} + \mathbf{V}|_{t=\infty} \\ &= \int_0^\infty \left[\mathbf{y_c}^{\mathrm{T}} \mathbf{y_c} - \gamma^2 \mathbf{w}^{\mathrm{T}} \mathbf{w} + \dot{\mathbf{V}} \right] dt \end{aligned} \tag{7.17}$$

Substituting Eq. 7.2 into Eq. 7.17 yields the inequality $J_\infty \leq \int_0^\infty \nu^T \mathbf{\Pi}_\infty \nu \, ds$ where:

$$\nu = \begin{bmatrix} \mathbf{x} & \eta_\mathbf{d} & \mathbf{w} \end{bmatrix}^{\mathrm{T}} \tag{7.18}$$

$$\mathbf{\Pi}_\infty := \begin{bmatrix} sym\left(\mathbf{P}^{\mathrm{T}} \begin{bmatrix} \mathbf{0} & \mathbf{I} \\ \bar{\mathbf{A}} & -\mathbf{I} \end{bmatrix} \right) + \begin{bmatrix} \bar{\mathbf{C}}^{\mathrm{T}} \\ \mathbf{0} \end{bmatrix} \begin{bmatrix} \bar{\mathbf{C}}^{\mathrm{T}} \\ \mathbf{0} \end{bmatrix}^{\mathrm{T}} & \mathbf{P}^{\mathrm{T}} \begin{bmatrix} \mathbf{0} \\ \mathbf{B_1} \end{bmatrix} + \begin{bmatrix} \bar{\mathbf{C}}^{\mathrm{T}} \mathbf{D_{12}} \\ \mathbf{0} \end{bmatrix} \\ \star & \mathbf{D_{12}}^{\mathrm{T}} \mathbf{D_{12}} - \gamma^2 \mathbf{I} \end{bmatrix} \tag{7.19}$$

where $sym(\mathbf{x}) = \mathbf{x} + \mathbf{x}^{\mathrm{T}}$. Applying the Schur complement lemma on the matrix $\mathbf{\Pi}_\infty$ of Eq. 7.19 yields:

$$\begin{bmatrix} sym\left(\mathbf{P}^{\mathrm{T}} \begin{bmatrix} \mathbf{0} & \mathbf{I} \\ \bar{\mathbf{A}} & -\mathbf{I} \end{bmatrix} \right) & \mathbf{P}^{\mathrm{T}} \begin{bmatrix} \mathbf{0} \\ \mathbf{B_1} \end{bmatrix} & \begin{bmatrix} \bar{\mathbf{C}}^{\mathrm{T}} \\ \mathbf{0} \end{bmatrix} \\ \star & -\gamma^2 \mathbf{I} & \mathbf{D_{12}}^{\mathrm{T}} \\ \star & \star & -\mathbf{I} \end{bmatrix} < \mathbf{0} \tag{7.20}$$

Let $\mathbf{X} = \mathbf{P}^{-1} = \begin{bmatrix} \mathbf{X_1} & \mathbf{0} \\ \mathbf{X_3} & \mathbf{X_2} \end{bmatrix}$ and a congruence transformation $\xi = diag(\mathbf{X}, \mathbf{I}, \mathbf{X_1})$. Pre- and post-multiplying ξ to the inequality 7.20 yields:

$$\begin{bmatrix} sym\left(\begin{bmatrix} \mathbf{0} & \mathbf{I} \\ \bar{\mathbf{A}} & -\mathbf{I} \end{bmatrix} \mathbf{X} \right) & \begin{bmatrix} \mathbf{0} \\ \mathbf{B_2} \end{bmatrix} & \mathbf{X} \begin{bmatrix} \bar{\mathbf{C}}^{\mathrm{T}} \\ \mathbf{0} \end{bmatrix} \\ \star & -\gamma^2 \mathbf{I} & \mathbf{D_{12}}^{\mathrm{T}} \\ \star & \star & -\mathbf{I} \end{bmatrix} < \mathbf{0} \tag{7.21}$$

Consider the equality constraint $\mathbf{C_2 X_1} = \hat{\mathbf{X}}_\mathbf{1} \mathbf{C_2}$ from Lemma 1, with $\hat{\mathbf{X}}_\mathbf{1}$ as a new LMI variable. Let $\tilde{\mathbf{X}}_\mathbf{1} = \mathbf{K_{2\infty}}(\mathbf{I} - \mathbf{D_{21} K_{2\infty}})^{-1} \hat{\mathbf{X}}_\mathbf{1}$. Then, the inequality 7.21 is represented in the following LMI form :

$$\begin{bmatrix} sym\left(\begin{bmatrix} \mathbf{X_3} & \mathbf{X_2} \\ \mathbf{A X_1} + \mathbf{B_1} \tilde{\mathbf{X}}_\mathbf{1} \mathbf{C_2} - \mathbf{X_3} & -\mathbf{X_2} \end{bmatrix} \right) & \begin{bmatrix} \mathbf{0} \\ \mathbf{B_2} \end{bmatrix} & \begin{bmatrix} (\mathbf{C_1 X_1} + \mathbf{D_1 1} \tilde{\mathbf{X}}_\mathbf{1} \mathbf{C_2})^{\mathrm{T}} \\ \mathbf{0} \end{bmatrix} \\ \star & -\gamma^2 \mathbf{I} & \mathbf{D_{12}}^{\mathrm{T}} \\ \star & \star & -\mathbf{I} \end{bmatrix} < \mathbf{0} \tag{7.22}$$

H_2 performance

Recall the Lyapunov function of Eq. 7.13. Under zero initial conditions and with $\mathbf{w} = \mathbf{0}$, the H_2 performance can be written as:

$$J_{H_2} \leq \int_0^\infty \left[\mathbf{x}^{\mathrm{T}} \mathbf{S_1 x} + \mathbf{u}^{\mathrm{T}} \mathbf{S_2 u} + \dot{\mathbf{V}} \right] dt = \int_0^\infty \nu^{\mathrm{T}} \mathbf{\Pi_2} \nu \, dt \tag{7.23}$$

where the vector ν and the matrix Π_2 are given by:

$$\nu = \left[\begin{array}{cc} \mathbf{x} & \eta_{\mathbf{d}} \end{array} \right]^{\mathrm{T}} \tag{7.24}$$

$$\mathbf{\Pi_2} = sym\left(\mathbf{P}^{\mathrm{T}} \left[\begin{array}{cc} \mathbf{0} & \mathbf{I} \\ \bar{\mathbf{A}} & -\mathbf{I} \end{array} \right]\right) + \left[\begin{array}{cc} \mathbf{S_1} + (\mathbf{K_{2\infty}}(\mathbf{I} - \mathbf{D_{21}}\mathbf{K_{2\infty}})^{-1}\mathbf{C_2})^{\mathrm{T}}\mathbf{S_2}(\mathbf{K_{2\infty}}(\mathbf{I} - \mathbf{D_{21}}\mathbf{K_{2\infty}})^{-1}\mathbf{C_2}) & \mathbf{0} \\ \mathbf{0} & \mathbf{0} \end{array} \right] < \mathbf{0} \tag{7.25}$$

Let a congruence transformation $\xi = diag\{\mathbf{X}, \mathbf{I}\}$. Applying the Schur complement lemma to the inequality 7.25 and then, pre- and post-multiplying ξ to the result yields:

$$\mathbf{\Pi_2} = \left[\begin{array}{cc} sym\left(\left[\begin{array}{cc} \mathbf{0} & \mathbf{I} \\ \bar{\mathbf{A}} & -\mathbf{I} \end{array} \right]\mathbf{X}\right) + \mathbf{X}^{\mathrm{T}} \left[\begin{array}{cc} \mathbf{S_1} & \mathbf{0} \\ \mathbf{0} & \mathbf{0} \end{array} \right]\mathbf{X} & \mathbf{X}^{\mathrm{T}} \left[\begin{array}{c} (\mathbf{K_{2\infty}}(\mathbf{I} - \mathbf{D_{21}}\mathbf{K_{2\infty}})^{-1}\mathbf{C_2})^{\mathrm{T}}\mathbf{S_2} \\ \mathbf{0} \end{array} \right] \\ \star & -\mathbf{S_2} \end{array} \right] \tag{7.26}$$

Let again $\tilde{\mathbf{X}}_\mathbf{1} = \mathbf{K_{2\infty}}(\mathbf{I} - \mathbf{D_{21}}\mathbf{K_{2\infty}})^{-1}\hat{\mathbf{X}}_\mathbf{1}$. Then, after substitution of $\mathbf{X} = \left[\begin{array}{cc} \mathbf{X_1} & \mathbf{0} \\ \mathbf{X_3} & \mathbf{X_2} \end{array} \right]$ into Eq. 7.26 and application of the Schur complement to the result, the following inequality is obtained:

$$\left[\begin{array}{ccc} sym\left(\left[\begin{array}{cc} \mathbf{X_3} & \mathbf{X_2} \\ \mathbf{AX_1} + \mathbf{B_1}\tilde{\mathbf{X}}_\mathbf{1}\mathbf{C_2} - \mathbf{X_3} & -\mathbf{X_2} \end{array} \right]\right) & \left[\begin{array}{c} (\tilde{\mathbf{X}}_\mathbf{1}\mathbf{C_2})^{\mathrm{T}}\mathbf{S_2} \\ \mathbf{0} \end{array} \right] & \left[\begin{array}{c} \mathbf{X_1}^{\mathrm{T}}\mathbf{S_1} \\ \mathbf{0} \end{array} \right] \\ \star & -\mathbf{S_2} & \mathbf{0} \\ \star & \star & -\mathbf{S_1} \end{array} \right] < \mathbf{0} \tag{7.27}$$

The controller gain $\mathbf{K_{2\infty}}$ can be obtained from the solution of the LMIs 7.22 and 7.27 as follows:

$$\mathbf{K_{2\infty}} = (\mathbf{I} + \tilde{\mathbf{X}}_\mathbf{1}\hat{\mathbf{X}}_\mathbf{1}^{-1}\mathbf{D_{21}})^{-1}\tilde{\mathbf{X}}_\mathbf{1}\hat{\mathbf{X}}_\mathbf{1}^{-1} \tag{7.28}$$

7.3 Experimental results

In this section, a mixed H_2/H_∞ controller for the 3-story building equipped with an MR damper is experimentally tested. Recall Eqs. 4.15, 4.20 - 4.21 that represent the dynamics of the structure and the MR damper. Let $F_{2\infty}$ be the control force estimated by the mixed H_2/H_∞ controller of Eq. 7.7. Then, the voltage signal to the MR damper is estimated with the following equation:

$$v = \frac{F_{2\infty}/S_F - (c_{mra}\dot{x_p} + k_{mra}x_p + \alpha_{mra}z)}{c_{mrb}\dot{x_p} + k_{mrb}x_p + \alpha_{mrb}z} \tag{7.29}$$

The vector of controlled signals is composed of the absolute accelerations and relative velocities of each floor. These signals are weighted by some weighting factors. The vector of controlled outputs was chosen as $\mathbf{y_c} = \left[\begin{array}{cc} (\mathbf{\Lambda_1}\mathbf{x_r})^{\mathrm{T}} & (\mathbf{\Lambda_2}\mathbf{x_a})^{\mathrm{T}} \end{array} \right]^{\mathrm{T}}$, where $\mathbf{x_r}$ is the vector of relative displacements, $\mathbf{x_a}$ is the vector of absolute accelerations and $\mathbf{\Lambda_1} = diag\{500, 500, 500\}$ and $\mathbf{\Lambda_2} = diag\{500, 150, 1000\}$ are the weighting matrices. The available measurements are the absolute accelerations of each floor. Thus, the matrices used to design the controller are:

$$\begin{array}{ccc} \mathbf{A} = \left[\begin{array}{cc} \mathbf{0} & \mathbf{I} \\ -\mathbf{M}^{-1}\mathbf{K} & -\mathbf{M}^{-1}\mathbf{C} \end{array} \right] & \mathbf{B}_1 = \left[\begin{array}{c} \mathbf{0} \\ \mathbf{M}^{-1}G_s \end{array} \right] & \mathbf{B}_2 = \left[\begin{array}{c} \mathbf{0} \\ -L_s \end{array} \right] \\ \mathbf{C}_1 = \left[\begin{array}{cc} \mathbf{0} & \mathbf{\Lambda_1 I} \\ -\mathbf{\Lambda_2}\mathbf{M}^{-1}\mathbf{K} & -\mathbf{\Lambda_2}\mathbf{M}^{-1}\mathbf{C} \end{array} \right] & \mathbf{D}_{11} = \left[\begin{array}{c} \mathbf{0} \\ \mathbf{\Lambda_2}\mathbf{M}^{-1}G_s \end{array} \right] & \mathbf{D}_{12} = \mathbf{0} \\ \mathbf{C}_2 = \left[\begin{array}{cc} -\mathbf{M}^{-1}\mathbf{K} & -\mathbf{M}^{-1}\mathbf{C} \end{array} \right] & \mathbf{D}_{21} = \mathbf{M}^{-1}G_s & \mathbf{D}_{22} = \mathbf{0} \\ \mathbf{S_1} = \mathbf{I} & \mathbf{S_2} = \mathbf{I} & \end{array} \tag{7.30}$$

A solution of the set of LMIs 7.22 and 7.27 was found with $\gamma = 131$. The resulting control gain is:

$$\mathbf{K_{2\infty}} = \begin{bmatrix} 493.90 & -4.20 & -95.95 \end{bmatrix} \tag{7.31}$$

The controller performance is evaluated by simulating the RTHT setup described in Section 4.3. The models of the 3-story building, the hydraulic actuator and the controller are implemented in Matlab/Simulink. The ordinary differential equation solver used is the 4^{th} order Runge-Kutta method with a time step $T_s = 5 \times 10^{-4}$ seconds. The structure is subject to the El Centro, Loma Prieta and Northridge seismic motion records; the scale amplitude used is 0.4. For comparison purposes, a controller based on the clipped optimal algorithm is implemented.

The H_∞ performance, measured as $\sqrt{||\mathbf{y_c}||}/\sqrt{||\mathbf{w}||}$ is shown in Table 7.1 for the different seismic motions and control cases. The performance bound ($\gamma = 131$) is satisfied by both controllers under the three seismic motions. In comparison, in the case of no MR damper actuating, the performance is higher than the bound. Furthermore, the H_2 performance was measured in all cases. For initial conditions $\mathbf{x(0)} = \begin{bmatrix} 0.005\,\text{in} & 0.008\,\text{in} & 0.01\,\text{in} & 0.5\,\text{in/s} & 0.8\,\text{in/s} & 1\,\text{in/s} \end{bmatrix}^{\mathrm{T}}$, the bound $J_0 = \mathbf{x(0)}^{\mathrm{T}}\mathbf{X_1^{-1}}\mathbf{x(0)} = 1.02 \times 10^9$ is greater than the J_{H_2} value achieved by the controllers in all cases, as can be seen in Table 7.2.

	Uncontrolled	H_2/H_∞ (with MRD dyn.)	H_2/H_∞ (Mod. Clipped Opt.)
El Centro	207.15	120.14	112.53
Loma Prieta	188.11	103.88	98.41
Northridge	182.42	113.08	110.92

Table 7.1: H_∞ performance indices under El Centro, Loma Prieta and Northridge earthquakes.

	H_2/H_∞ (with MRD dyn.)	H_2/H_∞ (Mod. Clipped Opt.)
El Centro	7.29×10^8	4.00×10^8
Loma Prieta	4.24×10^8	2.68×10^8
Northridge	5.43×10^8	2.78×10^8

Table 7.2: H_2 performance indices under El Centro, Loma Prieta and Northridge earthquakes.

The performance indices used to evaluate the controller performance are those of Table 5.1. The resulting indices for the different seismic excitations are shown in Table 7.3. Figures 7.2 - 7.4 show the structure response and the MR damper performance when the structures is subject to the El Centro seismic excitation. Figures 7.2 and 7.4 show the performance of the MR damper (the actual damper, i.e. not scaled). Additionally, Figures 7.5 and 7.6 show the power spectral density of the acceleration and displacement of each floor.

From Figures 7.2 and 7.4 it can be seen that both controllers are able to reduce the displacement response of the structure. The first floor acceleration of the structure is, in general, reduced with both controllers as well. However, the reduction achieved by the controller based on the damper model is not as significant as that achieved by the modified clipped optimal controller. This facts are numerically confirmed by performance indices J_1 - J_4. Indices J_5 and J_6 show that the controller based on the modified version of he clipped optimal algorithm, makes use of less control effort to achieve the results. This can also be observed in Figures 7.2 and 7.4. In the first case, the control signal, i.e. the voltage, remains mostly at low level values while in the second case, it remains at high values. Figure 7.5 shows that the first floor acceleration power spectral density is increased with the addition of the controllers while that of the second and third floors present no significant differences. In the case of the power spectral density, it can be seen in Figure 7.6 that it is decreased with both controllers.

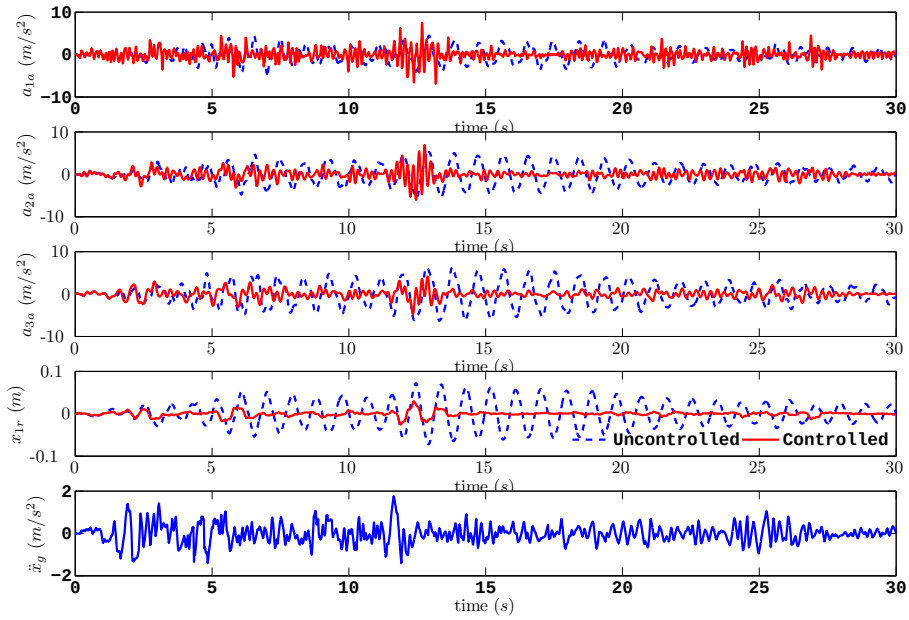

Figure 7.1: H_2/H_∞ (with MRD dynamics): Structure response under El Centro earthquake.

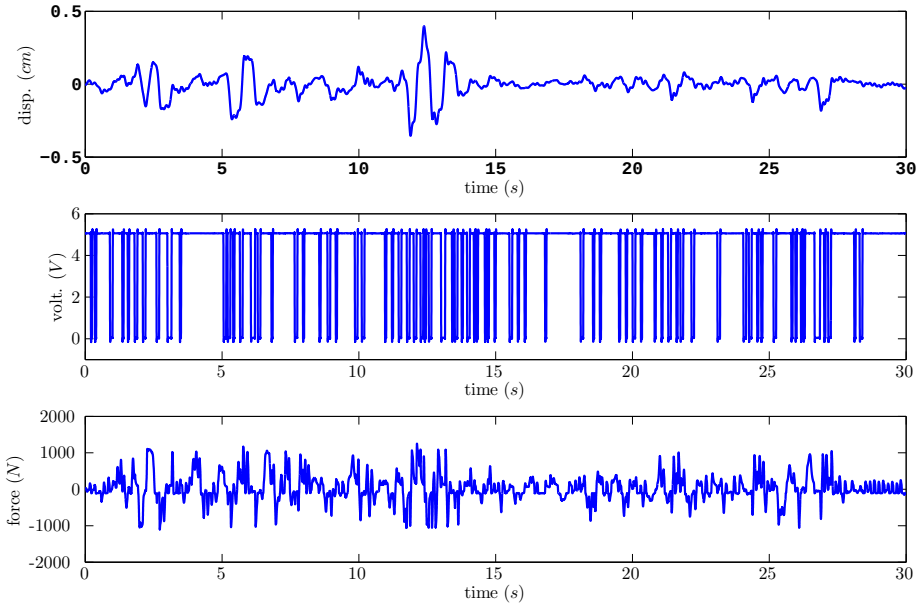

Figure 7.2: Mixed H_2/H_∞ (with MRD dynamics): MR damper response under El Centro earthquake.

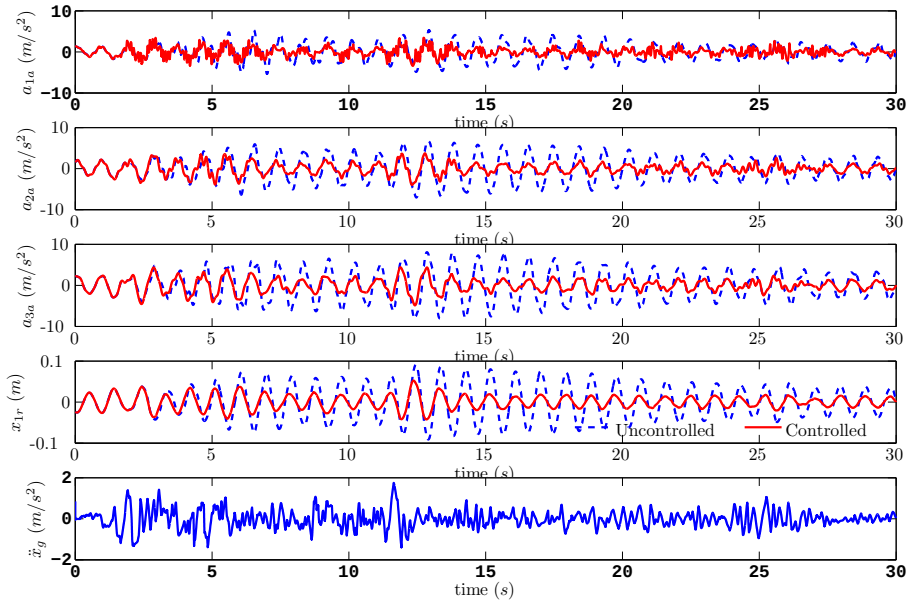

Figure 7.3: Mixed H_2/H_∞ (Mod. Clipped Optimal algorithm): Structure response under El Centro earthquake.

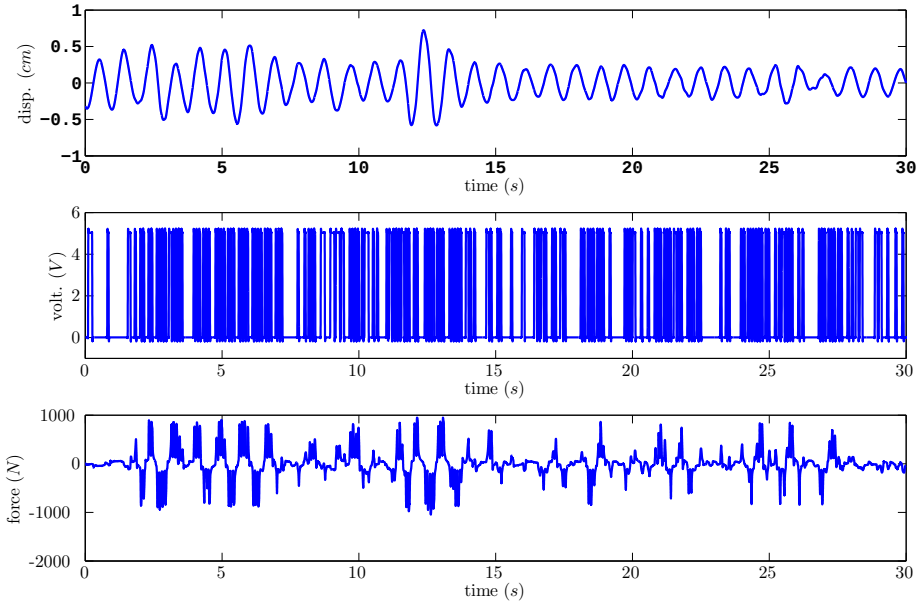

Figure 7.4: Mixed H_2/H_∞ (Mod. Clipped Optimal algorithm): MR damper response under El Centro earthquake.

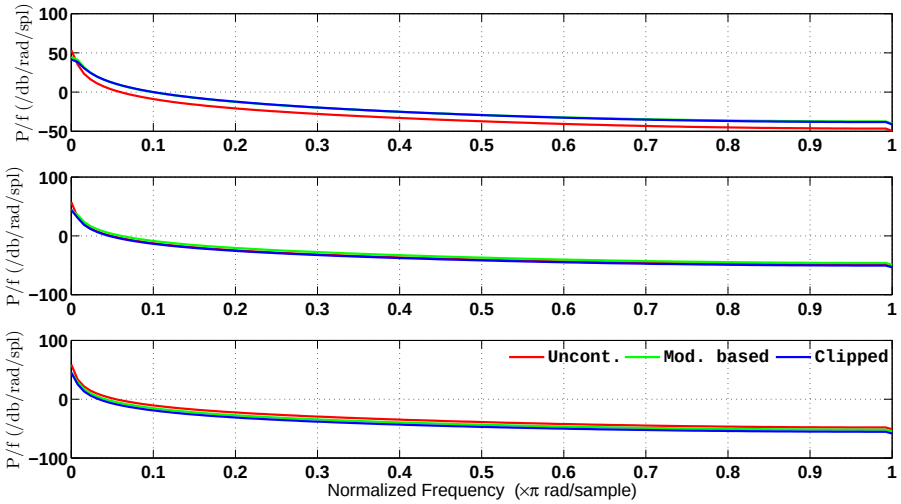

Figure 7.5: Acceleration power spectral density under El Centro earthquake.

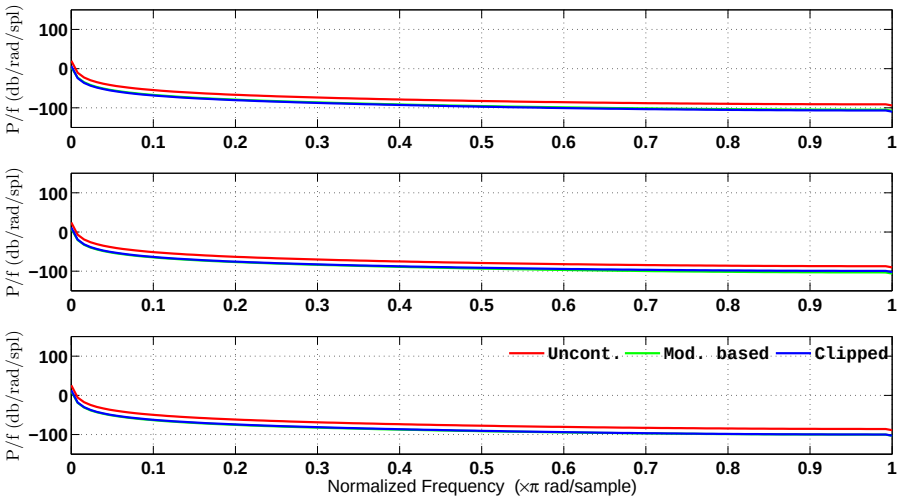

Figure 7.6: Displacement power spectral density under El Centro earthquake.

Earthquake	Controller	J_1	J_2	J_3 (cm)	J_4 (m/s^2)	J_5	J_6 (N)
El Centro	H_2/H_∞ (Mod. Clipped Opt.)	0.53	0.34	3.17	3.08	0.10	253.31
	H_2/H_∞ (with MRD dyn.)	1.14	0.38	2.64	7.23	0.12	361.22
Loma Prieta	H_2/H_∞ (Mod. Clipped Opt.)	0.58	0.27	3.25	3.07	0.11	227.40
	H_2/H_∞ (with MRD dyn.)	0.85	0.37	2.21	5.33	0.11	277.50
Northridge	H_2/H_∞ (Mod. Clipped Opt.)	0.73	0.34	4.95	5.53	0.13	241.30
	H_2/H_∞ (with MRD dyn.)	0.85	0.40	3.70	6.87	0.13	301.32

Table 7.3: Controller performance indices under El Centro, Loma Prieta and Northridge earthquakes.

7.4 Summary

In this chapter, an output feedback mixed H_2/H_∞ controller was formulated to reduce the vibrations of a 3-story building with MR damper when subject to seismic motions. The controller was designed following an LMI approach so that both H_2 and H_∞ performances could be achieved simultaneously. To generate the control signal, two algorithms were proposed: one based on a modified version of the clipped optimal algorithm and another based on the Bouc-Wen model of the damper. As a result, the experiments show a reduction in both acceleration and displacement responses. Furthermore, the power spectral density of the displacement of each floor decreased with both controllers. It was also found that the structure response decreased with the controller based on the modified clipped optimal algorithm making use of less control effort.

Chapter 8

Conclusions and future work

The main goal of this dissertation was to design semiactive controllers for magnetorheological dampers in order to mitigate vibrations in adaptronic systems. This problem is characterized by the existence of different factors such as nonlinear dynamics, parametric uncertainties, unknown disturbances and limited measurements. As discussed in Chapter 1, most of the existing solutions to this problem are based on time domain control techniques and others ignore the nonlinear dynamics of the MR damper.

The main contribution of this dissertation is, thus, the development of different semiactive control approaches that are capable of dealing with the nonlinearities, uncertainties, unknown disturbances and limited measurements of the system. Furthermore, control algorithms are developed in time (Backstepping), frequency (QFT) and time/frequency (H_2/H_∞) domains. Specifically, the contributions of the dissertation can be summarized as follows:

- In Chapters 1 - 4, an exhaustive study on the vibration mitigation problem in flexible structures was carried out. The search was focused on the solutions provided by the use of MR dampers. In consequence, a detailed study of this device was also presented and emphasis was made on the mathematical modeling of the damper. Comparison between parametric and non-parametric models was made. As a result, the Bouc-Wen model was chosen as a good system to represent the damper dynamics due to its numerical simplicity and accuracy. Moreover, this model suits well for control formulation as proposed in this dissertation. Finally, all the structure models used throughout the dissertation and the innovative experimental platform for validation were described in detail.

- In Chapter 5, control algorithms based on the Backstepping technique were proposed. This is a time domain technique based on the Lyapunov stability theory and it allows working with nonlinear systems. Thanks to this control technique, the nonlinear dynamics of the MR damper could be introduced in the controller formulation in a natural way. Furthermore, the parametric uncertainties of the structure were considered by adding adaptation terms. Unknown disturbances were also taken into account by adding some constraints during the controller formulation. Finally, the controller could be implemented with the need of a few measurements. For comparison purposes, two backstepping controllers were designed: one incorporating the dynamics of the MR damper; the other one based on the clipped optimal algorithm which does not take into account the damper dynamics.

  The backstepping controllers were designed and tested for different systems, namely, a base isolated 10-story building (numerically tested), a 3-story building with one MR damper (experimentally tested) and a vehicle semiactive suspension system (experimentally tested). As a result, a significant mitigation of vibrations was achieved through the reduction of the structure response in displacements and accelerations. Furthermore, the backstepping controller designed by incorporating the damper dynamics in the formulation performed, in general, better than the other with a reduction in the control effort.

- In Chapter 6, control algorithms based on Quantitative Feedback Theory (QFT) were proposed. This is an important contribution of this research since, as discussed in the initial chapters, little

work has been done to solve the vibration problem using frequency domain techniques. The QFT methodology allows to incorporate different constraints in the control formulation, particularly, but not limited to, frequency domain constraints. In this research, the controllers were formulated in such a way that all the design constraints were accomplished at the natural frequencies of the system. The controllers were designed for two structures: a 6-story building with two MR dampers (numerically tested) and a 3-story building with one MR damper (experimentally tested).

The key point of this controller formulation was the inclusion of the damper dynamics. QFT techniques were initially developed for LTI systems but it is possible to extend it to nonlinear systems. In order to apply this methodology to the problem in question, a particular model for the MR damper was proposed. It was modeled as an uncertain linear system whose dynamics approximately reproduce the actual dynamics of the damper. Two controllers were designed, like in the backstepping case: one based on the damper dynamics, and another one based on a modification of the clipped optimal algorithm.

The controllers were tested numerically and experimentally, and as a result, it was found that the structure response was reduced in comparison to the cases where no damping devices were actuating. Moreover, the controller formulated including the damper dynamics presented a similar performance to the other one but making use of less control effort.

- In Chapter 7, an output feedback mixed H_2/H_∞ controller was proposed and experimentally tested. This technique combines time domain specifications (H_2 control) and frequency domain specifications (H_∞ control). Through linear matrix inequalities (LMIs) formulation, it is possible to set constraints in such a way that both specifications are accomplished simultaneously. One important point to highlight here is that the technique allows to design the controller with a few output measurements.

  The controller was designed for the 3-story building and only acceleration measurements were considered. An algorithm was proposed to include the damper dynamics in the final control law. Experimental results showed a reduction in the structure response.

The controllers developed during this research accomplished the main objective, that is, reduced the displacement response of the structure (improving safety conditions) and the acceleration response (improving comfort). The controllers achieved a good degree of performance in comparison to two extreme cases: when there are no damping devices in the structure and when the damping devices are actuating at their maximum rate constantly (acting as purely passive devices). In comparison to uncontrolled cases, there is a significant reduction in both displacement and acceleration responses. In comparison to the passive cases, semiactive controllers improve, in general, the acceleration response while keeping a similar displacement response. This trade-off between acceleration and displacement response reduction is achieved thanks to the management of the energy resources provided by the semiactive controllers.

Among all of the controllers developed, the backstepping ones performed better, achieving higher structural responses than others. This can be caused by the fact that the backstepping methodology allows to include the nonlinear dynamics of the damper directly into the controller formulation. In the case of the QFT methodology, it is necessary to make an approximation of the nonlinear dynamics of the damper so that the controller can be formulated. The conservativeness of this approach may decrease the overall performance in comparison to the backstepping controllers. The same happens in the case of the H_2/H_∞ methodology; the fact that the dynamics of the damper are not accounted for directly during the controller formulation may lead to an average performance in comparison to the other controllers. The different degrees of performance obtained is something that should be expected and it has to be pointed out that each methodology offers diverse options that better suit to particular problems than others.

Based on the research progress of the thesis, the research activities are being carried out recently in two fields.

First, some alternative approaches for modeling and parameter identification of nonlinear dynamics are being investigated (Karimi, Zapateiro & Luo 2009*c*, 2008*c*). As a novelty, wavelets analysis is used for handling the nonlinear hysteretic terms. By using Haar wavelets, the properties of integral operational matrix and product operational matrix are introduced and utilized to find an algebraic representation form instead of the differential equations of the dynamical system. Consequently, parameter estimation is reduced to the solution of some algebraic equations which is simpler than solving systems of differential equations.

On the other hand, different studies are being done to handle the time delays in networked adaptronic systems in order to guarantee the stability and robustness of the controlled systems. An efficient approach has been developed for robust mixed H_2/H_∞ delayed state feedback control problem of uncertain neutral systems with discrete and distributed time-varying delays. New required sufficient conditions are established in terms of delay-range-dependent LMIs combined with the Lyapunov-Krasovskii method for the existence of the desired robust mixed H_2/H_∞ control such that the resulting closed-loop system is asymptotically stable and satisfies both H_2 performance with a guaranteed cost and a H_∞ level of performance (Karimi, Zapateiro & Luo 2008*d*). Also, new stability criteria for the stability analysis of the neutral systems with nonlinear parameter perturbations based on a descriptor model transformation have been developed (Karimi, Zapateiro & Luo 2009*b*,*a*). As an application study, delay-dependent state- and output feedback aspects of H_∞ control for vehicle engine-body vibration systems with a time-varying actuator delay have been developed (Karimi, Zapateiro & Luo 2008*a*).

Furthermore, the following research topics will be investigated in future:

- Extension of the obtained results to systems with other types of nonlinearities (friction, backlash, etc).
- Application to the vibration control of high rise buildings and long span bridges, and other mechatronic systems like aeronautic structures.
- Development of decentralized control schemes to enhance the reliability of the adaptronic systems.
- Development of autonomous damage and vibration control systems capable of making simultaneous damping of structural vibrations and detection of damage.

Bibliography

Acho, L., Pujol, G. & Pozo, F. (2008), Application of adaptive control to seismically excited highway bridges, *in* 'Proceedings of the 4^{th} European Conference on Structural Control', St. Petersburg, Russia, September 8-12.

Agrawal, A., Ciocanel, C., Martinez, T., Vieira, S., Naganathan, N., Robb, S. & Duggan, J. (2002), 'A bearing application using magnetorheological fluids', *Journal of Material Systems and Structures,* **13**, 667–673.

Aguirre, N., Ikhouane, F., Rodellar, J. & Christenson, R. (2008), Modeling and identification of large scale magnetorheological dampers, *in* 'Proceedings of the 4^{th} European Conference on Structural Control', St. Petersburg, Russia, September 8-12.

Ahn, Y., Yang, B., Ahmadian, M. & Morishita, S. (2005), 'A small-sized variable damping mount using magnetorheological fluid', *Journal of Material Systems and Structures,* **16**, 127–133.

Alvarez, L. & Jiménez, R. (2003), Semi-active control of civil structures using magnetorheological dampers, *in* 'Proceedings of the American Control Conference', Denver, U.S.A., June 4-6.

Atray, V. & Roschke, P. (2003), Design, fabrication, testing and fuzzy modeling of a large magnetorheological damper for vibration control in a railcar, *in* 'Proceedings of the 2003 IEEE/ASME Joint Rail Conference', Chicago, Illinois, U.S.A., April 22-24.

Attard, T. L., Pnevmatikos, N. G., Wesson, M. D., Sanchez, M. C. & Warton, C. (2008), Experimental shaking table tests of a steel structure using prototype MR damper, *in* 'Proceedings of the 4^{th} European Conference on Structural Control', St. Petersburg, Russia, September 8-12.

Baratta, A., Corbi, I. & Corbi, O. (2008), Hybrid and semi-active base isolation device for the smart control of structures, *in* 'Proceedings of the 4^{th} European Conference on Structural Control', St. Petersburg, Russia, September 8-12.

Butz, T. & von Stryk, O. (2002), 'Modeling and simulation of electro- and magnetorheological fluid dampers', *Zeitschrift für angewandthe Mathematik und Mechanik,* **82**, 3–20.

Canudas, C., Olsson, H., Astrom, K. & Lischinsky, P. (1995), 'A new model for control of systems with friction', *IEEE Transactions on Automatic Control,* **40**, 419–425.

Carlson, J. (1999), *Adaptronics and Smart Structures. Basics, Materials, Design and Applications*, Springer, chapter 6.6 (Magnetorheological fluid actuators), pp. 180–195.

Carrion, J. & Spencer, B. (2007), Model-based strategies for real-time hybrid testing, Technical report, NSEL-006, University of Illinois at Urbana-Champaign, http://www.ideals.uiuc.edu/handle/2142/3629.

Casciati, F., Faravelli, L. & Torelli, G. (1999), 'A fuzzy chip controller for nonlinear vibrations', *Nonlinear Dynamics,* **20**, 85–98.

Chang, Y. Y., Yang, Y. S., Wang, S. J., Lin, M. L., Wen, Y. T., Wang, K. J., Deng, H. Z., Lau, D. T. & Tsai, K. C. (2005), Hybrid testing of a multi-span bridge, *in* 'Proceedings of the First International Conference on Advances in Experimental Structural Engineering', Nagoya, Japan, July 19-21.

Charles, S. (2002), *Ferrofluids. Magnetically Controllable Fluids and their Applications*, Springer, chapter 1 (The preparation of magnetic fluids), pp. 3 –18.

Choi, K., Cho, S., Jung, H. & Lee, I. (2004), 'Semi-active fuzzy control for seismic response reduction using magnetorheological dampers', *Earthquake Engineering and Structural Dynamics,* **33**, 723–736.

Choi, S., Lee, S. & Park, Y. (2001), 'A hysteresis model for the field-dependent damping force of a magnetorheological damper', *Journal of Sound and Vibration,* **245**, 375–383.

Christenson, R. & Emmons, A. (2005), Semiactive structural control of a nonlinear building model: considering reliability, *in* 'ASCE Structures Congress 2005', New York, New York, U.S.A., April 20-24.

Darby, A., Blakeborough, A. & Williams, M. (2001), 'Improved control algorithm for real-time substructuring testing', *Earthquake Engineering and Structural Dynamics* **30**, 431–448.

Dias, C. (2005), Fuzzy control of magnetorheological dampers for vibration reduction of seismically excited structures, PhD thesis, Florida State University.

Dong, S., Lu, K., Sun, J. & Rudolph, K. (2006), 'Smart rehabilitation devices: Part II - adaptive motion control', *Journal of Material Systems and Structures,* **17**, 555–561.

Du, H., Lam, J. & Zhang, N. (2006), 'Modelling of a magneto-rheological damper by evolving radial basis function networks', *Engineering Applications of Artificial Intelligence,* **19**, 869–881.

Dyke, S. (2005), Current directions in structural control in the US, *in* '9^{th} World Seminar on Seismic Isolation, Energy Dissipation and Active Vibration', Kobe, Japan.

Dyke, S., Jr., B. S., Sain, M. & Carlson, J. (1998), 'An experimental study of MR dampers for seismic protection', *Smart Materials and Structures,* **7**, 693–703.

Dyke, S., Spencer, B., Sain, M. & Carlson, J. (1996), 'Modeling and control of magnetorheological dampers for seismic response reduction', *Smart Materials and Structures,* **5**, 565–575.

Dyke, S., Wang, Y. & Taylor, E. (2005), Seismic response modification using innovative damping devices, *in* 'Third Colombian Conference on Earthquake Engineering', Cali, Colombia, November 16-19.

Emmons, A. & Christenson, R. (2006), Proposed full-scale experimental verification of semiactive control applied to a nonlinear structure, *in* 'Proceedings of the 17^{th} Analysis and Computation Conference (ASCE)', St. Louis, Missouri, U.S.A., May 18-20.

Fan, X. & Smith, R. C. (2008), l_1 adaptive control of hysteretsis in smart materials, *in* 'Proceedings of the SPIE Smart Structures and Materials & Nondestructive Evaluation and Health Monitoring', San Diego, U.S.A., March 9-13.

Faravelli, L. & Venini, P. (1994), 'Active structural control by neural networks', *Journal of Structural Control,* **1**, 79–101.

Ferreira-Oliveira, C., Rogerio-Bairrao, Carneiro-Barros, R. & Guerreiro, L. (2008), The new generation of seismic active and semi-active protection systems, *in* 'Proceedings of the 4^{th} European Conference on Structural Control', St. Petersburg, Russia, September 8-12.

Flores, G. & Liu, J. (2002), 'Embolization of blood vessels as a cancer therapy using magnetorheological fluids', *Journal of Intelligent Material Systems and Structures,* **13**, 641–646.

Gamota, D. & Filisko, F. (1991), 'Dynamic mechanical studies of electrorheological materials: moderate frequencies', *Journal of Rheology,* **35**, 399–425.

Gavin, H. (2001), 'Multi-duct ER dampers', *Journal of Intelligent Material Systems and Structures,* **12**, 353–366.

Gavin, H., Hoagg, J. & Dobossy, M. (2001), Optimal design of MR dampers, *in* 'Proceedings U.S.-Japan Workshop on Smart Structures for Improved Seismic Performance in Urban Regions', Seattle, Washington, U.S.A., August 14.

Goncalves, F., Koo, J. & Ahmadian, M. (2006), 'A review of the state of the art in magnetorheological fluid technologies - Part I: MR fluid and MR fluid models', *The Shock and Vibration Digest,* **38**, 203–219.

Gu, Z. & Oyadiji, S. O. (2007), Application of MR damper in structural control using genetic algorithm and fuzzy logic PID tuning methods, *in* 'Proceedings of the ASME 2007 International Design Engineering Technical Conferences & Computers and Information in Engineering Conference', Las Vegas, U.S.A., September 4-7.

Guo, D., Hu, H. & Yi, J. (2004), 'Neural network control for a semi-active vehicle suspension with a magneto-rheological damper', *Journal of Vibration and Control,* **10**, 461–471.

Guo, S., Yang, S. & Pan, C. (2006), 'Dynamic modeling of magnetorheological damper behaviors', *Journal of Intelligent Material Systems and Structures,* **12**, 667–673.

Hakuno, M., Shidawara, M. & Hara, T. (1969), 'Dynamic destructive test of a cantilever beam controlled by an analog-computer', *Transactions of the Japanese Society of Civil Engineers* **171**, 1–9 (In Japanese).

Hirsch, G. (1999), *Adaptronics and Smart Structures. Basics, Materials, Design and Applications*, Springer, chapter 8.5 (Adaptronics in Civil Engineering Structures), pp. 334–351.

Ho, D. W. C. & Lu, G. (2003), 'Robust stabilization for a class of discrete-time nonlinear via output feedback: the unified LMI approach', *International Journal of Control,* **76 (2)**, 105–115.

Horiuchi, T., Inoue, M., Konno, T. & Namita, Y. (1999), 'Real-time hybrid experimental system with actuator delay compensation and its application to a piping system with energy absorber', *Earthquake Engineering and Structural Dynamics* **28**, 1121–1141.

Horiuchi, T., Sugano, M. & Konno, T. (1996), Development of a real-time hybrid experimental system with actuator delay compensation, *in* 'Proceedings 11^{th} World Conference on Earthquake Engineering', Acapulco, Mexico.

Houpis, C., Rasmussen, S. & Garcia-Sanz, M. (2006), *Quantitative Feedback Theory. Fundamentals and Applications.*, Taylor and Francis Group.

Housner, G. W., Bergman, L. G., Caughey, T. K., Chassiakos, A. G., Claus, R. O., Masri, S. F., Skelton, R. E., Soong, T. T., Spencer, B. F. & Yao, J. T. P. (1997), 'Structural control: past, present and future', *Journal of Engineering Mechanics* **123**, 897–971.

Ikhouane, F. & Dyke, S. (2007), 'Modeling and identification of a shear mode magnetorheological damper', *Smart Materials and Structures,* **16**, 1–12.

Ikhouane, F., Rabeh, A. & Giri, F. (1997), 'Transient performance oanalysis in robust nonlinear adaptive control', *Systems and Control Letters,* **31**, 21–31.

Ikhouane, F. & Rodellar, J. (2007), *Systems with hysteresis: Analysis, identification and control using the Bouc-Wen model*, John Wiley & Sons.

Jansen, L. & Dyke, S. (2000), 'Semiactive control strategies for MR dampers: comparative study', *Journal of Engineering Mechanics,* **126**, 795–803.

Jiménez, R. & Álvarez Icaza, L. (2005), 'LuGre friction model for a magnetorheological damper', *Structural Control and Health Monitoring,* **12**, 91–116.

Johnson, E., Baker, G., Spencer, B. & Fujino, Y. (2007), 'Semiactive damping of stay cables', *ASCE Journal of Engineering Mechanics,* **133**, 1–11.

Johnson, E., Ramallo, J., Jr., B. S. & Sain, M. (1998), Intelligent base isolation systems, *in* 'Second World Conference on Structural Control', Kyoto, Japan, June 28 - July 1.

Jolly, M., Bender, J. & Carlson, J. (1999), 'Properties and applications of commercial magnetorheological fluids', *Journal of Intelligent Material Systems and Structures,* **10**, 5–13.

Jung, R. Y. & Shing, P. B. (2006), 'Performance evaluation of a real-time pseudodynamic test system', *Eartquake Engineering and Structural Dynamics* **35**, 789–810.

Karimi, H. R., Zapateiro, M. & Luo, N. (2008*a*), 'A linear matrix inequality approach to H_∞ control of vehicle engine-body vibration systems with a time-varying actuator delay', *Proceedings of the Institute of Mechanical Engineers, Part I: Journal of Systems and Control Engineering* **8**, 883–899.

Karimi, H. R., Zapateiro, M. & Luo, N. (2008*b*), Robust mixed H_2/H_∞ vibration control of uncertain structures applied to a base isolated structure, *in* '4^{th} European Conference on Structural Control', St. Petersburg, Russia, September 8-11.

Karimi, H. R., Zapateiro, M. & Luo, N. (2008*c*), Semiactive control of nonlinear structures by using neural networks and wavelet analysis, *in* '4^{th} European Conference on Structural Control', St. Petersburg, Russia, September 8-11.

Karimi, H. R., Zapateiro, M. & Luo, N. (2009*a*), 'New delay-dependent stability criteria for uncertain systems with mixed time-varying delays and nonlinear perturbations', *Mathematical Problems in Engineering* **In press**.

Karimi, H. R., Zapateiro, M. & Luo, N. (2009*b*), 'Stability analysis and control synthesis of neutral systems with time-varying delays and nonlinear uncertainties', *Chaos, Solitons & Fractals* **In press**.

Karimi, H. R., Zapateiro, M. & Luo, N. (2009*c*), 'Wavelet-based parameter identification of a nonlinear magnetorheological damper', *International Journal of Wavelets, Multiresolution and Information Procesing,* **7**.

Karimi, K. R., Zapateiro, M. & Luo, N. (2008*d*), 'Robust mixed H_2/H_∞ delayed state feedback control of neutral delay systems with time varying delays', *Asian Journal of Control,* **10**, 569–580.

Kerschen, G., Worden, K., Vakadis, A. & Golinval, J. (2006), 'Past, present and future of nonlinear system identification in structural dynamics', *Mechanical Systems and Signal Processing,* **20**, 505–592.

Kilicarslan, A., Song, G. & Grigoriadis, K. (2008), ANFIS based modeling and control of a thin sma wire, *in* 'Proceedings of the SPIE Smart Structures and Materials & Nondestructive Evaluation and Health Monitoring', San Diego, U.S.A., March 9-13.

Kim, H. & Roschke, P. (2006), 'Fuzzy control of base-isolation system using multi-objective genetic algorithm', *Computer-Aided Civil and Infrastructure Engineering,* **21**, 436–446.

Kim, H., Roschke, P., Lin, P. & Loh, C. (2006), 'Neuro-fuzzy model of hybrid semi-active base isolation system with FPS bearings and an MR damper', *Engineering Structures,* **28**, 947–958.

Kim, J. & Oh, J. (2001), Development of an above-knee prosthesis using MR damper and leg simulator, *in* 'Proceedings of the 2001 IEEE International Conference on Robotics & Automation', Seoul, Korea, May 21-26.

Krstic, M., Kanellakopoulos, I. & Kokotovic, O. (1995), *Nonlinear and Adaptive Control Design.*, John Wiley and Sons, Inc.

Kuruta, N., Kobori, T., Takahashi, M., Niwa, N. & Midorikawa, H. (1999), 'Actual seismic response controlled building with semiactive damper system', *Earthquake Engineering and Structural Dynamics,* **28**, 1427–1447.

Li, Z., Chang, C. & Spencer, B. (2002), 'Intelligent technology-based control of motion and vibration using MR dampers', *Earthquake Engineering and Engineering Vibration,* **1**, 100–110.

Luo, N., Rodellar, J. & la Sen, M. D. (1999), *Advances in structural control*, CIMNE, chapter 6 (Sliding mode control of flexible structures), pp. 103–128.

Luo, N., Rodellar, J., la Sen, M. D. & Vehí, J. (2000), 'Output feedback sliding mode control of base isolated structures', *Journal of the Franklin Institute,* **337**, 555–577.

Luo, N., Rodellar, J., Vehí, J. & la Sen, M. D. (2001), 'Composite semiactive control of a class of seismically excited structures', *Journal of the Franklin Institute,* **338**, 225–240.

Luo, N., Rodellar, J. & Villamizar, R. (2003), Robust control law for a friction-based semiactive controller of a two-span bridge, *in* 'Proc. SPIE 10^{th} Annual International Symposium on Smart Structures and Materials', San Diego, California, U.S.A., March 2-6.

Luo, N., Villamizar, R. & Vehi, J. (2004), Quantitative feedback theory (QFT): application to structural control, *in* 'China-Japan-US Symposium on Health Monitoring and Control of Structures', Dalian, China, October 13-16.

Luo, N., Villamizar, R. & Vehi, J. (2007), Backstepping control of nonlinear building structures with hysteretic and frictional dynamics, *in* 'European Control Conference', Kos, Greece, July 2-5.

Luo, N., Villamizar, R., Vehi, J. & Dyke, S. (2006), Semiactive backstepping control for vibration attenuation in structures equipped with magnetorheological actuators, *in* 'Proceedings of the 2006 IEEE International Conference on Control Applications', Munich, Germany, October 4-6.

Ma, X., Wang, E., Rakheja, S. & Su, C. (2003), Evaluation of modified hysteresis models for magnetorheological fluid dampers, *in* 'Proceedings of the Fourth International Conference on Control and Automation (ICCA'03)', Montreal, Canada, June 10-12.

McClamroch, N. & Gavin, H. (1995), Closed loop structural control using electrorheological dampers, *in* 'Proceedings of the American Control Conference', Seattle, Washington, U.S.A., June 21-23.

McClamroch, N., Gavin, H., Ortiz, D. & Hanson, R. (1994), Electrorheological dampers and semi-active structural control, *in* 'Proceedings of the 33^{rd} Conference on Decision and Control', Lake Buena Vista, U.S.A., December 14-16.

Milecki, A. & Sedziak, D. (2005), 'The use of magnetorheological fluid dampers to reduce servo drive jumps due to load changes', *Journal of Intelligent Material Systems and Structures,* **16**, 501–510.

Moon, S., Bergman, L. & Voulgaris, P. (2003), 'Sliding mode control of cable-stayed bridge subjected to seismic excitation', *Journal of Engineering Mechanics,* **129**, 71–78.

Mosqueda, G., Stojadinovic, B. & Mahin, S. (2005), Implementaton and accuracy of continuous hybrid simulation with geographically distributed substructures, Technical report, Earthquake Engineering Research Center, University of California, Berkeley.

Nakashima, M. & Masaoka, N. (1999), 'Real-time on-line test for MDOF systems', *Earthquake Engineering and Structural Dynamics* **28**, 393–420.

Narasimhan, S. & Nagarajaiah, S. (2006), 'Smart base isolated buildings with variable friction systems: H_∞ controller and SAIVF device', *Earthquake Engineering and Structural Dynamics,* **35**, 921–942.

Narasimhan, S., Nagarajaiah, S., Johnson, E. & Gavin, H. (2006), 'Smart base isolated benchmark building part I: problem definition', *Journal of Structural Control,* **13**, 573–588.

Neelakantan, V. & Washington, G. (2005), 'Modeling and reduction of centrifuging in magnetorheological transmission clutches for automotive applications', *Journal of Intelligent Material Systems and Structures,* **16**, 703–711.

Neumann, D. (1999), *Adaptronics and Smart Structures. Basics, Materials, Design and Applications*, Springer, chapter 1 (Adaptronics - a concept for the development of adaptive and multifunctional structures), pp. 5–12.

Oh, J., Roschke, P., Lin, P., Carlson, J. & Sunakoda, K. (2004), 'Experimental behavior and neuro-fuzzy modeling of 30-ton magnetorheological damper', *KSCE Journal of Civil Engineering,* **8**, 213–219.

Park, C. & Jeon, D. (2002), 'Semiactive vibration control of a smart seat with an MR fluid damper considering its time delay', *Journal of Intelligent Material Systems and Structures,* **13**, 521–524.

Peschel, J. & Roschke, P. (2001), Neuro-fuzzy model of a large magnetorheological damper, *in* 'Proceedings of the Texas Section ASCE Spring Meeting', San Antonio, Texas, U.S.A., March 28-31.

Pozo, F., Ikhouane, F., Pujol, G. & Rodellar, J. (2006), 'Adaptive backstepping control of hysteretic base-isolated structures', *Journal of Vibration and Control,* **12**, 373–394.

Ramallo, J., Johnson, E. & Jr., B. S. (2002), '"Smart" based isolation systems', *Journal of Engineering Mechanics,* **128**, 1088–1099.

Rodellar, J. & Luo, N. (2003), State of the art report on methodological approaches and semiactive control of civil engineering structures, Technical report, SAMCO.

Rogers, C. A. & Giurgiutiu, V. (1999), *Adaptronics and Smart Structures. Basics, Materials, Design and Applications*, Springer, chapter 2 (Concepts of Adaptronics Structures), pp. 13–34.

Sain, P., Sain, M. & Spencer, B. (1997), Models for hysteresis and applications to structural control, *in* 'Proceedings of the American Control Conference', Albuquerque, U.S.A., June 4-6.

Saito, T., Ikeda, H. & Oguro, M. (2006), 'An application of magnetorheological suspension seal to pressure relief device', *Journal of Intelligent Material Systems and Structures,* **17**, 341–345.

Schurter, K. & Roschke, P. (2000), Fuzzy modeling of a magnetorheological damper using ANFIS, *in* 'The Ninth IEEE International Conference on Fuzzy Systems', San Antonio, Texas, U.S.A., May 7-10.

Schurter, K. & Roschke, P. (2001), 'Neuro-fuzzy control of structures using acceleration feedback', *Smart Materials and Structures,* **10**, 770–779.

Shames, I. H. & Cozzarelli, F. A. (1992), *Elastic and Inelastic Stress*, Englewood Cliffs, New Jersey, U.S:A., pp. 120–122.

Shield, C. K., French, C. W. & Timm, J. (2001), 'Development and implementation of the effective force testing method for seismic simulation of large-scale structures', *Philosophical Transactions of the Royal Society: Theme Issue on Dynamic Testing of Structures* **359**, 1911–1929.

Shing, P. B., Jung, R. Y., Wei, Z. & Stauffer, E. (2004), Fast hybrid testing at CU-NEES, *in* '17^{th} ASCE Engineering Mechanics Conference', Newark, Delaware, June 13-16.

Skelton, R. (1996), Some open problems in structural control, *in* 'Proceedings of the American Control Conference', Seattle, Washington, U.S.A.

Song, X., Ahmadian, M. & Southward, S. (2005), 'Modeling magnetorheological dampers with application of nonparametric approach', *Journal of Intelligent Material Systems and Structures,* **16**, 421–432.

Spencer, B., Dyke, S., Sain, M. & Carlson, J. (1997), 'Phenomenological model of a magnetorheological damper', *ASCE Journal of Engineering Mechanics,* **123**, 230–238.

Spencer, B. F., Elnashai, A., Nakata, N., Saliem, H., Yang, G., Futrelle, J., Glick, W., Marcusiu, D., Ricker, K., Finholt, T., Horn, D., Hubbard, P., Keahey, K., Liming, L., Zaluzec, N., Pearlman, L. & Stauffer, E. (2007), The MOST experiment: Earthquake engineering on the grid, Technical report, NEESgrid-2004-41.

Spencer, B. & Sain, M. (1997), 'Controlling buildings: a new frontier in feedback', *IEEE Control Systems Magazine,* **17**, 19–35.

Spencer, B. & Soong., T. (1999), New applications and development of active, semi-active and hybrid control techniques for seismic and non-seismic vibration in the USA, *in* 'Proceedings of International Post-SMIRT Conference Seminar on Seismic Isolation, Passive Energy Dissipation and Active Control of Vibration of Structures', Cheju, Korea, August 23-25.

Symans, M. D. & Constantinou, M. C. (1997), 'Seismic testing of a building structure with a semiacive fluid damper control system', *Earthquake Engineering and Structural Dynamics,* **26**, 759–777.

Utkin, V. I. (1992), *Sliding modes in control and optimization*, Springer Verlag, Berlin, Germany.

Villamizar, R. (2005), Robust control of systems subjected to uncertain disturbances and actuator dynamics, PhD thesis, University of Girona.

Villamizar, R., Luo, N., Vehi, J. & Rodellar, J. (2003), Semiactive sliding mode control of uncertain base isolated structures with actuator dynamics, *in* 'Proc. SPIE 10^{th} Annual International Symposium on Smart Structures and Materials', Warsaw, Poland.

Villamizar, R., Luo, N., Vehi, J. & Rodellar, J. (2004), Active and semiactive QFT control for the structural vibration attenuation, *in* 'International Conference on Mechanical Vibration and Noise', St. Louis, U.S.A., August 8-11.

Wang, D. & Liao, W. (2001), Neural network modeling and controllers for magnetorheological fluid dampers, *in* '2001 IEEE International Fuzzy Systems Conference', Melboune, Australia, December 2-5.

Wang, J., Feng, N., Meng, G. & Hahn, E. (2006), 'Vibration control of rotor by squeeze film damper with magnetorheological fluid', *Journal of Intelligent Material Systems and Structures,* **17**, 353–357.

Wang, S., Roschke, P. & Yeh, H. (2004), 'Robust control for structural systems with unstructured uncertainties', *Journal of Intelligent Material Systems and Structures,* **130**, 337–346.

Wang, X. & Gordaninejad, F. (2002), 'Lyapunov-based control of a bridge using magneto-rheological fluid dampers', *Journal of Intelligent Material Systems and Structures,* **13**, 415–419.

Weber, F., Feltrin, G. & Huth, O. (2006), Guidelines for structural control, Technical report, Structural Engineering Research Laboratory, Swiss Federal Laboratories for Materials Testing and Research.

Wen, Y. K. (1976), 'Method for random vibration of hysteretic systems', *Journal of Engineering Mechanics* **102**, 249–263.

Wu, B., Wang, Q. Y., Shi, P. F., Ou, J. P. & Guan, X. C. (2003), 'Real-time substructure test of jz20-2nw offshore platform with semi-active mr dampers', *Journal of Intelligent Material Systems and Structures* **14**, 35–42.

Xu, Z. & Guo, Y. (2006), 'Fuzzy control method for earthquake mitigation structures with magnetorheological dampers', *Journal of Intelligent Material Systems and Structures,* **17**, 871–881.

Yang, G. (2001), Large-scale magnetorheological fluid damper for vibration mitigation: modeling, testing and control, PhD thesis, University of Notre Dame.

Yang, G., Spencer, B., Carlson, J. & Sain, M. (2002), 'Large-scale MR fluid dampers: modeling and dynamic performance considerations', *Engineering Structures,* **24**, 309–323.

Yang, J., , Lin, S. & Jabbari, F. (2003), 'H_2-based control strategis for civil engineering structures', *Journal of Structural Control,* **10**, 205–230.

Yang, J., , Lin, S. & Jabbari, F. (2004), 'H_∞-based control strategis for civil engineering structures', *Structural Control and Health Monitoring,* **11**, 223–237.

Yang, S. & Shen, Y. (2006), Recent advances in dynamics and control of hysteretic nonlinear systems, *in* 'The Second International Conference on Dynamics, Vibration and Control', China, August 23-26.

Yi, F., Dyke, S., Caicedo, J. & Carlson., J. (1999), Seismic response control using smart dampers, *in* 'Proceedings of American Control Conference', San Diego, California, U.S.A., June 2-4.

Yi, F., Dyke, S., Caicedo, J. & Carlson, J. (2001), 'Experimental verification of multiinput seismic control strategies for smart dampers', *Journal of Engineering Mechanics,* **127**, 1152–1164.

Yoo, J. & Wereley, N. (2002), 'Design of a high-efficiency magnetorheological valve', *Journal of Intelligent Material Systems and Structures,* **13**, 679–685.

Yoshida, O. & Dyke, S. (2003), 'Response control in full scale irregular buildings using MR dampers', *ASCE Journal of Structural Engineering,* **131**, 734–742.

Yoshida, O., Dyke, S., Giacosa, L. & Truman, K. (2002), 'Experimental verification of torsional response control of asymmetric buildings using MR dampers', *Earthquake Engineering and Structural Dynamics,* **32**, 2085–2105.

Yoshioka, H., Ramallo, J. & Spencer, B. (2002), '"Smart" based isolation strategies employing magnetorheological dampers', *Journal of Engineering Mechanics,* **128**, 540–551.

Yu, M., Dong, X., Liao, C. & Chen, W. (2006), 'Adaptive fuzzy-neural network control for magnetorheological suspension', *IJCSNS International Journal of Computer Science and Network Security,* **6**, 66–71.

Yu, M., Liao, C., Chen, W. & Huang, S. (2006), 'Study on MR semi-active suspension systems and its road testing', *Journal of Intelligent Material Systems and Structures,* **17**, 801–806.

Zapateiro, M., Karimi, H. R. & Luo, N. (2008), Adaptive backstepping control for vibration reduction in a structure with frictional and hysteretical actuators, *in* 'IFAC World Congress', Seoul, Korea, July 6-11.

Zapateiro, M. & Luo, N. (2007*a*), MR dampers for seismic protection: design, modeling and identification, *in* '3^{er} Congreso Nacional de Ingeniería Sísmica', Girona, Spain, May 8-11.

Zapateiro, M. & Luo, N. (2007*b*), 'Parametric and non-parametric characterization of the dynamics of a shear-mode magnetorheological damper', *Journal of Vibroengineering,* **9**, 14–18.

Zapateiro, M., Luo, N. & Karimi, H. R. (2008), QFT control for vibration reduction in structures equipped with MR dampers, *in* 'American Control Conference', Seattle, U.S.A., June 11-13.

Zapateiro, M., Luo, N., Karimi, H. R. & Vehí, J. (2008), 'Vibration control of a class of semiactive suspension system using neural network and backstepping techniques', *Mechanical Systems and Signal Processing,* **DOI: 10.1016/j.ymssp.2008.10.003**.

Zapateiro, M., Luo, N., Taylor, E. & Dyke, S. J. (2008), 'Modeling and identification of a class of mr fluid foam dampers', *Journal of Smart Structures and Systems,* **In press**.

Zapateiro, M., Villamizar, R. & Luo, N. (2008), 'Semiactive seismic vibration control of structures equipped with magnetorheological dampers', *International Journal of Factory Automation, Robotics and Soft Computing,* **1**, 77–84.

Zhang, J. & Roschke, P. (1998), Neural network simulation of magnetorheological damper behavior, *in* 'Proceedings of the International Conference on Vibration Engineering', Dalian, China, August 6-9.

Appendix A

Publications

JCR Journal Papers

M. Zapateiro, H.R. Karimi, N. Luo, B.F. Spencer (2009). "Real-time hybrid testing of semiactive control strategies for vibration reduction i a structure with MR damper", *Structural Control and Health Monitoring*, Online available (DOI:10.1002/stc.321).

H. R. Karimi, **M. Zapateiro**, N. Luo (2009). "Wavelet-based parameter identification of a nonlinear magnetorheological damper", *International Journal of Wavelets, Multiresolution and Information Processing*, **7(1)**, 183-198.

M. Zapateiro, N. Luo, H. R. Karimi, J. Vehí (2008). "Vibration control of a class of semiactive suspension system using neural network and backstepping techniques, *Mechanical Systems and Signal Processing*, Online available (DOI: 10.1016/j.ymssp.2008.10.003).

H. R. Karimi, **M. Zapateiro**, N. Luo (2008)."Robust mixed H_2/H_∞ delayed state feedback control of neutral delay systems with time varying delays", *Asian Journal of Control*, **10(5)**, 569-580.

H. R. Karimi, **M. Zapateiro**, N. Luo (2008). "A Linear Matrix Inequality approach to H_∞ control of vehicle engine-body vibration systems with a time-varying actuator delay", *Proceedings of the Institute of Mechanical Engineers, Part I: Journal of Systems and Control Engineering*, **222(8)**, 883-899.

H. R. Karimi, **M. Zapateiro**, N. Luo (2008). "New delay-dependent stability criteria for uncertain systems with mixed time-varying delays and nonlinear perturbations", *Mathematical Problems in Engineering*, Online available (DOI:10.1155/2009/759248).

H. R. Karimi, **M. Zapateiro**, N. Luo (2008). "Stability analysis and control synthesis of neutral systems with time-varying delays and nonlinear uncertainties", *Chaos, Solitons & Fractals*, Online available (DOI: 10.1016/j.chaos.2009.01.028).

M. Zapateiro, N. Luo, E. Taylor, S.J. Dyke (2008). "Modeling and identification of a class of MR fluid foam dampers", *Journal of Smart Structures and Systems*, **In press**.

M. Zapateiro, H.R. Karimi, N. Luo, B.M. Phillips, B.F. Spencer. "Semiactive backstepping control for vibration reduction in a structure with magnetorheological damper subject to seismic motions". **Submitted to** Journal of Intelligent Material Systems and Structures.

M. Zapateiro, H.R. Karimi, N. Luo, B.F. Spencer. "Frequency domain control based on Quantitative Feedback Theory for vibration suppression in structures equipped with magnetorheological dampers". **Submitted to** Journal of Smart Materials and Structures.

M. Zapateiro, H.R. Karimi, N. Luo. "Vibration suppression in a building with frictional and hysteretic actuators through adaptive backstepping control. **Submitted to** International Journal of Control, Automation and Systems.

Other journal papers

M. Zapateiro, N. Luo, H.R. Karimi (2009). "Semiactive control of base isolated building using magnetorheological dampers", *International Journal of Modeling, Identification and Control*, **7(1)**.

M. Zapateiro, R. Villamizar, N. Luo (2008). "Semiactive seismic vibration control of structures equipped with magnetorheological dampers" *International Journal of Factory Automation, Robotics and Soft Computing*, Issue 1, 77-84.

M. Zapateiro, N. Luo, H. R. Karimi (2009). "Neural network - backstepping control for vibration reduction in a magnetorheological suspension system", *Solid State Phenomena*, **147-149**, 939-844.

M. Zapateiro, N. Luo (2007). "Parametric and non-parametric characterization of the dynamics of a shear-mode magnetorheological damper", *Journal of Vibroengineering*, **9**, 14-18.

Book chapters

M. Zapateiro, R. Villamizar, N. Luo (2008). "Semiactive seismic vibration control of structures equipped with magnetorheological dampers", *Recent Advances in Control Systems, Robotics and Automation*, 144-151.

M. Zapateiro, N. Luo (2007). "Neural network modeling of magnetorheological dampers", "Artificial Intelligence Research and Development", 351-358.

Conference papers

H.R. Karimi, **M. Zapateiro**, N. Luo (2009). "Stability analysis of a class of neutral systems with mixed time-varying delays and nonlinear parameter perturbations", *European Control Conference*, Budapest, Hungary, August 23-26.

H.R. Karimi, **M. Zapateiro**, N. Luo (2009). "Delay-dependent adaptive synchronization of master-slave systems with mixed time-delays and nonlinear perturbations", *Second IFAC meeting related to analysis and control of chaotic systems, CHAOS 09*, London, U.K., June 22-24.

H.R. Karimi, **M. Zapateiro**, N. Luo (2009). "An LMI approach to H_∞ synchronization of second-order neutral master-salve systems", *American Control Conference*, St. Louis, U.S.A., June 10-12.

N. Luo, H.R. Karimi, **M. Zapateiro** (2009). "Robust control of networked structural control systems with wireless sensing", *International Workshop on Dynamics and Control*, Tossa de Mar, Spain, May 31 - June 2.

M. Zapateiro, H.R. Karimi, N. Luo (2009). "Semiactive suspension for aircraft landing vibration", *ECCOMAS Thematic Conference: Smart Structures and Materials*, Porto, Portugal, July 13-15.

H.R. Karimi, **M. Zapateiro**, N. Luo (2009). "Networked structural control with wireless sensing using H_∞ output feedback", *ECCOMAS Thematic Conference: Smart Structures and Materials*, Porto, Portugal, July 13-15.

H. R. Karimi, **M. Zapateiro**, N. Luo (2008). "Semiactive control of nonlinear structures by using neural networks and wavelet analysis", 4^{th} *European Conference on Structural Control*, St. Petersburg, Russia,

September 8-11.

H. R. Karimi, **M. Zapateiro**, N. Luo (2008). "Robust mixed H_2/H_∞ vibration control of uncertain structures applied to a base isolated structure", *4^{th} European Conference on Structural Control*, St. Petersburg, Russia, September 8-11.

M. Zapateiro, N. Luo, H. R. Karimi (2008). "QFT robust control for structures with hysteretic dynamics and parametric uncertainties, *4^{th} European Conference on Structural Control*, St. Petersburg, Russia, September 8-11.

J. Rodellar, **M. Zapateiro**, N. Luo, A. Rodríguez (2008). "Modeling and identification of hysteretic dynamics of MR dampers and application to semiactive vibration control of smart structures, *14^{th} World Conference on Earthquake Engineering*, Beijing, China, October 12-17.

H. R. Karimi, **M. Zapateiro**, N. Luo (2008). "Intelligent vibration attenuation in smart structures with nonlinear actuator dynamics", *9^{th} International Conference on Motion and Vibration Control (MOVIC)*, Munich, Germany, September 15-18.

M. Zapateiro, H. R. Karimi, N. Luo (2008). "Adaptive backstepping control for vibration reduction in a structure with frictional and hysteretical actuators", *IFAC World Congress*, Seoul, Korea, July 6-11.

A. Khosravi, J. Melendez, **M. Zapateiro**, J. Colomer (2008). "Classification of voltage sags based on MPCA and CBR", *IFAC World Congress*, Seoul, Korea, July 6-11.

M. Zapateiro, N. Luo (2008). "Semiactive control of a base isolated building using magnetorheological dampers", *International Conference on Modeling, Identification and Control*, Shanghai, China, June 29 - July 2.

M. Zapateiro, N. Luo (2008). "A neural-network backstepping based control for a magnetorheological damper suspension", *Mechatronic Systems and Materials*, Bialystok, Poland, July 14-17.

M. Zapateiro, H.R. Karimi, N. Luo (2008). "QFT control for vibration reduction in structures equipped with MR dampers", *American Control Conference*, Seattle, U.S.A., June 11-13.

M. Zapateiro, N. Luo (2008). "Vibration control of hysteretic systems via neural network adaptive backstepping" *(SPIE) Symposium on Smart Structures and Materials & Nondestructive Evaluation and Health Monitoring*, San Diego, U.S.A., March 9-13.

M. Zapateiro, N. Luo (2007). "Neural network modeling of magnetorheological damper", *Congrés Internacional de l'Associació d'Intel.ligència Artificial (CCIA)*, Sant Julià de Lòria, Andorra, October 25-26 .

M. Zapateiro, N. Luo (2007). "Parametric and non-parametric characterization of a shear mode magnetorheological damper" *3^{rd} International Conference on Mechatronic Systems and Materials 2007*, Kaunas, Lithuania, September 27-29.

M. Zapateiro, N. Luo, E. Taylor, S.J. Dyke. "Experimental identification of a shear-mode MR damper and numerical evaluation of hysteretic models", *21^{st} Biennial Conference on Mechanical Vibration and Noise (DETC-VIB)*, Las Vegas, U.S.A., September 12-15.

M. Zapateiro, N. Luo, E. Taylor, S.J. Dyke (2007). "Modeling and identification of a class of MR fluid foam damper", *III ECCOMAS Thematic Conference, Smart Structures and Materials*, Gdansk, Poland July 9-11.

M. Zapateiro, N. Luo (2007). "MR dampers for seismic protection: design, modeling and identification", *Proceedings of the 3er Congreso Nacional de Ingeniería Sísmica*, Girona, Spain, May 8-11.

N. Luo, J. Rodellar, F. Ikhouane, **M. Zapateiro** (2007). "Modeling, identification and control of mechatronic systems equipped with smart actuators: research advances in Spain", *World Forum on Smart Materials and Smart Structures Technology (SMSST)*, Chongqing-Nagjing, China, May 22-27.

M. Zapateiro, E. Taylor, S.J. Dyke, N. Luo (2007). "Modeling and identification of the hysteretic dynamics of an MR actuator for its application to semiactive control of flexible structures", *SPIE Symposium on Smart Structures and Materials & Nondestructive Evaluation and Health Monitoring*, San Diego, California, U.S.A., March 18-22.

Technical Reports

M. Zapateiro, H.R. Karimi, N. Luo, B.F. Spencer (2008). "Design and experimental testing of semiactive controllers for seismic vibration mitigation in structures with MR dampers". Technical Report IIiA 08-02-RR. Institute of Informatics and Applications, University of Girona.

M. Zapateiro (2007). "Identification, modeling and control of magnetorheological dampers for adaptronics and smart structures". Research Report for Diploma of Advanced Studies in PhD program of Information Technology, graded with an "Excellent Unanimously", University of Girona.

M. Zapateiro and N. Luo (2006). "Magnetic circuit design for magnetorheological dampers". Technical Report IIiA 06-15-RR. Institute of Informatics and Applications, University of Girona.

M. Zapateiro and N. Luo (2006). "Magnetorheological dampers for structural control". Technical Report IIiA 06-13-RR. Institute of Informatics and Applications, University of Girona.

M. Zapateiro and N. Luo (2006). "Magnetorheological fluids: characteristics, preparation and applications to vibration control". Technical Report IIiA 06-12-RR. Institute of Informatics and Applications, University of Girona.

M. Zapateiro and N. Luo (2006). "Mathematical modeling of magnetorheological dampers". Technical Report IIiA 06-14-RR. Institute of Informatics and Applications, University of Girona.